Self-assembling amphiphilic oligopeptides

Structural and functional characterization

ALBERT VAN HELL

ISBN 978-90-393-4986-1

Structural and functional characterization of self-assembling amphiphilic oligopeptides

Albert Jan van Hell

PhD Thesis with summary in Dutch

Department of Pharmaceutics, Utrecht University, The Netherlands

December 2008

Financial support for the publication of this thesis was kindly provided by the Utrecht Institute for Pharmaceutical Sciences, Utrecht, The Netherlands.

Printed by PrintPartners Ipskamp, Enschede, The Netherlands.

Structural and functional characterization of self-assembling amphiphilic oligopeptides

Structurele en functionele karakterisering van zelf-associërende amfifiele oligopeptiden

(met samenvatting in het Nederlands)

PROEFSCHRIFT

ter verkrijging van de graad van doctor aan de Universiteit Utrecht op gezag van de rector magnificus, prof. dr. J.C. Stoof, ingevolge het besluit van het college voor promoties in het openbaar te verdedigen op maandag 12 januari 2009 des middags te 2.30 uur

door

ALBERT JAN VAN HELL

geboren op 28 april 1981 te Pretoria, Zuid-Afrika

Promotor: Prof. dr. DJA Crommelin
Prof. dr. ir. WE Hennink

Co-promotor: Dr. E Mastrobattista

Table of Contents

Chapter 1

General introduction

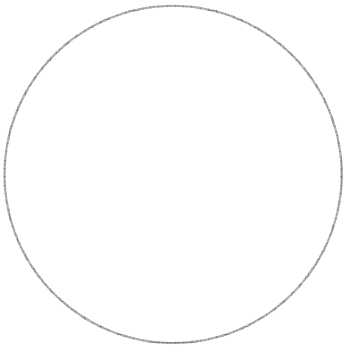

Albert J van Hell

Department of Pharmaceutics, Utrecht Institute for Pharmaceutical Sciences, Utrecht University, The Netherlands

1.1 Molecular self-assembly

Molecular self-assembly is defined as the spontaneous association of molecules under equilibrium conditions into stable, structurally well-defined aggregates joined by noncovalent bonds [1, 2]. Molecules that spontaneously self-organize into larger, supramolecular structures are a universal phenomenon in nature and in fact are essential to life. For example, actin proteins assemble into cytoskeleton filaments, lipids self-organize into membranes and virus capsids spontaneously form by assembly of the virus coat proteins.

Over the past decades, scientists have utilized the supramolecular assembly of molecules as a powerful toolbox for creating new and functional materials. Different forces contribute to the stabilization of supramolecular assemblies, including hydrophobic forces, hydrogen bonding, electrostatic interactions and van der Waals forces. This intricate interplay of forces allows the formation of an almost unlimited number of supramolecular assemblies. Interestingly, by precise control over the intermolecular interactions, materials were obtained with smart properties, which were unattainable by covalent bond chemistry [2-4]. For example, a flexible filament of polymer material has been demonstrated to shape spontaneously into a 2 mm wide tube upon a shift in temperature [5] or a self-healing rubber material was designed based on supramolecular interactions; when the piece of rubber is broken the material regains its initial strength at the site of scission, simply by holding both ends together [6]. These examples illustrate the level of control that can be obtained at the mesoscale by carefully controlling supramolecular interactions.

Nanostructures can be defined as assemblies of bonded atoms that have dimensions in the range of 1 to 10^2 nanometers [1]. Particularly, molecular self-assembly is a practical approach to form well-defined nanosized objects [4], which are of use for a variety of different applications, including molecular sensors in detection arrays [7], diagnostic imaging agents [8, 9], templates for nanolithography [10, 11], nanovessels for chemical reactions [12] and drug carriers [13, 14]. The techniques that are available to modify or shape such small structures after their synthesis are limited. Among the few techniques that are applicable, like dip-pen

nanolithography, most are very costly, or not suited for large scale productions [15, 16]. Therefore, molecular self-organization is the most frequently exploited route for the assembly of nanostructures.

The selection of self-assembling molecules is greatly defined by the intended application of the material or nanostructure. For biomedical applications, like drug delivery, medical imaging, or tissue engineering, the self-assembled structures should at least be stable in biological fluids, have low toxicity and be poorly immunogenic. Examples of molecular building blocks that have successfully been used as biomaterials are metals [17], polysaccharides [18], lipids [19] and synthetic polymers [20]. In addition to synthetic polymers, which represent the predominant class so far [21], genetically engineered protein-based polymers, such as silk-like or elastin-like polymers are increasingly being used as building blocks to generate novel biomaterials by self-assembly [22, 23].

1.2 Peptides in molecular assembly

Among the candidates for self-assembly of molecules, (poly)peptide polymers based on amino acids combine sequential control with a wide diversity of molecular characteristics [23]. Even when only considering the 20 encoding amino acids, peptides as the molecular building blocks allow the selection of a broad range of physicochemical features. Four out of the 20 encoding amino acids contain charged side groups that can establish coulombic intermolecular interactions, various amino acids exhibit apolar side chains, either aliphatic or aromatic which may contribute to hydrophobic clustering. Furthermore, the aromatic amino acids can orderly arrange via π-π stacking, and many peptide side chains, and the peptide backbone itself, can form hydrogen bonds. The variety of intermolecular interactions available for the self-assembly of peptides is reflected by the diversity of developed supramolecular structures [24-30]. In aqueous environment peptide design exclusively based on the 20 encoding amino acids has generated supramolecular architectures like peptide hydrogels [31-34], adjustable fibrous scaffolds [35, 36], rigid or dynamic nanotubes [10, 37, 38], micelles and peptide sheets [39, 40].

Even peptides as short as two amino acids (dipeptides) can orderly arrange into a variety of different structures. The dipeptides are characterized by the presence of at least one phenylalanine. For example, well-defined nanospheres are formed by a glycine-phenylalanine peptide. The Fmoc-diphenylalanine peptide spontaneously forms hydrogels, whereas a plain diphenylalanine peptide assembles into hollow peptide tubes of 50 up to 1000 nm in diameter [10, 41, 42]. The diphenylalanine tubes are rigid and withstand highly disruptive conditions. The Youngs' elastic modulus of 19 GPa places these dipeptide nanotubes among the stiffest biological materials that are known to date [38, 43].

Polypeptides, whose controllable synthesis up to extensive block lengths has become feasible by the discovery of nickel mediated NCA polymerization, represent a contrasting class of self-assembling peptide molecules [28, 44]. Dependent on the lengths and ratios of the hydrophilic and the hydrophobic blocks, long polypeptides of up to 400 amino acids in length assemble into sheets, micelles, vesicles or hydrogels [28, 39]. The $L_{40}K_{160}$ polypeptides assemble into a hydrogel of high water content, only containing 0.25–2.0 weight percent of the polymer material. The polypeptide assemblies display a soft and highly deformable nature rapid recovering after mechanical stress [28, 45]. The stiff phenylalanine dipeptide structures and the soft polyleucine-*b*-polylysine polypeptide assemblies exemplify the broad range of supramolecular structures and variety of physicochemical characteristics achievable, even when restrictively using the 20 natural amino acids as the building blocks. It can be envisioned that many supramolecular morphologies and physicochemical characteristics in between the outlined examples are achievable by variations of (poly)peptide lengths and composition. Further insights into the details of the forces driving self-assembly will lead to rationally design of (poly)peptide materials.

1.2.1 Self-assembling amphiphilic oligopeptides

Small oligopeptides varying in size from 8-30 amino acids are particularly interesting building blocks for molecular self assembly. By their small size the supramolecular self-organization in aqueous environment can be more readily predicted as compared to larger peptides or proteins, whose folding behavior

remains complicated. Moreover, when hydrophobic peptide segments are utilized, small peptides limit the tendency to form peptide aggregates [24, 29]. Amphiphilicity is a main driving force in self-assembly, and it dominantly drives the structuring of self-assembling oligopeptides as well [25]. Two different topologies of amphiphilicity can be distinguished in oligopeptides. One is the hydrophobic and hydrophilic moieties on the opposing sides of the backbone's longitudinal axis. For example, alternating hydrophobic and charged amino acids in EAK16 ionic self-complementary peptides contain repetitions of negatively and positively charged amino acids, spaced by a single alanine [46]. The beta-sheet conformation of these peptides presents the apolar alanines to one side, while the complementary charged species face the opposite side of the peptide backbone. The manifestation of amphiphilicity in these peptides is thus dependent on the secondary conformation of the peptide. In the EAK16 peptides the attractive coulombic interactions promote self-association of the peptides, whereas the opposing sides associate via hydrophobic interactions. As a result, the beta-sheeted oligopeptide assemblies gelate into a stable macroscopic hydrogel.

The other type of amphiphilicity is represented along the longitudinal axis of the peptide backbone, in which the hydrophobic block is attached to the hydrophilic block. This type is not specific for oligopeptides, as it is present in e.g. amphiphilic block-co-polymers and lipids. By their size these amphiphilic oligopeptide resemble the molecular dimensions of phospholipids. Such lipid-like or detergent-like peptides were shown to assemble into thin peptide membranes that form a network of nanotubes [37, 47, 48]. Interestingly, these tubes appeared open at their ends, and the oligopeptide assembly into these tubes occurred spontaneously upon dispersion in water, thereby revealing marked distinctions from classical hydrocarbon amphiphile assembly [49]. Despite observation of some spherical architectures in these assemblies, oligopeptides that solely formed nanovesicles were not reported so far [50, 51].

Various promising results of biomedical applications of oligopeptide assemblies have been reported. This is remarkable giving the fact that self-assembling oligopeptides are explored only since recently [46]. Oligopeptide hydrogels, like the

EAK16 peptide gels, were shown to promote biological processes, like neurite outgrowth and synapse formation of neurons, as well as angiogenesis in 3D cell cultures and wound healing in human skin tissue culture models [52-56]. Moreover, oligopeptides can be directly extended to incorporate and present biofunctional peptide sequences, like 6-10 amino acids laminin 1 or collagen IV motifs for cell adherence to the oligopeptide scaffolds. These straightforward extensions of the peptide sequence indeed improved the long-term effects and functionality of the peptide assemblies [53, 57, 58]. The biocompatibility of such oligopeptides was furthermore demonstrated by the *in vivo* application of oligopeptide hydrogels. The intrinsic promotion of neural growth and function *in vivo* resulted in the restoration of vision in mice after severe nerve injury. The self-assembling oligopeptides were immunologically inert [59] .

1.2.2 Production of amphiphilic oligopeptides and effects on self-assembly

Recently it was reported that the production of lipid-like oligopeptides with several hydrophobic amino acids in a row is challenging by means of current solid phase synthesis techniques [60]. Other, more sophisticated synthesis routes might be opted for, like NCA polymerization synthesis; however, this route lacks sequential control on the peptides. Moreover, purification of synthetic peptides is difficult and labor-intensive. The impurities may consist of peptides differing only one or two amino acids in length. Such impurities may significantly affect the self-assembling behavior of amphiphilic peptides [60]. An alternative route of synthesis, production of proteins or polypeptides in biological systems like *E. coli* bacteria, is feasible up to long polypeptide lengths, while keeping full sequential control of the peptide [23, 61, 62]. Moreover, the incorporation of synthetic, non-natural amino acids by bacteria by expanding the genetic code may increase the chemical diversity of peptide biosynthesis [63, 64]. The use of fusion proteins (e.g. glutathione *S*-transferase, thioredoxin, small ubiquitin modifying protein) can further facilitate peptide expression and purification [65, 66]. Recombinant production is cost-effective, in particular at larger scales [67, 68]. For difficult to synthesize peptides, biotechnology may provide production routes alternative to solid-phase synthesis.

1.2.3 Peptide hydrogen bonding and secondary conformation

The design of supramolecular assemblies requires full understanding and control over intermolecular interactions. The intramolecular (secondary) organization of peptides determines the spatial arrangement of amino acids relative to each other in a peptide, and thereby dictating the intermolecular interactions that may occur. Peptides deviate significantly from many self-assembling synthetic polymers and hydrocarbon amphiphiles by the chemical nature of their backbone. The amide hydrogen and carbonyl oxygen in the backbone are a hydrogen bond donor and acceptor, respectively and in the case of amphiphilic peptides the backbone itself exhibits an apolar character. As mentioned above, supramolecular assemblies frequently are based on the formation of a hydrophobic domain [25]. The energetic penalty of burying the free hydrogen bond donor and acceptor into an apolar, dehydrated environment has been estimated at 2.5 kcal/mol [69]. In contrast, the gain in energy of hydrophobic desolvation of apolar amino acid side chains is at maximum -2.2 kcal/mol, and for many amino acid side chains like alanine or valine these values are lower [70]. Therefore, burial of free amides and carbonyls in the hydrophobic domains is energetically restricted, and in the hydrophobic domain of proteins rarely found [71].

Many peptides in assemblies establish hydrogen bonds, thereby saturating the amide and carbonyl hydrogen bond donors and acceptors [24-27, 55]. Typically, hydrogen bonding occurs in a well defined pattern. For example, the alpha-helix turns 360° each 3.6 amino acids, and thereby saturates the peptide backbone hydrogen bond donors and acceptors intramolecularly. In supramolecular assemblies, such secondary peptide conformation can distinguish between molecular organization and peptide aggregation. Assembly of polylysine-*b*-polyleucine into vesicles was demonstrated to rely on alpha-helix formation of the hydrophobic leucine block; if a racemic mixture of the leucines was used, unable to adopt the alpha-helical conformation, large unordered aggregates were formed instead [39].

A slightly different helical structure, the coiled coil conformation, has been extensively exploited for example in the design of longitudinally interacting peptides. Upon interaction of two or more helices a slight switch to a 3.5 amino

acid periodicity takes place. Due to the restricted conformational freedom of such peptide conformation precise modification of the peptide structures is facilitated. Peptide coiled coil fibers can be grown in a highly ordered way, of demonstrated use for biomedical tissue engineering applications [36, 72]. Kinks as well as branches can be controllably introduced in the fibers, whereas insertion of biofunctional peptide sequences is of use for the controllable attachment of cells [35, 73-75].

Many other peptide self-assemblies adopt the beta-sheet conformation, which involve intermolecular hydrogen bonding. Typically, beta-sheeted peptides self-associate into fibers, which in turn may form a mesoscale network. Using the well-defined nature of the beta-sheets, peptide assembly was shown to be highly controllable and adjustable, in analogy to the self-assembling coiled coil fibers [76-81]. Interestingly, the peptide fibers and networks were found to be robust and biocompatible [59, 78, 79] In conclusion, the utilization of the secondary peptide conformation provides an additional level of control over the supramolecular assembly of peptide molecules [82-85].

In small peptides as well as in proteins, the significance and the characteristics of a thus far largely unexplored secondary conformation has become increasingly evident [86-88]. The polyproline type II (PPII) conformation in its extended form turns counterclockwise (left-handed) each 3.0 amino acids and is a well-known structure in collagen and polyproline peptides. However, the PPII conformation extends beyond these typical examples. Detailed insights by spectroscopic techniques on short non-proline peptides has confirmed that the typical PPII dihedral angles (Φ -75°, Ψ 145°) are the preferential orientation of peptide bonds occurring in many, thus far designated as unordered, peptide sequences [86, 88-93].

Besides the impact these findings may have on the early steps in protein folding, the light shed on the PPII conformation may be of value in the design of peptide self-assembling systems. Contrary to the alpha-helix conformation and the beta-sheet, the PPII conformation is not cooperative and is typically found in equilibrium with the dihedral angles of the extended beta-sheet [94]. In other words, in contrast to e.g. the alpha-helix, the PPII conformation is not stabilized by hydrogen bonds and the PPII dihedral angles of one amino acid is not

energetically favored by the equal conformation of the neighboring amino acids [95]. Consequently, non-proline peptides that adopt the PPII conformation not necessarily exhibit a rigid and stiff rod-like character, like the alpha-helical or beta-sheet conformation, and may retain significant flexibility [96]. In peptide self-assembly, the PPII conformation as an intramolecularly ordered and stretched conformation thus far has remained largely unexplored.

1.3 Molecular self-assembly to obtain drug delivery systems

Advanced drug delivery strategies aim at maximizing the therapeutic activity of drugs while minimizing their toxic side effects [21]. To achieve this, various supramolecular structures have been used to entrap pharmaca. The design of such self-assembling structures can follow a top-down approach in which structures from nature with known self-assembling characteristics are being used to create the supramolecular assemblies. Some of the many examples are liposomes, virus-like particles, alginate beads, gelatins and silk-like polymers. Alternatively, a bottom-up approach is followed in which molecules are designed *de novo* in such a way that they will self-assemble in a controlled and predictable manner. The latter approach of supramolecular assembly aims at, as was mentioned before, a full control on the mechanisms that underlie the self-assembly into the desired structure.

By utilizing either approaches of molecular self-association a broad range of different structures can function as a drug carrier, like macroscopic hydrogels, or nanoscaled particles like tubes, rods, micelles and vesicles. Hydrogels can be used to entrap and release protein pharmaceuticals, micelles for the delivery of low molecular weight drugs that are poorly water soluble, or polyplexes for the delivery of genetic material. Self-assembled nanostructures can also function in selectively protecting the drugs from undesired interactions with the body fluid or enzymatic degradation. In contrast, drugs or prodrugs can be attached to supramolecular structures, and may be released specifically upon enzymatic cleavage of the supramolecular components in particular tissue [97, 98].

Morphological characteristics of the supramolecular nanoparticles like shape [99], surface patterning [100] and size [101] influence the behavior and efficiency of a drug carrier. For example, the shape of micelles can affect the circulation time. Filamentous PEG-polyethylethylene polymer micelles showed superior *in vivo* circulation kinetics as compared to spherical micelles [99]. The particle size is one of the key parameters, particularly when used for intravenous delivery of drugs to tumor tissue [101, 102]. In order to avoid rapid liver clearance, particles should be smaller than 200 nm in diameter. Moreover, several studies have demonstrated the poor penetration of particles of a size in between 50 and 200 nm into diseased tissues [103]. Large particles do not diffuse readily across the extracellular matrix. Spheres of 100 nm in diameter or larger are excluded from penetration into the extracellular collagen matrix [104] and injection of 100 nm nanoparticles in tumor tissue resulted in the delivery of the particles to only those tumor cells located along the needle track [105]. In contrast, particles with a diameter of 40 nm were shown to penetrate into the collagen-rich regions and uniformly distributed throughout the tumor tissue [104, 106].

Besides carrying the drug through the body, the supramolecular structures can also provide additional control over the properties of the drug. For example, by its particular physico-chemical characteristics the supramolecular assembly can shift the effective pK_a of the bound low molecular weight drug, establishing more desirable pK_a values for drug release [107]. Frequently, the biodistribution is modulated by the characteristics of the drug carrier and can be enhanced towards specific organ or tumor accumulation, thereby optimizing the biodistribution profile. Circulation kinetics can be extended by the nanoparticle or the carrier can actively transport its payload to specific (sub)cellular target locations [108, 109]. Hence, the success of a drug delivery vehicle largely depends on the ability to optimize the supramolecular assembly for specific applications [101].

1.4 Nanovesicles

Vesicles of nanometer scale have been seen repeatedly as a platform for the intelligent delivery of drug molecules to diseased sites in the body. Design of such smart drug delivery vehicles may include elements for recognition of the

target sites and subsequent triggered release of one or even multiple stocks of active drug molecules [101, 110]. So far, several vesicular systems for intravenous delivery of drugs have reached the market [111]. However, further improvement of their performance is still needed. Therefore, an extension of the arsenal of nanosized delivery systems is desired.

In order to develop nano-particles and, more specifically, vesicular architectures several types of molecular building blocks can be considered. Hydrocarbon amphiphiles, like lipids and detergents, are well-characterized with respect to their self assembling behavior [49, 112] and have been extensively studied for their potential as a drug delivery platform [113-115]. Many lipids, in particular phospholipids have been used because of their vesicle-forming capacity when dispersed in aqueous media. Such lipid vesicles are often referred to as liposomes and can be considered as an archetype of colloidal drug delivery systems obtained by molecular self-assembly. Similarly, non-ionic surfactants can also form vesicles, the so-called niosomes (Table 1). Both hydrophobic and hydrophilic drugs can be encapsulated in the bilayer or the enclosed aqueous compartment, respectively. Niosomes, however, face some challenges with respect to the stable entrapment of low molecular weight hydrophilic molecules [116]. One of the advantages of using lipids for biomedical applications is the stability of the assembly which can be attuned to the desired situation [117]. Moreover, the building blocks are biocompatible – only limited adverse effects have been reported for lipid carriers by systemic administration. In fact, several approved pharmaceutical products are based on drugs entrapped in liposomes, such as Doxil® and Daunoxome® and are successfully used in the clinic [118-120]. However, the design of smart liposomal carriers, for example by inclusion of stimuli-responsiveness, is challenging. The attachment of targeting and biofunctional moieties on liposomes has faced significant hurdles as well [121]. Chemical modifications of the lipids required for attaching the targeting molecule can be precarious, and unnatural linker moieties may elicit undesired side effects in the body [122].

Synthetic polymers comprise a diverse class of building blocks for assembling nanosized particles, which can be varied in polymer design, block lengths, and molecular composition [123-126]. The wide variety of possible polymer compositions

allows steering the characteristics of nanoparticles over a broad range, representing a major advantage of polymers as building blocks for supramolecular assembly. Various di- and triblock polymer architectures have been used to form vesicles (polymersomes) [127-130]. The bilayer of the amphiphilic polymer can be increased as compared to e.g. liposomes; whereas lipid bilayers span 3-5 nm, 10-20 nm thickness is readily achievable for polymer membranes [128]. Polymersomes can thereby typically display high rigidity and low permeability for hydrophilic low molecular weight molecules [128, 131]. Stable entrapment of small molecules can be advantageous for storage of the formulation. However, if triggered mechanisms of release are unavailable, an impermeable membrane may also imply restrictions on the availability of the drug molecules upon reaching the target site. In addition to encapsulation of drugs in the polymersome, the polymer membrane can be functionalized via the attachment of enzymes or incorporation of membrane proteins into the polymer bilayer [132, 133]. Several polymeric vesicles have been examined with respect to their *in vivo* behavior. For example, PEO-PEE vesicles circulate for 15 to 20 hours, comparable to the circulation properties of clinically approved stealth liposomes [134]. A major issue to be considered in the case of biomedical applications of polymers is the biodegradability, biocompatibility and the toxicity of low molecular weight molecules residual to the polymer synthesis, clearly restricting the synthesis routes and polymers that are suited for drug delivery applications.

Table 1. Currently available vesicles for drug delivery

	Liposomes	Niosomes	Polymersomes
Components	Phospholipids, cholesterol	Non-ionic surfactants, cholesterol	Amphiphilic di- or tri-block-polymers
Nanosize dimensions (diameter, nm)	<100, sizing required	<100, sizing required	≥100
Stability	High - moderate	Low	High
Crosslinkable	-/+	-	+
Permeability	Moderate-Low	High	Low

The vesicles that have been developed for drug delivery purposes so far typically are relatively large and require sizing for intravenous administration (Table 1). Polymer vesicles are limited in their size towards smaller diameters below 75 nm, due to the restricted curvature modulus and the development of lipid vesicles for drug delivery of sizes below 75 nm faces challenges as well [39, 49, 113, 135]. Therefore, in order to enhance penetration into inflammatory and tumorigenic tissues, the development of stable and biocompatible vesicles of a size smaller than 50 nm may be of benefit for the delivery of both hydrophobic and hydrophilic drugs to the diseased tissues.

1.5 Aim

The aim of this thesis was to develop nanovesicles by molecular self-assembly of oligopeptides and to obtain insight into the intermolecular interactions that govern the self-organization of the oligopeptides. Furthermore, the potential of such oligopeptide vesicles as a drug carrier is investigated.

1.6 Outline

Chapter 2 reports the design, production and characterization of amphiphilic oligopeptides. First, the recombinant production of the oligopeptides is described and subsequently the reversible assembly of the peptides into nano-sized vesicles is demonstrated. The entrapment of hydrophilic low molecular weight molecules was feasible using calcein as a small hydrophilic model molecule.

In **Chapter 3** multiple cysteines are introduced in the hydrophobic domain of the self-assembling amphiphilic oligopeptides. As was shown using dynamic light scattering analysis in different solvents, after oxidation intermolecularly crosslinked vesicles were obtained. Dynamic light scattering, electron microscopy and atomic force microscopy were applied to gain further insight into the size distribution of the oligopeptide vesicles.

Chapter 4 describes the secondary conformation of the vesicle-forming amphiphilic oligopeptides. By both circular dichroism and Fourier transform

infrared spectroscopy it is demonstrated that the oligopeptides adopt the polyproline type II as their dominant conformation. It is further demonstrated that this peptide conformation is a critical factor in the assembly of the oligopeptides into nanovesicles.

Knowing the intramolecular order of the oligopeptides, subsequently the intermolecular peptide organization was studied in **Chapter 5**. The vesicular assemblies are driven by the formation of a hydrophobic domain, as was demonstrated with fluorescence spectroscopy. In addition to hydrophobic interactions, both experimental and computational techniques demonstrated that also hydrogen bonds within the hydrophobic domains of the assemblies stabilize the oligopeptide vesicles. Either direct intermolecular hydrogen bonds are formed within the hydrophobic domain, or peptide backbones are stably bridged by single hydrogen-bonded water molecules.

Chapter 6 investigates the potential use of the oligopeptide nanovesicles for drug delivery applications. The (route of) cellular internalization of the peptide vesicles was revealed by flow cytometry and fluorescence microscopy. Poorly-water soluble phthalocyanines could be entrapped in the peptide vesicles. Using the peptide vesicles as a carrier for the intracellular delivery of the hydrophobic drugs resulted in a phototoxic response towards cells.

Chapter 7 is a brief summary of the thesis and future perspectives of self-assembling oligopeptides for drug delivery applications are outlined, with a special focus on the optimization of peptide vesicle characteristics.

Chapter 2

Self-assembly of recombinant amphiphilic oligopeptides into vesicles

Albert J van Hell

Cristina Costa

Frits M Flesch

Marc Sutter*

Wim Jiskoot*

Daan JA Crommelin

Wim E Hennink

Enrico Mastrobattista

Department of Pharmaceutics, Utrecht Institute for Pharmaceutical Sciences (UIPS), Utrecht University, The Netherlands

*Division of Drug Delivery Technology, Leiden / Amsterdam Center for Drug Research (LACDR), Leiden University, The Netherlands

Published in Biomacromolecules

Abstract

The aim of the present study was to design amphiphilic oligopeptides that can self-assemble into vesicular structures. The ratio hydrophilic to hydrophobic block length was varied and peptides were designed to have a hydrophobic tail in which the bulkiness of the amino acid side groups increases towards the hydrophilic domain (Ac-Ala-Ala-Val-Val-Leu-Leu-Leu-Trp-$Glu_{2/7}$-COOH). These peptides were recombinantly produced in bacteria as an alternative to solid-phase synthesis. We demonstrate with different complementary techniques (dynamic and static light scattering, tryptophan fluorescence anisotropy and electron microscopy), that these amphiphilic peptides spontaneously form vesicles with a radius of approximately 60 nm and a low polydispersity when dispersed in aqueous solution at neutral pH. Morphology and size of the vesicles were relatively insensitive to the variations in hydrophilic block length. Exposure to acidic pH resulted in formation of visible aggregates, which could be fully reversed to vesicles upon pH neutralization. In addition, it was demonstrated that water-soluble molecules can be entrapped inside these peptide vesicles. Such peptide vesicles may find applications as biodegradable drug delivery systems with a pH dependent release profile.

Introduction

The self-assembly of biomolecules has gained increasing attention as a means to design novel biomaterials from biomolecular building blocks (e.g. DNA, proteins and peptides) [24, 136]. A variety of supramolecular structures have been formed with self-assembling peptides, such as macroscopic hydrogels [45, 53, 79], fibers [137], β-sheeted tapes [78], polypeptide vesicles [39, 138] and nanotubes [37, 47]. The biocompatability of peptide assemblies is underscored by their successful utilization in various biological and medical applications, like stem cell differentiation, tissue engineering, *in vivo* nerve regeneration and as scaffolds to deposit hydroxyapatite minerals as a mimic for extracellular bone matrix [33, 57, 59, 139, 140].

Zhang et al showed that small amphiphilic oligopeptides self-assembled into nanotubes [37, 47, 48, 141]. They proposed a model of assembly in which the peptides stick together tail-to-tail, forming a bilayer similar to lipids in aqueous environment [37, 48]. These peptides were found to predominantly assemble into open-ended tubes. A vesicular architecture, however, might be useful in a variety of applications, e.g. to encapsulate and deliver pharmaceutically active compounds, like low molecular weight drugs as well as biotherapeutics (protein, siRNA and pDNA) [111, 142].

Extensive research about the self-assembling behavior of amphiphiles has provided valuable information about critical parameters determining the final assembled architecture. The surface area occupied by a monomer, relative to the length of the hydrophobic block determines the packaging shape of a monomer within a supramolecular assembly [112]. A slightly increased surface area is favorable for the formation of vesicles, when compared to the formation of planar bilayers [49, 143]. Besides the size and charge of the hydrophilic residues, such a surface area is influenced by the length of the hydrophilic block; an extension of the hydrophilic block favors an increase of occupied surface area per monomer [128, 144]. Therefore, the ratio hydrophobic to hydrophilic block length can be varied, in order to obtain a vesicular architecture [127]. The aim of the current study was develop amphiphilic oligopeptides that self-assemble into vesicles in aqueous environment. Two peptides were designed to be amphipatic, negatively charged at neutral pH and to occupy a relatively large interfacial surface area.

These self-assembling (SA) peptides were recombinantly produced in bacteria as an alternative to solid-phase synthesis; a production route that might be advantageous e.g. for large scale production [145]. After purification and N-terminal acetylation, these peptides were characterized for their self-assembling behavior by fluorescence spectroscopy, electron microscopy and dynamic and static light scattering.

Results

Peptide design

SA2 and SA7 peptides were designed to be amphipathic, containing glutamic acid residues as the hydrophilic domain (Figure 1) that, due to their side chain size and electrostatic repulsion, will occupy a relatively large interfacial area. A relative increase in hydrophilic block length also may enlarge the surface area [128]. Therefore, the mass fraction of the hydrophilic block was varied from 25% (SA2) to 50% (SA7) of total peptide mass, while keeping the length of hydrophobic domain unchanged. In the hydrophobic domain of the SA peptides a conical shape was introduced by using hydrophobic amino acids with decreasing bulkiness of the side chains towards the N-terminus (Figure 1). Tryptophans suit well on a polar-apolar interphase, due to the polarity of the amide group present in the further hydrophobic indole side chain [146]. The N-terminus of the peptide was acetylated to prevent undesired charge interactions with the negatively charged glutamic acid residues and to increase hydrophobicity [147].

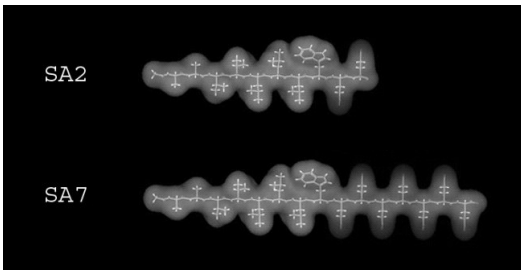

Figure 1. Space filling molecular models of stretched SA peptides, with amino acid sequence Ac-Ala-Ala-Val-Val-Leu-Leu-Leu-Trp-$Glu_{2\text{-}7}$-COOH.

Recombinant production and purification of amphiphilic peptides

The amphiphilic oligopeptides SA2 and SA7 were recombinantly produced as a cost-effective alternative to solid phase synthesis. To prevent degradation or toxicity of the unfolded, amphiphilic peptides in bacteria, SUMO protein was used as a fusion protein that has been reported to increase solubility and yield of recombinant proteins [68, 148, 149]. DNA constructs, encoding the different SA peptides (Figure 1), were cloned into the pET-SUMO vector in frame with and downstream of the SUMO gene. The resulting gene constructs were expressed in

E. coli strain BL21(DE3). The SUMO fusion protein contained an N-terminal hexahistidine tag which allowed purification by IMAC. The SA peptide was cleaved from the C-terminus of the SUMO protein by SUMO protease, which cleaves by recognizing the three dimensional structure of the SUMO protein, rather than a specific amino acid (sequence), yielding SA peptides without any undesired amino acids on their N-termini [149].

A typical example of SA peptide production in *E. coli* is shown in Figure 2. Total protein content of the BL21(DE3) bacteria expressing SUMO-SA2 fusion proteins was analyzed on a SDS-PAGE gel, before and after induction of recombinant protein expression with IPTG (Fig. 2A). In the IPTG treated sample, a protein band with an apparent molecular weight of ca. 17 kDa appeared, which is close to the theoretical mass of the fusion protein (13 kDa). After 3 hrs of induction by IPTG, ~40% of the soluble fraction of bacterial proteins consisted of the SUMO-peptide (SUMO-SA2) fusion protein (Fig. 2A, third lane). One-step IMAC was performed to purify the fusion protein from the soluble fraction of the bacterial lysate (Fig. 2A, fourth lane). From the purified fusion protein imidazole was removed by desalting and the protein was incubated with SUMO protease to release the SA peptide. Cleavage is clearly visualized by monitoring the release of protein (UV_{280}) from a Superdex peptide column (Fig. 2B) (void volume peak no. 1, optimal separation range 1-15 kDa) before (dashed line) and after cleavage by SUMO protease (dotted line).

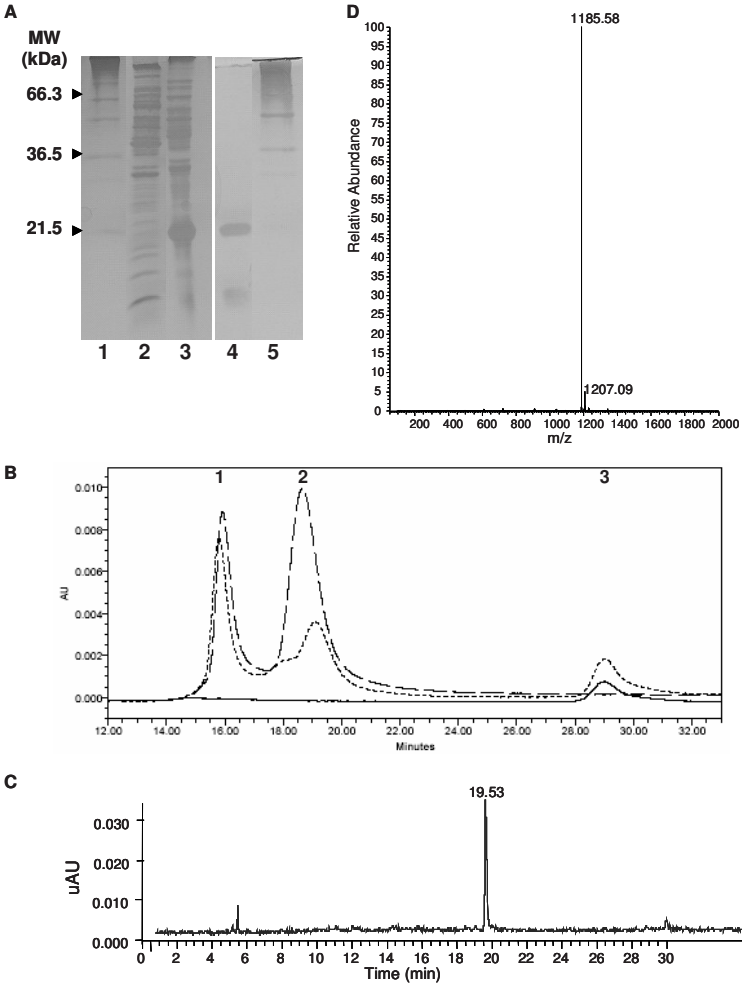

Figure 2. Recombinant production of SA2 oligopeptide in *E. coli* BL21(DE3). A. Expression and subsequent purification of SUMO-SA2 peptide fusion protein, analyzed on a 15% SDS-PAGE and visualized by silver staining. Lanes 1 and 5: Mark12 protein standard (Invitrogen); Lane 2: Total bacterial protein, uninduced; Lane 3: Total bacterial protein, IPTG induced; Lane 4: IMAC purified SA2-SUMO fusion protein. B. Enzymatic release of the SA2 peptide from the SUMO fusion protein using SUMO protease, analyzed by size exclusion chromatography (Superdex Peptide 10/300 GL column monitored at UV_{280}). SUMO fusion protein (peak 2) before (dashed line) and after (dotted line) incubation with SUMO protease. The cleaved peptide (peak 3) was purified by removing co-purified proteins (peak 1), the SUMO fusion protein and the SUMO protease, both bearing hexahistidine tags, with IMAC (solid line). C. HPLC analysis on the purified and acetylated SA peptide, monitored at UV_{280}. D. ESI-MS mass spectrum of the 19.53 min. peak in C (19.47-19.84 min, expected mass 1183.65).

After cleavage a low molecular weight peak appeared (no. 3) that corresponded with the SA2 peptide as was revealed by MS analysis. The cleavage efficiency depended on incubation time and temperature. After 6 hours incubation at ambient temperature cleavage was complete. In the void volume of the column (peak 1) some co-purified bacterial proteins and aggregated fusion proteins came off. However, by applying the mixture of cleaved SA peptide on a Ni-NTA column the co-purified proteins, the His-tagged SUMO protease and the SUMO fusion protein could be removed and yielded the SA peptides (solid line, Fig. 2B). Subsequently, the purified SA peptide was acetylated on its N-terminus and analyzed with ESI-MS (Fig. 2C). The observed mass of N-acetyl-SA2 was 1184.58, which is in good agreement with the expected mass of 1183.65. Non-acetylated peptide was neither detected by ESI-MS nor by the free amine sensitive 2, 4, 6-trinitrobenzene sulfonic acid assay. SA7 peptide was produced in the same way. Typically, from a batch of 25 gram bacteria (dry cell weight) 300 mg purified fusion protein was obtained, which yielded 30 mg of acetylated SA2 peptide.

Determination of the critical aggregation concentration

After purification and subsequent acetylation of their N-termini, the SA peptides were studied for their self-assembling behavior in aqueous solution. To investigate the CAC of the peptide assemblies, tryptophan fluorescence anisotropy was used. Steady-state anisotropy is a measure for the rotational motion of fluorophores [150]. At the critical aggregation concentration (CAC), the average rotational rate of the peptide molecules and of their intrinsic tryptophan residues will decrease abruptly, because of formation of peptide assemblies. This will manifest itself as a sudden increase of intrinsic tryptophan anisotropy [151].

As can be seen in Figure 3 A and B, both peptide dispersions displayed a sharp rise of anisotropy with increasing peptide concentration. This allowed determination of the CAC, which is defined at the intersection of a linear fit through the points at low anisotropy values and a linear fit through the points describing a steep anisotropy increase. The CAC determined in this way was found to be 4.9×10^{-7} M for SA2, whereas the CAC of SA7 was 1.6×10^{-5} M. Measurements with a SA5 peptide, containing an identical hydrophobic block as SA2 and SA7 and 5 glutamic acids residues, gave a CAC of 1.3×10^{-6} M (data not

shown). This confirms that there is a trend for increasing CAC with increasing length of the hydrophilic block of the peptide. At higher concentrations, a plateau value of maximal anisotropy was reached of around 0.23 for SA2 and 0.19 for SA7.

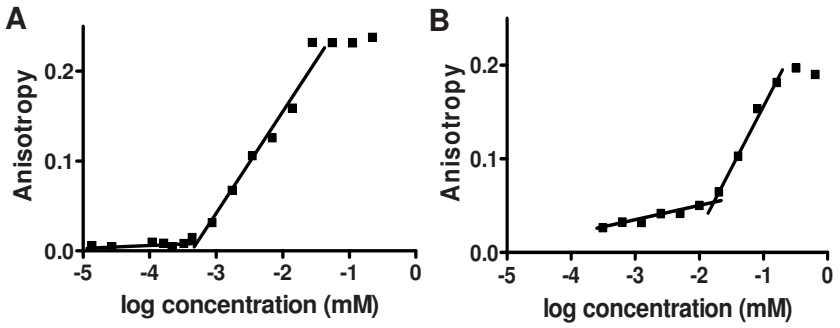

Figure 3. Tryptophan steady-state anisotropy as a function of SA2 (A) and SA7 (B) peptide concentration. CAC was determined at the intersection of the two linear fits in A (SA2, 4.9 x 10^{-7} M) and B (SA7, 1.6 x 10^{-5} M).

Morphology of the peptide self-assemblies

Transmission electron microscopy was used to elucidate the morphology of the SA2 and SA7 peptide assemblies (Fig. 4). The use of the quick-freeze technique with subsequent transmission electron microscopy (TEM) provides an impression of the particles in solution and avoids potential artifacts induced by staining of the sample. As can be seen in Figure 4, the assemblies were situated apart, some seemed attached or even fused to each other (see arrow in 4D). All assemblies appeared as spherical particles and neither tubes nor fibrils were observed. The morphology of the particles was insensitive to increased hydrophilic block length, since for SA2 (Fig. 4A, C) and SA7 (Fig. 4B) only spherical particles of comparable sizes were observed. Peptide particles were also visualized with Atomic Force Microscopy (AFM) by immobilization of the particles on ornithine-modified silica matrix, giving similar morphologies and size distributions as seen with TEM (data not shown). The spherically assembled peptide structures displayed a relatively soft nature, since minor forces were needed to destroy the peptide assemblies by the AFM cantilever.

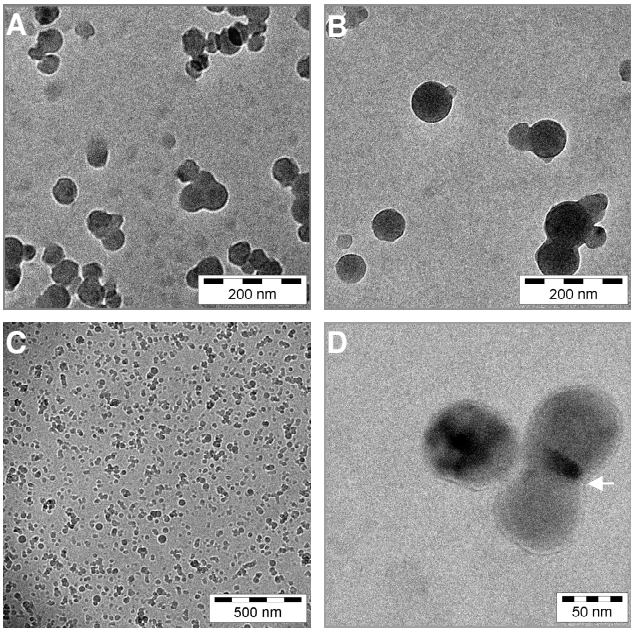

Figure 4. Transmission electron microscopy of peptide self-assemblies. Both for the SA2 (A) and SA7 (B) spherical assemblies were observed. The spheres are abundantly present in solution (C, overview of SA2 assemblies). Some assemblies lie overlaid, attached (A, D) or even fused (D, arrow).

Dynamic and static light scattering and zeta potential measurements

The SA2 and SA7 assemblies were analyzed by dynamic light scattering (DLS) to obtain the hydrodynamic radius (R_h) of the assemblies (Table 1). The radii found (63 nm for SA2 and 59 nm for SA7) correspond with the largest particles observed in TEM micrographs (Fig. 4). The particles sizes were stable over time (> three months, 4°C) and at physiological conditions (150 mM sodium chloride, 10 mM sodium phosphate, pH 7.4). The polydispersity index (PD) of the self-assemblies was ca. 0.2, which indicates little heterogeneity of particle size, as was also observed by TEM.

Static light scattering provides information about the radius of gyration (R_g) and the molecular weight of the particles. Results of static light scattering (SLS) data analysis are shown in Table 1. The ρ-parameter (R_g/R_h), sheds light onto the density distribution of the particles and thereby on particle morphology.[152] In case of uniform spheres, $R_g = (3/5)^{1/2}R_h$, so that $\rho = (3/5)^{1/2} = 0.775$; for hollow spheres

(vesicles), assuming an infinitely thin wall, $R_g = R_h$, so that ρ = 1.0 [152-155]. The R_g values of the SA particles coincided with the R_h values, resulting in ρ values of around 1 (Table 1). SLS data furthermore revealed the molecular weight of the particles and division by the molecular weight of the monomer resulted in the number of peptides per particle (Table 1). The aggregation number allowed the calculation of the surface area per monomer, assuming an equal distribution of peptides over the inner and outer side of a peptide bilayer [48]. As can be seen in Table 1, the SA7 peptides containing a longer charged hydrophilic domain, occupied a larger surface area within the assembly, when compared to SA2 peptides. Furthermore, these assemblies with the larger surface area per peptide also displayed a less negative zeta potential.

Table 1. Macromolecular properties of the peptide assemblies

	Zeta potenti	R_h[a] (nm)	Polydispersity Index	R_g[b] (nm)	ρ paramete	Particle molecular	Aggregation number
SA2	-48 (±1)	63 (±1)	0.21	66 (±2)	1.04 (±0.03)	3.0 (±0.1) x10^7	2.5 (±0.1) x10^4
SA7	-26 (±1)	59 (±3)	0.24	54 (±1)	0.92 (±0.06)	1.8 (±0.1) x10^7	9.8 (±0.2) x10^3

[a] hydrodynamic radius; [b] radius of gyration

pH dependency of the self-assembled structures

The stability of the SA peptide vesicles was studied as a function of pH by DLS measurements. As can be seen in Figure 5, the peptide assemblies were stable above pH 5.0 as no change in particle size (distribution) was observed. Lowering the pH to 4.0 resulted in the formation of aggregates, as indicated by a dramatic increase in particle size and PD (Fig. 5A, C). These aggregates were clearly visible by the naked eye. Reversing the pH to neutral values (Fig. 5B, D) elicited the formation of self-assemblies of a size and polydispersity similar to values before acidification. Interestingly, hysteresis was observed when reversing the pH values. Whereas destabilization took place around pH 4, re-assembly only occurred at pH values ≥ 7 (Fig. 5B, D). The vanishing aggregates and appearing assemblies in the re-assembly process can also be seen in the DLS size

distribution graphs (Fig. 5E). At pH 5, large particles were present (1 µm peak), that diminished at pH 6 and were completely gone at pH 7. The size distribution graph after acidification is similar to the initial particle size distribution (Fig. 5E).

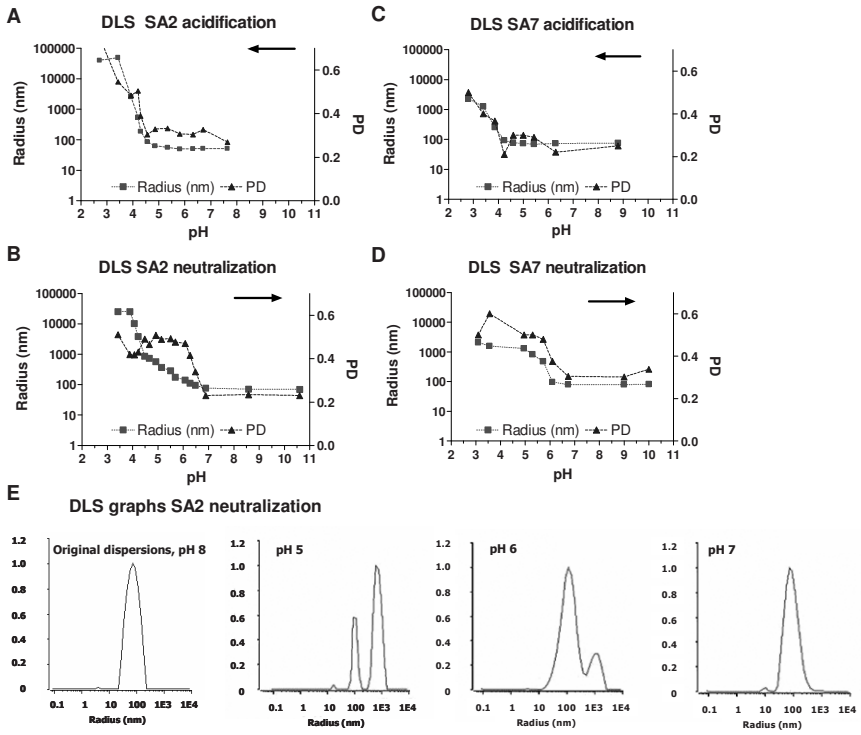

Figure 5. Effect of pH on the size of the SA peptide assemblies, as monitored by DLS measurements. Aggregation of the SA2 and SA7 peptides occurs below pH values of 4.0. The destabilization process is reversed by neutralization of the pH values, displaying hysteresis and restoring size and polydispersity (PD) to initial values. The process is further visualized by DLS size distribution graphs of SA2 peptides (E).

Calcein encapsulation

A vesicular nature of the peptide assemblies would allow entrapment of hydrophilic molecules in the interior of the assemblies. To test this, the SA2 assemblies (0.2 mg/ml) were prepared either in presence or absence of the fluorescent marker calcein. By using Sephadex G50 size exclusion spin columns the calcein-vesicle fraction can be rapidly separated from free calcein with only minor dilution of the vesicle dispersion, which could potentially destabilize the vesicles [156]. As a positive control for calcein encapsulation, negatively charged

unilamellar egg phosphatidylglycerol (EPG) liposomes with comparable size and light scattering intensities as the SA-peptide vesicles were used. The eluted fractions were collected and analyzed for calcein fluorescence. As can be seen for the liposomes containing calcein, the first two fractions represented encapsulated calcein (void volume), whereas free calcein started eluting from fraction 4 onward (Fig. 6A). SA2 assemblies, prepared in the presence of 4 mM calcein, showed high calcein fluorescence in the first two fractions. Calcein fluorescence decreased in the third fraction and increased again in next fractions, a trend that confirms the presence of two different calcein populations. In contrast, when calcein was added to peptides after assembly, spin column separation shows minimal calcein fluorescence in the void volume, comparable to the elution profile of free calcein. At similar light scattering intensity, the degree of calcein encapsulation is 2.5 times lower when compared to negatively charged EPG liposomes (Fig. 6A). The degree of calcein entrapment linearly increased with SA peptide concentration (Fig. 6B).

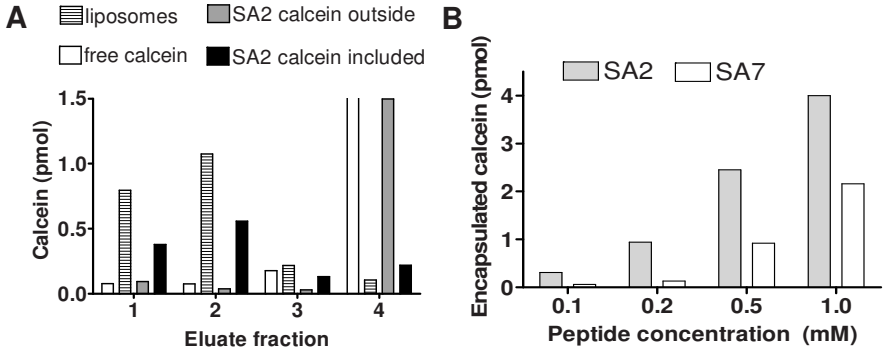

Figure 6. Calcein incorporation in SA2 peptide assemblies. A. Free calcein elutes in fraction 5 and onwards, whereas liposomes come off the column in the first two fractions (void volume). SA2 peptide was dispersed in presence of calcein, prior to spin column separation (0.2 mM SA2 peptide, 4.0 mM calcein). As a negative control calcein was added to SA2 assemblies after preparation. B. At increasing concentrations of peptide, assemblies were prepared in presence of a constant calcein concentration.

Discussion

In this study, amphiphilic oligopeptides were recombinantly produced in bacteria and assessed for their self-assembling behavior. Recombinant production represents a cost-effective alternative to solid-phase synthesis, as it does not require expensive chemicals and can be easily scaled up to gram-quantities. However, recombinant production of small amphiphilic peptides may induce toxicity to the host cells. This toxicity problem was circumvented by using a fusion partner that increases the overall hydrophilicity of the recombinant polypeptide to be produced [65]. Removal of the peptide from its SUMO fusion partner by SUMO protease was specific and yielded peptides without undesired N-terminal amino acids. Furthermore, the method used for purification of the SA peptides is, in principle, independent of the size, polarity and charge of the peptide and thus does not require setting up elaborate purification schemes for each peptide when different peptides have to be produced. Recombinant production may also provide means for the extension of peptide lengths towards longer (heteropolymeric) polypeptides.

The use of the intrinsic tryptophan fluorescence of the peptides for CAC determination avoids the need for an external fluorophore, which might interfere with the self-assembling behavior. An increasing CAC with increasing hydrophilic block length was observed, and this trend was confirmed by the CAC value of a peptide containing 5 glutamic acids. Such an effect has also been observed for other small amphiphilic peptides [157]. The maximal anisotropy value of any fluorophore in isotropic solution is 0.4, in case of minimal rotational movement; for tryptophans this value is near 0.3 [150]. The SA2 peptide assemblies, however, display a maximal anisotropy of 0.23 and for SA7 assemblies, this value was around 0.19, both clearly below the maximum tryptophan anisotropy. Local rotational motions of tryptophan residues within the assemblies are possibly responsible for this difference.

The polydispersity index of the peptide assemblies derived from dynamic light scattering indicated the formation of an ordered structure. This was confirmed by TEM investigations, which revealed highly organized, spherical structures. The particles are formed spontaneously by resuspension of the acid precipitated

peptides and no sizing is required to obtain such a relatively monodisperse size distribution. Further studies by SLS confirmed the vesicular nature of the spherical assemblies. The calculated ρ values indicated the specific density distribution at the particle edge that is characteristic for a vesicle. Assuming a peptide bilayer, as was proposed by Vauthey for similar amphiphilic peptides [37], the surface area occupied by the peptides (4.0 nm^2 for SA2 and 8.9 nm^2 for SA7) are in good agreement with values found for other vesicles [127, 158]. An increased length of the hydrophilic block indeed resulted in a larger surface area per monomer, as has been suggested before [128, 143]. However, the increased hydrophilic mass fraction had no influence on the size and shape of the vesicles.

Furthermore, the vesicular nature of the assemblies was confirmed by the ability to entrap calcein, a small water soluble fluorescent molecule, inside these peptide vesicles. The quantity of entrapped calcein was positively correlated with the peptide concentration used and was not due to diffusion of calcein into the spherical assemblies, as the addition of equal concentrations of calcein to the peptide vesicles after rehydration yielded much lower calcein fluorescence levels associated with the peptide vesicles (Fig. 6). The SA2 vesicles entrapped somewhat higher amount of calcein. These peptides display a lower CAC than SA7 peptides (Fig. 3), and the SA2 peptides within assembly might be packed denser, resulting in an increased ability to entrap water soluble compounds. Such a difference in packaging density of SA peptides is supported by the SLS data, which show a larger surface area per monomer for SA7, and by the maximal SA7 anisotropy value, which indicates an increased movement for the SA7 peptides. The quantity of encapsulated calcein in SA2 vesicles is 2.5 times lower compared to the amount entrapped in negatively charged phospholipid vesicles of similar size and comparable scattering intensity. This difference may be related to the preparation methods of these two types of vesicles (lipid-film hydration vs. precipitate dispersion) or to the amount of vesicles present, since scattering intensity is not only dependent on particle concentration, but also on refractive index of the particles, which may differ for liposomes compared to peptide vesicles.

Interestingly, the self-assembly behavior of the SA peptides presented here are different from other amphiphilic oligopeptides described, like G_8D_2 or A_6D that predominantly form branched nanotubes [37, 47]. It might well be that differences in molecular geometry cause differences in the self-assembly of the SA peptides [49, 159]. A truncated cone has been proposed as the optimal packaging shape of the monomers in vesicle-forming amphiphiles [49, 112]. Such a geometry is influenced by the length of the hydrophobic domain of the amphiphile in relation to the size of the interfacial surface area of the monomer within the assembly [128, 159], which is larger for the SA peptides compared to e.g. G_8D_2 or A_6D, due to the larger glutamic acid side chain. Furthermore, the geometry of the peptide monomers also favors a conical shape as the hydrophobic amino acids increase in size towards the hydrophilic domain.

The spontaneous nature of the self-assembly of peptides into vesicular structures is illustrated by their pH dependency. As studied by DLS measurements, the peptide vesicles aggregate below the pKa of the side chain carboxyl group of glutamic acid (4.3). It could not be determined whether this aggregation caused disruption of the vesicular assemblies. However, the assembly can be restored by re-adjusting the pH to neutral or basic values. The observed hysteresis upon pH neutralization might be caused by the shielding of peptides from the environment within the large aggregates, which may hinder deprotonation. Nevertheless, the experiments show that assembly and disassembly of the SA peptide vesicles can be controlled by changing the pH of the surrounding medium, which may be useful for drug delivery applications.

According to the DLVO theory, the higher Coulombic repulsions between the particles, the more stable the colloids are [49, 160]. The SA2 assemblies display a more negative zeta potential compared to SA7 assemblies (Table 1), which might favor the long-term stability. Also, the SA2 displayed a lower CAC, which is favorable for *in vivo* applications. Even further decrease of CAC might be established by modification or extension of the hydrophobic block, or by enhancement of secondary structure formation [161].

Conclusion

In conclusion, a versatile method to recombinantly produce amphiphilic peptides in bacteria was developed. It was demonstrated that these SA peptides assemble spontaneously into nanosized vesicles above their critical aggregation concentration at neutral or basic pH. Furthermore, the study elucidates the characteristic of fully reversible assembling process of these peptides when brought into acidic solution. Interestingly, hydrophilic compounds could be encapsulated within the peptide vesicles and may therefore be useful as drug delivery systems, exhibiting a pH dependent release profile.

Materials and Methods

DNA design and construction

Oligo DNA 5' GCGGCGGTGGTGCTGCTGCTGTGGGAAGAA(G/T)AA(G/T)AA(G/T)AA TGATAGACTCGGATCC 3' and 5' GCGGCGGTGGTGCTGCTGCTGTGGGAAGAAGAAGAA(G/T)AA(G/T)AA(G/T) AATGATAGACTCGGATCC 3' were made double stranded by annealing 5' TTCGGATCCGAGTCTA 3' oligo DNA and strand extension by incubation at 65 °C with Taq polymerase (Fermentas, Burlington, Canada), generating adenine overhangs. The double stranded DNA was directly ligated in pET SUMO plasmid (Invitrogen, Carlsbad, USA) by TA cloning and the constructs were transformed into *Escherichia coli* (*E. coli*) strain Mach1 T1 competent cells (Invitrogen, Carlsbad, USA) for colony screening. Correct insertion of oligo DNA was confirmed by DNA sequencing.

Protein and peptide biosynthesis and purification

The *E. coli* strain BL21(DE3) (Invitrogen Carlsbad, USA) was transformed with the constructed DNA plasmids to express the SUMO-SA fusion proteins. Five liters of Luria-Bertani (LB) medium, supplemented with 10 µg/ml kanamycin and trace metal solution [67], was inoculated with a 100 ml overnight shaking-flask bacterial culture. Bacteria were grown in a Labfors 3 fermentor (Infors HT, Bottmingen, Switzerland), with air flow, pH (7.0), and temperature (37°C) control and growth dependent glucose supply. Protein expression was induced by addition of

isopropyl-β-D-thiogalactopyranoside (IPTG) (Fisher Emergo, Landsmeer, Netherlands) to a final concentration of 1.0 mM. Three hours after induction, cells were harvested by centrifugation. Bacterial pellets were resuspended in lysis buffer (150 mM NaCl, 20 mM NaH_2PO_4, 10 mM imidazole, pH 8.0). Lysis was performed by a single cycle of freezing and thawing of the bacteria, 30 minutes incubation with lysozyme (1 mg/ml) at ambient temperature and subsequent sonication on ice, using a Braun Labsonic tip-sonicator (Braun Biotech, Melsungen, Germany). Bacterial lysates were centrifuged (30 minutes, 70 000 x g, 5°C) and supernatant was filtered through a 0.45 µm syringe filter. SUMO-SA fusion proteins were captured from the cleared supernatant using an Akta Purifier equipped with 5 ml His-Trap HP columns (GE Healthcare, Uppsala, Sweden). After capture, columns were washed extensively (25 column volumes 1.1 M NaCl and 25 column volumes 50 mM imidazole) and His-tagged protein was eluted at 400 mM imidazole (150 mM NaCl, 20 mM NaH_2PO_4, 400 mM imidazole, pH 8.0). Elution buffer was exchanged to SUMO protease cleavage buffer (20 mM hepes, 150 mM NaCl, 1.0 mM dithiothreitol (DTT), pH 8.0) using a HiPrep 26/10 desalting column (GE Healthcare, Uppsala, Sweden). To release the peptides 1 unit SUMO protease (Invitrogen, Carlsbad, USA) per ml protein solution was added and incubated at ambient temperature for 6 hours. Cleavage was confirmed by size exclusion chromatography on a Superdex Peptide 10/300 GL column (GE Healthcare, Uppsala, Sweden) at a flow rate of 0.5 ml/min with phosphate buffered saline (pH 7.4) as mobile phase. Column performance was determined with Gel Filtration LMW Calibration kit (GE Healthcare, Uppsala, Sweden). Second immobilized metal affinity chromatography (IMAC) purification was performed with nickel-nitrilotriacetic acid (Ni-NTA) Superflow (Qiagen, Hilden, Germany) to remove both the His-tagged SUMO protease and protein.

Gel electrophoresis

For sodium dodecyl sulfate-polyacrylamide gel electrophoresis (SDS-PAGE), samples were boiled in Laemmli sample buffer (Bio-Rad Laboratories, Hercules, CA, USA) for 5 min and loaded to a 15% acrylamide gel. Electrophoresis was performed at room temperature applying 10 mA per gel until the running front reached the end. The gel was fixed in 50% methanol, 12% acetic acid and bands were visualized by silver staining. Mark12 protein standard (Invitrogen, Carlsbad, USA) was used as a reference.

Peptide acetylation and self-assembly

The N-termini of the peptides were acetylated by incubating the purified peptide in 25% acetic anhydride, 50% methanol, 25% water (volume) for 1 hour at ambient temperature [162]. The extent of acetylation was determined with 2,4,6-trinitrobenzene sulfonic acid assay (Pierce, Rockford, USA), measuring UV_{335} absorbance, according to manufacturer's protocol. Solvents were removed by reduced pressure evaporation and remaining peptides were washed once in H_2O as follows: peptides were rehydrated and subsequently precipitated by acidification. The precipitated peptides were harvested by centrifugation (30 minutes at 17 000 x g). Self-assembly of the peptides was performed by dispersing the precipitated peptide in 1.0 mM NaOH in H_2O while gently shaking (pH > 7.0). Peptide dispersions were centrifuged for 5 min. at 13 000 x g to sediment any dust particles present. Peptide concentration was determined by UV_{280} measurements based on the molar extinction coefficient of the tryptophan residue of 5690 $M^{-1}cm^{-1}$.

HPLC analysis and mass spectrometry

Acetylated peptide was injected onto a Sunfire C18 column (Waters Corporation, Milford, USA). A gradient was run at 1.0 ml/min flow rate from 5% acetonitrile, 0.1% trifluoroacetic acid, 95% water in 30 minutes to 95% acetonitrile, 0.1% trifluoroacetic acid, 5% water, and running an additional 10 minutes as such. UV was monitored at λ= 280 nm. Online electron spray ionization - mass spectrometry (ESI-MS) in positive ion mode was performed on a Finnigan LCQ Deca MAX (Thermo Electron Corporation, Waltham, USA).

Fluorescence anisotropy

To determine the CAC of the peptides, dilution series of peptide (1000 - 0.1 μg/ml) were prepared in 10 mM sodium phosphate (pH 8.0). Tryptophan steady-state fluorescence anisotropy was measured with a Horiba Fluorolog fluorometer (Horiba Jobin Yvon, Longjumeau Cedex, France) using quartz cuvettes (Hellma, Müllheim, Germany). Experiments were performed at 22°C. Samples were excited at 290 nm and emission was recorded at 360 nm. Integration time of 10 seconds was used and the excitation and emission band slits were set at 7 and 10 nm, respectively. The fluorescence intensities I_{VV} and I_{VH} were measured with the polarizers of the instrument in vertical-vertical (VV) and vertical-horizontal

(VH) positions, respectively. The anisotropy (r) was calculated from the measured intensities I_{VV} and I_{VH} using

$r=(I_{VV}-GI_{VH})/(I_{VV}+2GI_{VH})$ (1)

The factor G corrects for differences in sensitivity of the detection system of vertically and horizontally polarized light and was determined with peptide samples at concentrations below CAC by using

$G= I_{HV}/I_{HH}$ (2)

where I_{HV} and I_{HH} are the fluorescence intensities with the polarizers in horizontal-vertical (HV) and horizontal-horizontal (HH) positions, respectively. For each peptide anisotropy was plotted against the peptide concentration.

Cryogenic transmission electron microscopy

Cryogenic transmission electron microscopy (TEM) analysis was performed on 1 and 3 mg/ml peptide dispersions. Quick freezing of the samples was performed using a Vitrobot (FEI Company, Eindhoven, The Netherlands). Samples were applied on glow-discharged 200 mesh grids, covered with Quantifoil holey carbon foil (Micro Tools GmbH, Jena, Germany) and blotted for 0.5 second at 100% relative humidity. Immediately the samples were vitrified by plunging the grid into liquid ethane and subsequently put in dry liquid nitrogen. Grids were introduced in a Tecnai12 transmission electron microscope (Philips, Eindhoven, The Netherlands) using a GATAN 626 cryoholder (Gatan GmbH, München, Germany). Samples were observed at 120 kV with low-dose imaging conditions to avoid melting of the vitrified film. Images were recorded on TemCam-0124 camera (TVIPS GmBH, Gauting, Germany) and processed with AnalySIS software.

Zeta potential and light scattering techniques

Buffers used to dilute the peptide dispersions were filtered through 0.02 µm filters (Whatman, Kent, UK). Static light scattering (SLS) and dynamic light scattering (DLS) measurements were performed in a Malvern ALV CGS-3 goniometer (Malvern Instruments, Malvern, UK) containing a HeNe laser source (λ = 632.8 nm, 22 mW output power). The DLS time-correlation was analyzed by ALV Correlator 3.0 software (ALV, Langen, Germany). For pH dependent DLS measurements 10 mM citrate buffer was used. pH values were adjusted with 1.0 M HCl or 1.0 M NaOH. SLS was performed at angles between 150° and 30° for

four different peptide concentrations (40, 50, 60 and 80 µg/ml). A Guinier plot was constructed [163] using ALVStat 4.31 software (ALV, Langen, Germany) (dn/dc of peptides in hepes buffer: 0.185 ml/g). Zeta potential measurements were performed in 5.0 mM Hepes (pH 8.0) in a dip-in cell on a Zetasizer 2000 (Malvern Instruments, Malvern, UK).

Calcein encapsulation assay

Spin columns containing 250 mg Sephadex G50 (medium bead size; Amersham Bioscience, Uppsala, Sweden) were prepared according to Fry et al [156]. SA2 peptides precipitated by acidification were re-dispersed in the absence or presence of a 4.0 mM calcein solution in hepes buffer (5.0 mM hepes, pH 8.0). Fifty microliters of the peptide dispersion (0.2 mg/ml) were then applied to the spin column and subsequently spun for 3 min at 350 x g in a swing-out rotor and eluent was collected. Consecutive elution steps (applying 50 µl of hepes buffer followed by centrifugation at 350 x g for 3 min) were performed and eluted fractions were collected and analyzed for calcein fluorescence using a Fluorostar Optima microplate reader (BMG Labtech GmbH, Offenburg, Germany) set at 488 nm excitation and 514 nm emission wavelengths. As a reference, EPG liposomes were prepared in hepes buffer containing 4.0 mM calcein by lipid-film hydration and extrusion as described by Olson et al [164]. After extrusion the average size of the EPG liposomes was 45 nm in radius with a PD of 0.17. The liposome sample was adjusted to give a similar light scattering intensity as the peptide dispersion prior to loading 50 µl onto the spin column.

Acknowledgements

We thank Aissa Ramzi and Ed Moret for their valuable contributions and Arjen Scholten, John Kruijtzer and Annemarie Dechense for performing the mass spectrometry analyses. The Electron Microscope Facility of the Department of Biology, Utrecht University is thanked for the use of their microscopes and support and Hans Meeldijk is specially thanked for his comments and assistance.

Chapter 3

Crosslinkable oligopeptide vesicles

Albert J van Hell

Daan JA Crommelin

Wim E Hennink

Enrico Mastrobattista

Department of Pharmaceutics, Utrecht Institute for Pharmaceutical Sciences, Utrecht University, The Netherlands

Submitted

Abstract

Previously, we have shown that amphiphilic oligopeptides (e.g. Ac-Ala-Ala-Val-Val -Leu-Leu-Leu-Trp-Glu-Glu-COOH) spontaneously assemble into peptide vesicles in aqueous environment. In order to improve the stability of such vesicles, in the present study peptides were produced using recombinant techniques containing either two or three cysteines in their hydrophobic domain (Ac-Ala-Cys-Val-Cys-Leu-(Leu/Cys)-Leu-Trp-Glu-Glu-COOH). The peptides were assessed for their self-assembling behavior. Light scattering, electron and atomic force microscopy as well as encapsulation assays showed that the peptides spontaneously assemble into nano-sized vesicles of 15-20 nm in mean particle radius, which enclose aqueous compartments. Hydrophilic molecules could be encapsulated and released slowly over time. Importantly, crosslinking of the supramolecular structure by disulfide bond formation rendered the assemblies resistant to disruptive environments, such as exposure to high concentrations of dimethyl formamide (DMF) and did not the affect the supramolecular structure. Such small and crosslinkable oligopeptide vesicles hold promise for, e.g. drug delivery applications.

Introduction

Self-assembly of peptides can result in a whole array of different supramolecular morphologies [10, 45, 59, 79, 142, 165]. Long polypeptides as well as oligopeptides have been exploited to develop new (bio)materials. Several of these (bio)materials exhibit unique and useful macromolecular characteristics [24, 46, 78]. Recently, we have shown that amphiphilic oligopeptides (e.g. Ac-Ala-Ala-Val-Val-Leu-Leu-Leu-Trp-Glu-Glu) assemble into nanosized vesicles in aqueous environment (Chapter 2). These peptides display a 'lipid-like' design, containing charged amino acids as the hydrophilic domain, whereas a stretch of up to 8 hydrophobic amino acids functions as the hydrophobic domain [24]. Similar surfactant-like peptides, with a different primary sequence (e.g. Ac-Gly_8-Asp_2, Ac-Val_6-Asp) formed open-ended tubes [37, 47].

The individual intermolecular interactions, like hydrophobic interactions, van der Waals forces, and hydrogen bonding that may stabilize the supramolecular structure in peptide self-assemblies, are relatively weak. Indeed, it was found for both the tubular and the vesicular assemblies that they exhibit a dynamic character [37, 50]. The assembly exists in equilibrium with oligopeptides in free form and the amphiphilic oligopeptides display a critical aggregation concentration (CAC). For example, the CAC for the vesicle-forming SA2 peptides is around 0.5 μM [50, 157]. As a consequence, the supramolecular peptide assemblies destabilize upon dilution. For certain applications of these peptide vesicles, e.g. for use as drug delivery systems, a more stable structure is favorable, because injection into the bloodstream or tissue may rapidly destabilize the peptide assemblies. Hence, in this study we aimed for stabilization of the oligopeptide vesicles after self-assembly by introducing intermolecular disulfide bonds in the peptides.

Results and Discussion

Peptide design and production

Amphiphilic peptides that were previously shown to assemble into vesicles were used as the basic motif to develop crosslinkable peptide vesicles. The hydrophobic domain of the peptide exhibits a conical shape, in which the amino acid side groups decrease in size from the interface along its hydrophobic chain (Table 1) [50]. Considering that thiols can function as an elegant and reversible route to stabilize the peptide assemblies [166], two (SA2C2) or three (SA2C3) cysteines were introduced in the hydrophobic domain (Table 1). The cysteine-containing peptides fused to the small-ubiquitin modifying protein (SUMO) were recombinantly produced in *E. coli* as previously described [50]. SDS-PAGE (Fig. 1) showed that the purified SUMO-SA2C2 and SUMO-SA2C3 fusion proteins appeared around 17 kDa. Although the expected mass of the fusion proteins (15 kDa) is lower, the SUMO protein is known to run at a somewhat higher apparent molecular weight on SDS-PAGE [149]. The SUMO protease specifically cleaves SUMO protein by means of recognition of the folded SUMO protein [149]. In lanes 4 and 5 (Fig. 1A) an intermediate of the cleavage process (1 hour incubation at 30°C) was analyzed on the gel and the two different proteins are visible: the upper band corresponds to the SUMO-peptide fusion protein and the lower band to the cleaved SUMO protein. Because of the small size of the released peptide

(MW 1.2 kDa), the monomeric peptide is not visible on gel under the tested conditions. SDS-PAGE showed that almost quantitative cleavage (> 95%) was achieved by prolongation of the incubation time to 4 hours at 30°C. Since the SUMO-peptide fusion protein contains two (SUMO-SA2C2) or three (SUMO-SA2C3) thiols, protein dimerization was also investigated using SDS-PAGE under non-reducing conditions. As can be seen in Figure 1B, the non-cleaved fusion proteins in lane 3 (SUMO-SA2C2) and 5 (SUMO-SA2C3) revealed the presence of protein dimers, whereas after cleavage (Fig. 1B, lane 2 and 4) dimerization of SUMO was not observed. This is expected since the SUMO protein itself does not contain cysteines.

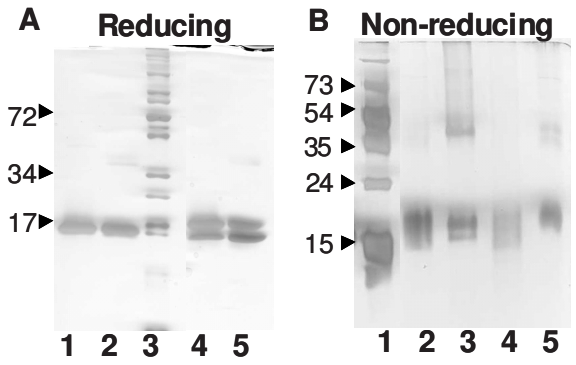

Figure 1. SDS-PAGE analysis on the purified fusion proteins. Reducing conditions (A): lane 1 SUMO-SA2C2, lane 2 SUMO-SA2C3, lane 3 molecular weight markers, lane 4 SUMO-SA2C2 partially cleaved, lane 5 SA2C3 partially cleaved. Non-reducing conditions (B): lane 1 the molecular weight marker, lane 2 SUMO-SA2C2 cleaved and not cleaved (lane 3), lane 4 SUMO-SA2C3 cleaved and not cleaved (lane 5).

Peptide self-assembly and intermolecular crosslinking of the peptide vesicles

Acetylated SA2C2 and SA2C3 peptides were first precipitated at low pH, upon which the pH was elevated by adding an aqueous PB solution of pH 8.0. Dispersion of the peptides occurred spontaneously by elevation of the pH without application of external mechanical input. Upon incubation at RT, a clear solution was obtained within half an hour after addition of the PB and DLS was used to determine the size of the formed peptide assemblies (Table 2).

Table 1. Synthesized peptides

Peptide	Sequence
SA2C2	Ac-Ala-Cys-Val-Cys-Leu-Leu-Leu-Trp-Glu-Glu-COOH
SA2C3	Ac-Ala-Cys-Val-Cys-Leu-Cys-Leu-Trp-Glu-Glu-COOH
SA2 [50]	Ac-Ala-Ala-Val-Val-Leu-Leu-Leu-Trp-Glu-Glu-COOH

Table 2 shows that both peptides assembled into supramolecular structures. The SA2C3 particle radius (75 nm) was in good agreement with the non-crosslinked SA2 peptide assemblies (63 nm); in the case of SA2C2 peptides a somewhat larger mean particle radius (106 nm) was observed. It was investigated whether the assemblies relied on the oxidation of the cysteines by adding DTT to the assemblies. Subsequent DLS analysis showed that the assemblies were stable under reducing conditions and loss of scattering intensity was not observed (Table 2). Moreover, the reducing conditions did not significantly change the mean particle size, indicating that the assembled structures were not affected by the cleavage of the disulfide bonds.

As was established using the Ellman's free thiol assay, by air exposure a final reduction of free thiols to 5% had been achieved, which confirmed disulfide formation in the oxidized peptide assemblies. In order to assess whether this disulfide bond formation indeed stabilized the peptide assemblies, the organic solvent DMF was added to the peptide dispersion to a final concentration of 95% (v/v). This solvent disrupts hydrogen bonds as well as hydrophobic domains and was found a good solvent for hydrophobic or amphiphilic (poly)peptides [44]. When the peptides were reduced with DTT and subsequently injected into DMF, the particle light scattering dropped to background levels instantaneously (Table 2), indicating full disintegration of the assembled structures. In contrast, when the oxidized peptide assemblies were brought into DMF, the scattering intensity remained and was stable over time. DLS analysis on the assembled structures in

DMF indicated a mean particle radius of 50-65 nm. Next to the direct effects of the solvent, noncovalent interparticle interactions may be broken by DMF as well, resulting in the observed lower mean particle radius. In conclusion, the stability of the oxidized peptide assemblies in DMF demonstrated that intermolecular disulfide bonds were formed, which covalently crosslinked the peptide assemblies.

Table 2. DLS analysis of the peptide assemblies with and without disulfide bonds in different solvents

	Solvent	Radius (nm)	Mean count rate (kcps)
SA2Ac	PB	63 (±1)	380
	DMF	-	11
SA2C2Ac, reduced	PB, DTT	102 (±3)	340
	DMF	-	10
SA2C2Ac, oxidized	PB	106 (±2)	185
	DMF	50 (±1)	200
SA2C3Ac, reduced	PB, DTT	69 (±8)	355
	DMF	-	10
SA2C3Ac, oxidized	PB	75 (±5)	280
	DMF	63 (±1)	510

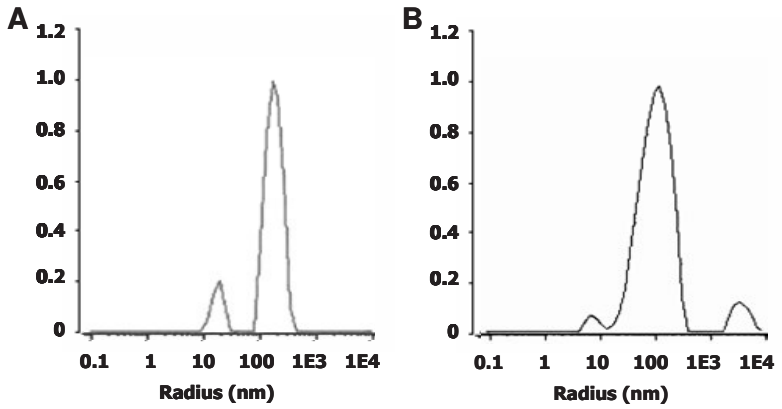

Figure 2. Dynamic light scattering size distribution graphs of the oxidized SA2C2 (A) and SA2C3 (B) peptide assemblies in 10 mM PB of pH 8.0.

The particle size derived from DLS readings was more closely examined. In Figure 2, the particle size distribution of SA2C2 and SA2C3 assemblies was plotted as a function of the scattering intensity. The peptide assemblies displayed a wide distribution of particle sizes. The peak around 100 nm, which was the dominant peak, confirms the mean particle radii of Table 2. Besides the 100 nm particles, light scattering by smaller particles (peak around 10 nm, radius) was detected as well for the oxidized SA2C2 and SA2C3 peptide dispersions (Fig. 2A and B). Since the size distribution graphs are based on the scattering intensity, in number the smaller particles may constitute the major fraction of the peptide structures. In Figure 2B also a 1000 nm peak was observed, which was not present for the SA2C3 dispersion. The 1000 nm peak diminished when the oxidized assemblies were brought in DMF (data not shown), what might indicate some clustering of particles in aqueous environment. The peak around 10 nm (radius) remained in DMF for both peptide assemblies, underscoring the significance of the smaller particles detected.

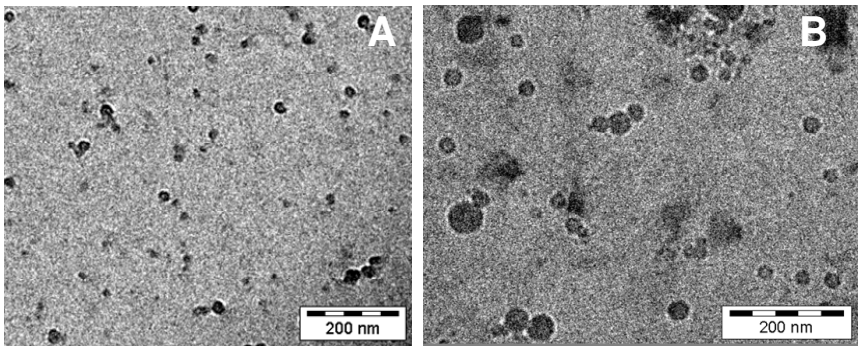

Figure 3. Cryogenic transmission electron microscopy micrographs of the crosslinked SA2C2 (A) and SA2C3 (B) peptide assemblies.

Cryogenic Electron Microscopy analysis of peptide assemblies

Although the peptides formed particles with a radius that would agree with a vesicular architecture [48], other morphologies (tubes from oligopeptides) also have been reported to display comparable hydrodynamic radii in DLS measurements [47]. Therefore, to discern tubes or other aggregated morphologies from spherical particles, and to further investigate the particle sizes, cryogenic transmission electron microscopy (cryoTEM) was performed. The vitrification of the sample in cryoTEM allowed the direct examination of the peptide structures as present in solution. Representative micrographs of the crosslinked peptide assemblies are shown in Figure 3. As can be seen in the micrographs, both SA2C2 and SA2C3 samples (oxidized) showed spherical structures and neither tubes nor fibrils were observed. The size of the particles was examined by measuring the diameter of 85 particles on average at random tracks. Table 3 shows that the mean particle radii for both the SA2C2 and SA2C3 assemblies was < 20 nm, which is substantially smaller than the size detected by DLS (75 nm or larger; Table 2). Some assemblies indeed were clustered, which may in part explain the large sizes detected with DLS (Figure 2).

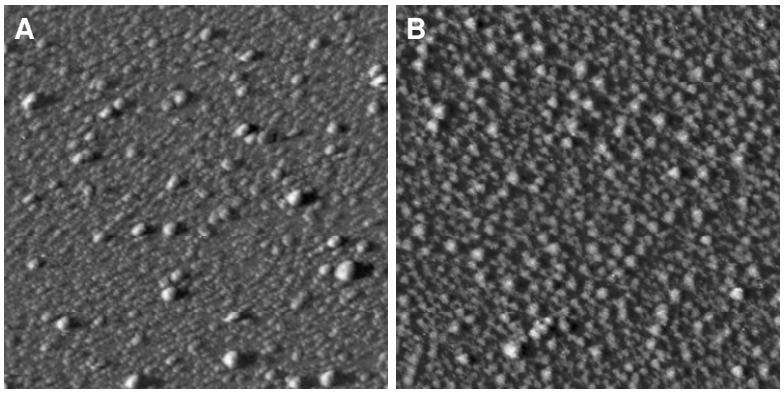

Figure 4. Atomic force microscopy of SA2C2 (A) and SA2C3 (B) crosslinked assemblies immobilized on poly(ornithine) coated mica. The scan size of the images is 1.0 x 1.0 μm and the z-scale is 16 nm.

Atomic Force Microscopy

Atomic Force Microscopy (AFM) was used to provide further evidence regarding the particle morphology and size distribution of the SA2C2 and SA2C3 peptide assemblies. After coating of the mica with polyornithine [50], the negatively charged peptide assemblies were immobilized on the surface and AFM was performed in solution. Figure 4 shows representative AFM micrographs of the crosslinked peptide assemblies. In accordance with the cryoTEM, only spherical particles were observed with AFM. The particle size and size distribution were analyzed using AFM analysis software [167]. As can be seen in Table 3, the particle sizes derived from the AFM measurements are in good agreement with the sizes found by cryoTEM. The mean particle radius from either technique is approximately 20 nm for the SA2C3 assemblies, and 16 nm for the SA2C2, respectively. AFM on the reduced assemblies showed no significant different morphologies or particle sizes, while contrary to non-crosslinked particles, contact with the AFM-tip did not damage the crosslinked assembled structures and instead could move the spheres intact over the mica (results not shown). These findings indicate that the intermolecular disulfide crosslinks indeed preserved the peptide supramolecular structure, making them more resistant to external disruptive forces, and confirm the particle sizes that were found with cryoTEM.

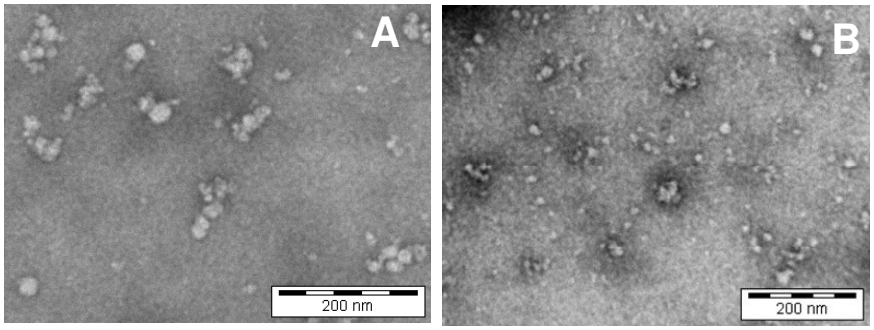

Figure 5. Negative staining transmission electron microscopy micrographs of the crosslinked SA2C2 (A) and SA2C3 (B) peptide assemblies.

Negative staining Electron Microscopy

Due to the blotting performed in the sample preparation, cryoTEM might be slightly biased in disfavor of the larger particles, which are easier removed during blotting [168]. Also with AFM, large particles in a population can be more difficult to detect. Therefore, to exclude biased conclusions based on artifacts in cryoTEM and AFM particle analysis, a complementary imaging technique, namely negative staining transmission electron microscopy (nsTEM) was exploited. As can be seen in Figure 5, imaging of the assemblies by the negative staining was feasible for the crosslinked peptides; this technique remained elusive for non-crosslinked peptides (data not shown). Evidently, the nsTEM technique was harsh, involving staining and dehydration of the sample and the spheres tended to cluster together and some were damaged. Nevertheless, taking into account the individual structures, predominantly spherical particles were observed and no tubes, fibrils nor irregular aggregates were observed (Figure 5). The mean radius of the individual spheres was 10 nm for the SA2C3 and 11 nm for SA2C2 (Table 3). More importantly, throughout the nsTEM investigations, no individual particles or structures larger than observed with cryoTEM and AFM were found (Figure 5, Table 3). The extensive dehydration of the sample in nsTEM may explain the smaller mean particle size observed by nsTEM as compared to the cryoTEM and AFM analysis. The nsTEM showed that the only larger structures that were present, were clusters of smaller (3 – 35 nm, radius) particles and thus confirmed that the particle size distribution observed with AFM and cryoTEM were not biased against a specific subset of large particles.

Microscopy based size distribution

Using the data on particle size obtained with cryoTEM and AFM, a microscopy based size distribution graph was constructed (Figure 6). In agreement with DLS (Fig. 2), the peptide assemblies displayed a wide particle size distribution. The mean particle size as was determined by DLS, the technique that is often used to establish the particle size and size distribution [125, 169], matched the largest particles present in the particle population. This is explained by the fact that this technique is exceptionally sensitive to the larger particles in a population or a cluster of particles (scattering proportional to (radius of hydration)^6) (Fig. 2) [152]. The actual size of the particles is relevant for e.g. drug delivery applications. With respect to *in vivo* biodistribution kinetics, reduction of the particle size typically correlates to an enhanced penetration in diseased tissue, like tumors [14, 102, 170]. Moreover, small particle sizes may facilitate the cellular entry of the drug carriers by endocytic processes [171, 172].

Table 3. Radii of stabilized oligopeptide assemblies based on microscopic analyses

Particle radius (nm)	SA2C2			SA2C3		
	Mean (stdev)	Min	Max	Mean (stdev)	Min	Max
CryoTEM	14 (4)	7	56	19 (7)	8	38
AFM	17 (7)	7	48	21 (8)	8	51
nsTEM	11 (5)	3	31	10 (5)	5	35

Based on the microscopic examination it can be concluded that the majority in number (>90%) of the crosslinked oligopeptide assemblies exhibited a radius between 7 and 30 nm for the SA2C2 assemblies, and between 10 and 30 nm for SA2C3 assemblies. Performing a number weighting on the DLS analysis resulted in a size distribution analogous to the EM and AFM size distribution. Interestingly, the amphiphilic peptide assemblies displayed an asymmetric size distribution curve (Fig. 6), which is typical for assemblies in which the hydrophobic chain repulsion is dominant, as opposed to a symmetrical size distribution for assemblies in which the head group repulsion dominates [49]. The difference in hydrophobic block composition might thereby also have effectuated the observed difference in mean size (distribution) of the SA2C2 compared to the SA2C3 assemblies (Fig. 6).

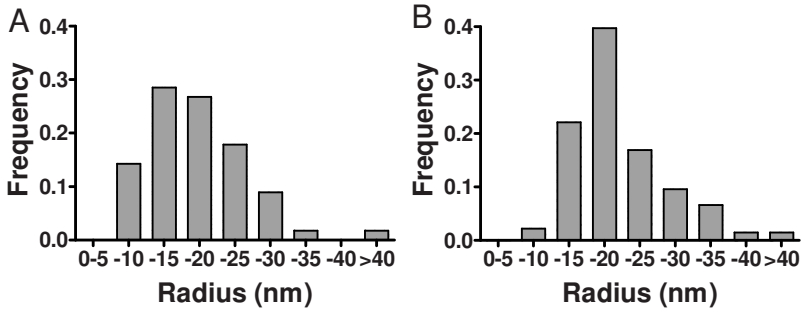

Figure 6. Size distributions in number of the SA2C2 (A) and SA2C3 (B) crosslinked assemblies, based on cryoTEM and AFM analysis.

Calcein encapsulation and release

To confirm a vesicular architecture of the crosslinked SA2C2 and SA2C3 peptide structures, a calcein entrapment assay was performed [155]. Calcein was entrapped by hydration of the acid-precipitated peptides in a buffered calcein solution (pH 8.0). Separation of the free calcein from the calcein associated with the peptide assemblies was done on a SEC spin column [156]. The peptide assemblies, eluting in the void volume of the column, entrapped considerable amounts of calcein (Fig. 7A). As a control calcein was added to the outside of the peptide vesicles and separated on the column, resulting in minimal calcein co-elution (Fig. 7A). Besides small molecules as calcein, larger hydrophilic compounds like dextran 10 000 could be entrapped as well (Fig. 7C).

To demonstrate release of water-soluble compounds from the peptide vesicles, calcein was entrapped in the peptide assemblies at self-quenching concentrations. After separation from non-encapsulated calcein, the release of the entrapped calcein can be conveniently monitored as an increase in fluorescence intensity, due to the dilution of the calcein into the bulk volume [173]. Indeed, a typical calcein release profile was observed for the SA2C2 and SA2C3 assemblies, as is shown in Figure 7. After 24 hours 50% of the entrapped calcein was released and continued slowly releasing further. During the time schedule the particles were stable as no changes in particle size were observed by DLS. The calcein release indicated that the assembled structures exhibit a vesicular

architecture. Moreover, Figure 7B shows that the release of calcein from the oxidized cysteine peptide assemblies was comparable to the SA2 peptides, which were shown to form vesicles previously. The comparable release profile of the crosslinked (SA2C2, SA2C3) assemblies and the non-crosslinked (SA2) vesicles suggests that the covalent bonds between the peptide monomers within the vesicular assembly do not form an additional barrier for diffusion of calcein.

The size of the assemblies (Fig. 6) is in good agreement with a vesicular nature, as was demonstrated by molecular dynamic simulations on surfactant-like peptides, similar to the ones we have studied here [37, 48]. These peptides form stable assemblies with a hydrophilic interior and exhibit radii comparable to the SA2C2 and SA2C3 assemblies. The smallest particles detected with cryoTEM and AFM theoretically can exhibit a vesicular architecture; moreover, it was demonstrated before that the SA2 peptides, which display a similar size distribution, also exhibit a vesicular architecture [50].

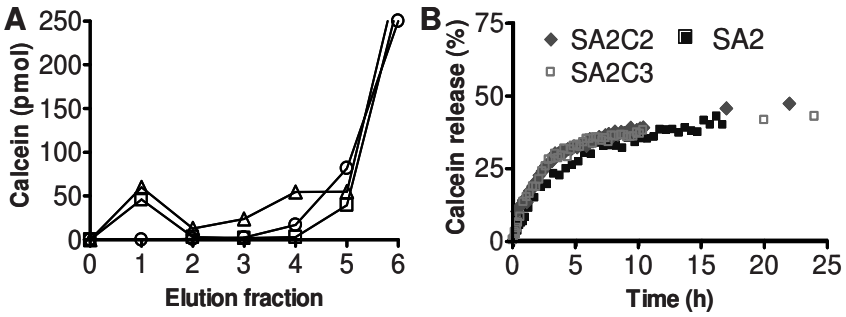

Figure 7. Calcein encapsulation (A) and calcein release (B) from the peptide assemblies. A. Crosslinked SA2C2 (triangles) and SA2C3 (blocks) assemblies prepared in the presence of calcein were separated on a size exclusion spin column. Fraction 1 and 2 represented the void volume containing the peptide assemblies. When calcein was added to preformed assembled peptide (control, circles) no calcein elution in the void volume was observed. B. Release of calcein from the crosslinked SA2C2 (diamonds) SA2C3 (open blocks) and the non-crosslinked SA2 (filled blocks) peptide assemblies.

Conclusion

Although various strategies for the covalent stabilization of supramolecular assemblies have been exploited [166], disulfide bond formation represent an attractive route for crosslinking self-assembled oligopeptide vesicles. We showed that the particle size of supramolecular structure was preserved after intermolecular disulfide bond crosslinking. By using different, complementary sizing techniques we demonstrated that the disulfide cross-linked particles are small in size (7-30 nm in radius, 14-60 nm in diameter) and that at least part of these particles, if not all, have a vesicular nature in which water-soluble compounds can be entrapped. The encapsulation of hydrophilic molecules, as well as the small size of the particles is relevant in the case these peptide vesicles will be used for drug delivery applications. The *in vivo* circulation kinetics of the peptide vesicles and their cellular uptake is subject of subsequent investigations.

Materials and Methods

Materials

Chemicals were from Sigma (St. Louis, USA) unless indicated otherwise. Hepes, acetic anhydride was from Fluka, Ellman's reagent was from Pierce (Rockford, USA). pET SUMO and chemically competent TOP10 and BL21(DE3) *E. coli* cells were from Invitrogen (Carlsbad, USA). SUMO protease was from (LifeSensors, Malvern, USA).

DNA design and construction

Two sets of complementary oligo DNA (5' GCGTGCGTGTGTCTGCTGCTGTGGGAAGAATGAGGATCCA 3'; 5' GGATCCTCATTCTTCCCACAGCAGCAGACACACGCACGCA 3' and GCGTGCGTGTGTCTGTGCCTGTGGGAAGAATGAGGATCCA 3'; 5' GGATCCTCATTCTTCCCACAGGCACAGACACACGCACGCA 3') were designed to have 3' A-overhangs for directional ligation (TA cloning) and a BamHI recognition site after the peptide coding region and stop codon. Both complementary oligos were annealed at a 5.0 µM DNA concentration using temperature gradients (cooling at

0.2° per second; 10 minutes 95°C, cooling to 30°C, 10 minutes 75°C, cooling to 30°C, 10 minutes 65°C, cooling to 30°C) and ligated into pET SUMO with T4 DNA ligase (Fermentas, Burlington, USA). After transformation of TOP10 *E. coli* cells, colonies were screened for the right DNA construct by colony PCR and subsequent BamHI (Fermentas, Burlington, USA) restriction analysis on purified plasmid DNA. Correct insertion of the dsDNA was confirmed by DNA sequencing (BaseClear, Leiden, The Netherlands).

Peptide biosynthesis

E. coli BL21(DE3) cells were transformed with plasmids encoding the SUMO-peptide fusion protein, and expression and protein purification were performed as described before [50]. Briefly, bacteria were cultured in a 5L Luria Broth pO_2-stat fed-batch fermentation. Protein expression was induced by addition of isopropyl-β-D-thiogalactopyranoside (IPTG) (Fisher Emergo, Landsmeer, The Netherlands) to a final concentration of 1.0 mM. After 3 hours, cells were harvested by centrifugation for 15 minutes at 3500 x g and lysed by means of a single freeze-thaw step and passing twice through an Avestin C5 cell-cracker (ATA Scientific, Lucas Heights, Australia). The cleared lysate, the His-tagged fusion protein was purified on a 20 ml HisTrap column (GE Healthcare, Upsala, Sweden) by automated flow purification. After elution with a 300 mM phosphate buffer (pH 8.0) containing 400 mM imidazole and buffer exchange to Hepes buffered saline (HBS, 20 mM Hepes, 150 mM NaCl, pH 8.0) supplemented with 2.5 mM dithiotreitol (DTT), the peptides were cleaved off the fusion protein by incubation with 2 u/ml SUMO protease at 30°C. The peptide was purified from the SUMO protein and protease using a size exclusion column of Sephadex™ G–25 Fine material (GE Healthcare, Upsala, Sweden) in a buffer of 10 mM Hepes, 75 mM NaCl, 2.5 mM DTT, pH 8.0. Subsequently, N-terminally acytelation was performed for 1 hour in 50% ddH_2O, 25% methanol 25% acetic anhydride (v/v). Acetylation was confirmed (>95%) by determination of free amines using 2,4,6-trinitrobenzene sulfonic acid (Pierce, Rockford, USA) according manufacture's protocol. The solvents were removed by reduced pressure evaporation. The correct peptide mass was confirmed by mass spectrometry after S-carboxymethylation of the cysteine residues by iodoacetic acid [174] (SA2C2 expected mass 1294.1; found mass 1294.0; SA2C3 expected mass 1282.4; found mass 1281.5 (diiodoacetylated)).

Gel electrophoresis

For sodium dodecyl sulfate polyacrylamide gel electrophoresis (SDS-PAGE), samples were boiled in Laemmli sample buffer without (non-reducing conditions) or with 25% β-mercaptoethanol (v/v) for 5 min and loaded onto a 15% acrylamide gel. Electrophoresis was performed at room temperature, applying 10 mA per gel until the running front reached the end of the gel. The gel was fixed in a 38/50/12 (v/v/v) mixture of water/methanol/acetic acid followed by silver staining. PageRuler prestained protein ladders were obtained from Fermentas (Burlington, USA)

Peptide self-assembly

The acetylated peptides were reconstituted in ddH_2O and washed as follows. Typically, 8.0 µmol of peptides were sedimented after acidifying with HCl (pH < 2.5) the peptide solution (15 ml), by centrifugation for 30 minutes at 13 000 x g and the supernatant was carefully removed. Peptide self-assembly was performed by adding 3.0 ml of 20 mM phosphate buffer (PB), pH 8.0 on top of the pellet, excluding mechanical input. The peptide solutions were exposed to air for 16 hours. The peptide concentration in the dispersions was determined by UV absorbance of the tryptophan residue at 280 nm, using a molar extinction coefficient of 5690 l mol^{-1} cm^{-1}. The measurements were checked on light scattering and if needed corrected for, according to ref. 175.

Ellman's reaction

To the peptide dispersions diluted in 0.1 M sodium phosphate, 1.0 mM EDTA, pH 7.0 Ellman's Reagent was added, to a concentration of 71 µg/ml. The conversion to 2-nitro-5-thiobenzoic acid was monitored at 412 nm in a Shimadzu spectrophotometer. The conversion was considered complete when the signal became stable over time (typically after 16 hours). Subsequently, the free thiols were quantified using the molar extinction coefficient of 2-nitro-5-thiobenzoic acid (14 150 l mol^{-1} cm^{-1})[176].

Dynamic Light scattering

Dynamic light scattering measurements were performed in a Malvern ALV CGS-3 goniometer (Malvern Instruments, Malvern, U. K.) containing a He-Ne laser source (λ = 632.8 nm, 22 mW output power) under an angle of 90°. The DLS time correlation was analyzed by ALV Correlator 3.0 software (ALV, Langen,

Germany). The refractive indices used were 1.333 (water) and 1.431 (DMF). In general, the solvents used to dilute the peptides were filtered through a 0.2 µm filter before use, and three independent light scattering experiments were performed on the peptide samples.

Electron Microscopy

Cryogenic transmission electron microscopy (TEM) analysis was performed on 2.5 mM peptide dispersions. Samples were applied on glow-discharged 200 mesh grids, covered with Quantifoil holey carbon foil (Micro Tools GmbH, Jena, Germany) and blotted for 0.5 second at 100% relative humidity. Immediately, the samples were vitrified by plunging the grid into liquid ethane using a Vitrobot (FEI Company, Eindhoven, The Netherlands) and subsequently put in dry liquid nitrogen. Grids were introduced in a Tecnai12 transmission electron microscope (FEI co, Eindhoven, The Netherlands). Samples were observed at 120 kV with low-dose imaging conditions to avoid melting of the vitrified film. Images were recorded on TemCam-0124 camera (TVIPS GmBH, Gauting, Germany) and processed with AnalySIS software. For negative stain EM, the peptide samples were adsorbed onto a glow discharged Formvar-carbon-coated copper grid and washed twice with 20 µl of ddH_2O. The samples were stained with 2% uranyl acetate (w/v) and examined in Tecnai10 transmission electron microscope (FEI Company, Eindhoven, The Netherlands) at 100 kV acceleration voltage.

Atomic Force Microscopy

Freshly cleaved mica was incubated for 5 min with 0.1 mg/ml poly-ornithine (30-70 kDa, Sigma, St. Louis, USA) and subsequently washed 4 times with water. A 0.3 mM peptide dispersion was applied on the coated mica and incubated for 5 minutes. The peptide dispersion was removed, the mica was rinsed and 10 mM PB was applied. Tapping mode AFM was performed in aqueous environment with a Multimode AFM and Nanoscope IIIa controller, equipped with a Silicon Nitride NP cantilever (Veeco, Santa Barbara, USA). A 12 µm piezoscanner (E scanner) was employed for imaging (Veeco, Santa Barbara, USA).

Calcein entrapment and release assay

Twenty five nanomol peptide was reduced in 20 mM, freshly prepared DTT for 40 minutes at 45°C. The peptides were precipitated by addition of 1.0 M HCl to pH < 3.0, centrifuged for 10 minutes at 13 000 g, and the pellet was washed twice with

100 µl 10 mM HCl. Peptide self-assembly was performed in 50 µl calcein solution (40 mg/ml calcein, 20 mM Hepes, pH 8.0) at anaerobic conditions (degassed solution, under argon) and subsequently exposed to air for 16 hours. Size exclusion spin columns were prepared as described by Fry et al [156]. Four milliliter of G25 Sephadex Medium Coarse size (GE Healthcare, Upsala, Sweden) swollen in Hepes buffered saline (HBS, 150 mM NaCl, 20 mM Hepes, pH 8.0) was used per column. The solution was applied on top of the column and centrifuged for 3 minutes at 350 g. The flow through was collected (fraction 1) and 50 µl of isotonic HBS were used for elution of the subsequent fractions. The void volume fractions (1 and 2) were directly measured over time in a Horiba Fluorolog fluorescence spectrometer (excitation 495 nm, emission 518 nm, slits 1.0 nm). The total encapsulated calcein was quantified after reduction in 20 mM DTT and disruption of the supramolecular structure in DMF (90% DMF, 10% HBS). Concentration series of calcein from 1.0 µM to 1.0 nM in 90% DMF, 10% HBS was used for calibration.

Acknowledgements

We thank Ronnie Willaert from the Flanders Institute for Biotechnology at the Vrije Universiteit Brussel for AFM measurements, and Fritsch Flesch for EM measurements. The Electron Microscope Facility of the Department of Biology, Utrecht Uiversity is acknowledged for the use of their microscopes.

Chapter 4

The Polyproline Type II Conformation is Critical for the Self-Assembly of Short Amphiphilic Oligopeptides into Vesicles

Albert J van Hell

Wim E Hennink

Daan JA Crommelin

Wim Jiskoot*

Enrico Mastrobattista

Department of Pharmaceutics, Utrecht Institute for Pharmaceutical Sciences, Utrecht University, The Netherlands

* Division of Drug Delivery Technology, Leiden / Amsterdam Center for Drug Research, Leiden University, The Netherlands

Submitted

Abstract

The secondary conformation of peptides determines their intramolecular organization and thereby critically affects self-assembling behavior of peptides. Amphiphilic oligopeptides have been designed that spontaneously self-organize into nano-sized vesicles, while their secondary conformation has thus far remained unknown. Here, we investigate the intramolecular organization of these amphiphilic oligopeptides with circular dichroism and Fourier transform infrared spectroscopy. We show that these non-proline containing oligopeptides (Ac-Ala-Ala-Val-Val-Leu-Leu-Leu-Trp-$Glu_{(2/7)}$-COOH) exhibit the polyproline type II (PPII) as its dominant peptide conformation. Moreover, the PPII conformation appears critical for the correct peptide self-assembly.

Introduction

With an increased understanding of the mechanisms that underlie peptide self-assembly, we can now exploit peptides as versatile building blocks for the design of supramolecular nanomaterials. Because of the chemical diversity of the 20 coding amino acids, (oligo)peptides can possess a virtually unlimited number of conformations and intermolecular interactions. Moreover, peptide polymers have the ability to adopt a secondary structure. This intramolecular level of organization determines the spatial distribution of amino acids within the peptides and thereby their self-assembling characteristics [27, 39, 82]. The secondary structure of peptides is therefore critically important in predicting its self-assembling behavior. For example, β-sheet forming peptides are well known for their ability to assemble into long fibrous structures, which is seen in amyloid structures associated with diseases like Alzheimer's and Parkinson's disease. Alpha-helices can give rise to fibrous structures by forming coiled-coils [27, 39, 82]. Besides fibrils, other supramolecular structures have been observed with alpha-helix forming peptides. The ability of poly-lysine-*b*-poly-leucines to adopt an alpha-helix was shown to be responsible for the formation of vesicles [27, 39, 82].

In a previous study, we have shown that small amphiphilic peptides $SA_{2/7}$ (Ac-Ala-Ala-Val-Val-Leu-Leu-Leu-Trp-$Glu_{(2/7)}$-COOH) self-assemble in aqueous

environment [50]. At pH > 7 these peptides form nanospheres, with an average size of around 130 nm. The vesicular nature of these nanospheres was demonstrated by both static light scattering and by entrapping a water-soluble fluorescent marker in the nanospheres [50]. Other groups reported that similar amphiphilic oligopeptides, but with a different primary peptide sequence, assemble into nanotubes [37]. Circular dichroism spectroscopic analysis revealed that alpha-helix and beta-sheet conformations were absent in these self-assembled surfactant-like peptides [37].

A secondary conformation which is frequently found in small peptides and which has gained increased attention is the polyproline type II conformation [87]. In its extended form (like in collagen) the PPII is a left-handed helix and exhibits 3.0 amino acids per turn [87]. The PPII conformation is not restricted to proline-containing sequences and has been described for many regions in proteins as well as for small peptides (e.g. short alanine peptides) that were previously assigned as unordered [90]. Detailed insights from spectroscopic techniques on short peptides [86, 90, 91] suggest that the typical PPII dihedral angles (Φ -75°, Ψ 145°) are the preferential orientation of many peptide bonds [92, 93]. Consequently, the PPII helix has been proposed as the major conformation in previously assigned unordered peptide sequences [87, 177]. The PPII conformation in supramolecular self-assembly so far has been largely unexplored [51]. Here, we studied whether the polyproline type II conformation plays a role in the self-assembling characteristics of SA2 and SA7 amphiphilic oligopeptides.

Results and Discussion

First, CD measurements were performed on the SA2 peptide, in its self-assembled, vesicular state (Fig. 1). The CD spectrum of the SA2 vesicles showed a steep, negative peak around 200 nm, which is typical for peptides that exhibit a PPII conformation [90, 177]. Dependent on the amino acid content and charged state of peptides, either positive, neutral or slightly negative 220 nm CD values have been observed [178], which thus far have hindered the development of a generally applicable quantification of the PPII content [179]. However, clearly the intensity and

the shape of the CD spectrum indicate a substantial PPII content in the SA2 peptide [91].

To investigate the relevance of the peptide conformation on the self-organized state of the SA2 peptide, the secondary structure was also investigated at acidic conditions. At pH<4 the SA2 peptide has been shown to form large aggregates [50]. As can be seen in Figure 1, the disruption of the vesicular assemblies upon exposure to low pH was clearly accompanied by a change in the peptide conformation. A shift of the minimum in the CD spectra from 200 nm to 219 nm was observed and the x-axis is crossed at 205 nm, indicating the formation of beta-sheets [180-182]. The hydrogen bond patterning in beta-sheets may favor the hydrophobic residue alignment, thereby strengthening the peptide aggregation.

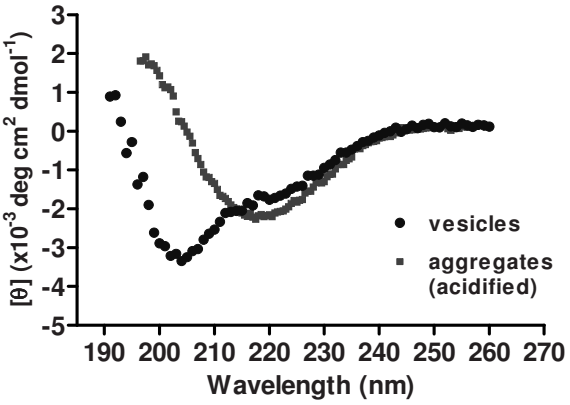

Figure 1. Circular dichroism spectra of the SA2 peptides assembled into vesicles (spheres) and in acid-induced aggregated form (blocks).

To substantiate the CD results, the effect of the SA2 secondary structure on the peptide organization was investigated with FTIR (Fig 2). The infrared absorption in the amide I' region is sensitive to the secondary structure of peptides and beta-sheets typically absorb around 1620 cm^{-1}, frequently accompanied by a peak around 1680 cm^{-1} [180-182]. The PPII helix appears around 1645 cm^{-1}, in proximity to the alpha-helix position (1650 cm^{-1}) [86, 180-182]. The SA2 peptide in their self-organized form, displaying a vesicle size distribution of around 65 nm in radius (Fig. 2A), showed a main infrared absorption at 1645 cm^{-1} (Fig. 2D and G). This

peak position indicates that the PPII structure is predominantly present, in agreement with the CD data. The higher-wavenumber shoulder (Fig. 2G) is typically observed for the PPII conformation in various peptides [86, 177].

Aggregation of the peptide by acidification is reflected by the 1-µm peak in the size distribution graph (Fig. 2B). As well, large, visible particles appeared in the solution. FTIR showed that the absorbance peak shifted towards lower wavenumbers (Fig. 2E). Although a minor 1650-1645 cm^{-1} absorbance was still observed (Fig. 2H), the main IR absorbance was at 1620 cm^{-1} with a minor peak at 1680 cm^{-1}. The latter peaks indicate the presence of beta-sheets [180-182] in the aggregated SA2 peptide, which is consistent with the CD data.

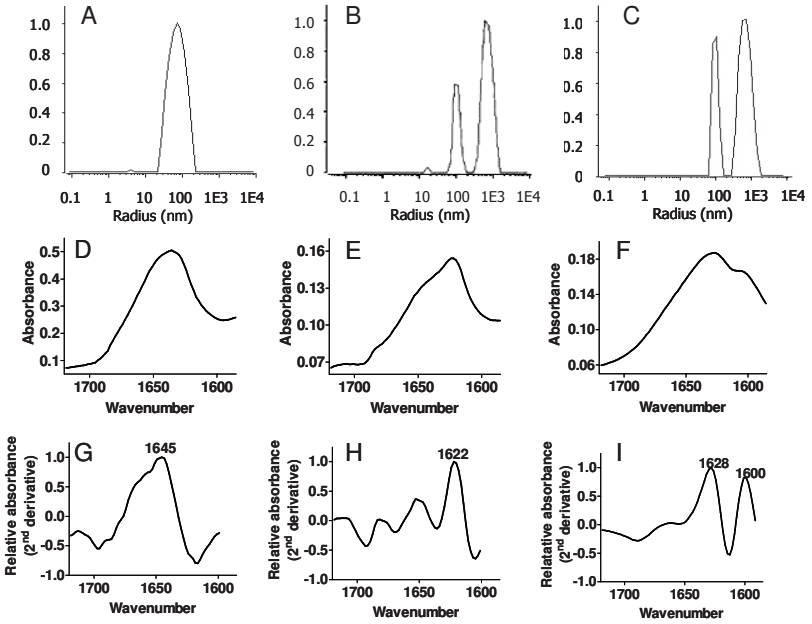

Figure 2. Dynamic light scattering and Fourier transform Infrared Spectroscopy on self-assembled and aggregated SA2 peptides. Dynamic light scattering size distribution graphs of the peptide in assembly (A), aggregated by acidification (B) and aggregated by organic solvents (C). Depicted in the row below: the corresponding amide I' FTIR absorption graphs of the vesicular peptide assemblies (D), acid-induced peptide aggregation (E) and organic solvent induced aggregation (F). Resolution enhancement by the second-derivative was used to denote the major infrared absorbance peaks of the peptide vesicles (G), acid-aggregated (H) and organic solvent aggregated (I) peptide.

Table 1. Dynamic light scattering analysis before and after heating the SA2 assemblies to 85°C

	Hydrodynamic radius (nm)	Polydispersity index
Before heating	58 nm	0.25
After heating	48 nm	0.26

Since acidification of the sample results in the protonation of the peptide, and consequently the charged state of the peptides is changed, another method (solvent change of the sample) inducing aggregation was investigated. SA2 peptide assemblies were injected into heated (68°C) acetonitrile. Immediate peptide aggregation was observed, as reflected in the dynamic light scattering size distribution graphs (Fig. 2C). After removal of the acetonitrile, the aggregated peptide in D_2O showed a strong shift of the amide I' peak to a lower wavenumber (Fig. 2 F and I) as compared to the peptide in vesicular assembly, resulting in a peak in the beta-sheet region at 1628 cm^{-1} and a shoulder around 1600 cm^{-1}. Especially, the 1600 cm^{-1} peak represents extensively dehydrated and strongly intermolecular hydrogen bonded strands of aggregated peptide [180-182]. This is in agreement with the observation that the acetonitrile induced aggregation was irreversible: the size distribution as displayed in Fig. 2A could not be restored upon reversal to initial conditions, contrary to the acid aggregated SA2 peptides [50].

To further investigate PPII as the predominant conformation of the peptide organized into vesicles, the effect of guanidine hydrochloride (GND) on the peptide self-assembly and conformation was studied. GND, like urea, is known to disrupt secondary structures like alpha-helix and beta-sheets, but it stabilizes the PPII helix in peptides and (denatured) proteins [177, 183, 184] . The peptide assemblies were titrated with GND and dynamic light scattering of the peptide dispersions was studied. Surprisingly, GND at concentrations up to 6 M did not disrupt the peptide assemblies (Fig. 3B). The scattering intensity was stable over time and the vesicle radius only slightly increased with GND concentration.

Moreover, the secondary structure was not affected by GND, as can be seen from the CD analysis; the addition of GND did not result in a significant change in shape or intensity of the CD spectrum down to 210 nm (Fig. 3A). In the case peptides adopt the PPII conformation partially, GND has been reported to increase the PPII content [10,183, 184]. For the SA2 peptides the PPII increasing effect of GND was not observed, which underscores that the PPII conformation is dominantly present in the peptide. Also, these results show that the PPII-preserving characteristics of GND counterbalanced its weakening of the hydrophobic interactions in the peptide assemblies. Therefore, the stability of the assemblies at high GND concentrations indicates the importance of the PPII conformation on the stability of the self-assembled structure of SA2 peptides.

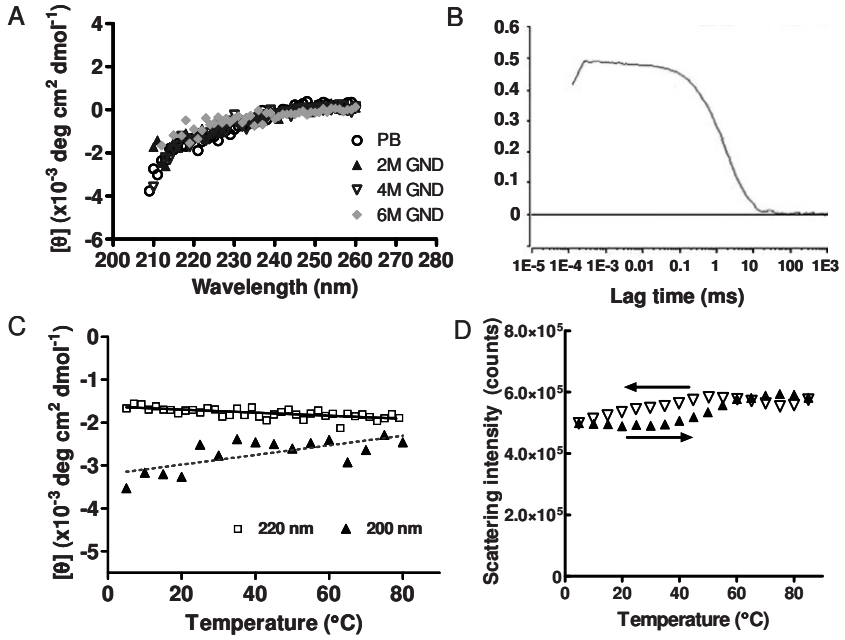

Figure 3. Effect of guadinium HCl (GND) and temperature on the peptide assemblies. A. Circular dichroism of the self-assembled SA2 peptide in presence of increasing concentrations of GND as compared to the peptide in phosphate buffer (PB). B. Dynamic light scattering correlation function of the SA2 assemblies in 6M GND. C. Dependence of the SA2 CD intensities on temperature. D. Effect of temperature on scattering intensity of the SA2 assemblies: heating (closed triangles), cooling (open triangles).

Characteristically, the tendency of peptide bonds to adopt the PPII conformation increases at lower temperature, as detected by a decrease in intensity of the (negative) peak around 200 nm and an intensity increase of the (negative) 220 nm signal [91, 93, 177]. Therefore, the temperature of the peptide dispersion was increased from 5 to 85°C, while monitoring CD and the particle characteristics by light scattering. Notably, the peptide assemblies were stable upon heating to 85°C and subsequent cooling. No change in scattering intensity was observed (Fig. 3D), neither particle size nor polydispersity were affected by the temperature trajectory (Table 1). During the temperature trajectory a slight gradual change in CD intensities was observed (Fig. 3C), while sharp transitions in the CD profile were absent. The negative slope of the 200 nm CD signal versus temperature and the positive slope of the 220 nm signal reflect an increase in PPII conformation upon lowering the temperature [87, 91].

The effect of temperature on the PPII conformation in the SA2 peptide is less pronounced as compared to the PPII conformation in the GGAGG peptide [91]. The latter peptide decreased in 200 nm CD values from -500 to -800 deg cm^2 $dmol^{-1}$ upon cooling from 55°C to 4°C, whereas the SA2 peptide showed a decrease from -2600 to -3100 deg cm^2 $dmol^{-1}$ in 200 nm values upon the same temperature change (Fig. 3B). In dissolved peptides like the GGAGG peptide, the PPII conformation is stabilized by water structuring around the peptide. With increasing temperature the water hydrogen bonding with the peptide backbone is reduced [87, 185]. With respect to the SA2 peptides in assembly the intermolecular steric effects may have a more pronounced influence on the PPII conformation as compared to effects of water structuring.

To determine whether the PPII conformation is induced by self-assembly of the SA-peptides into vesicles or that the PPII conformation is already present in monomeric peptides, the secondary structure of these peptides above and below the critical aggregation concentration was measured by CD. No dependence of the SA2 conformation on changes in the peptide concentration above its critical aggregation concentration (CAC) was observed with CD (Fig. 4A). Unfortunately, due to the low CAC of the SA2 peptides (0.5 μM) no reliable CD spectra were obtained at peptide concentrations below this CAC. Therefore, SA7 peptides

were used in this experiment. SA2 and SA7 peptides have identical hydrophobic blocks and only differ in length of the hydrophilic domain (2 vs 7 glutamic acid residues). This difference affects the CAC (16 μM for SA7 compared to 0.5 μM for SA2) but peptide vesicles obtained above the CAC are, in terms of size and morphology indistinguishable from SA2 peptide vesicles [50].

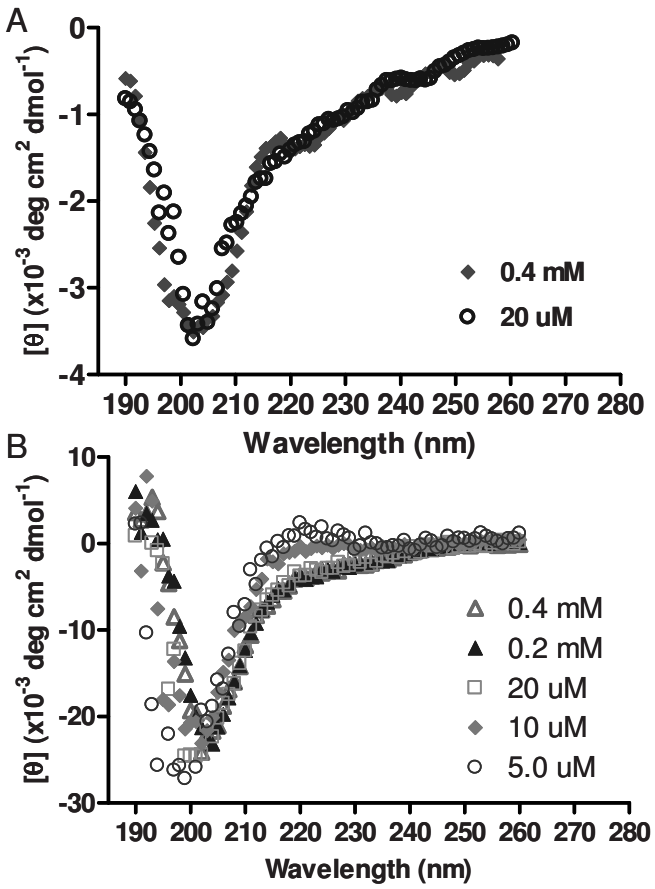

Figure 4. Circular dichroism spectra of the self-assembling peptides SA2 (A) and SA7 (B) at different peptide concentrations. The CAC of the SA2 and SA7 peptide is 0.5 μM and 16 μM, respectively.

The CD spectra of the SA7 peptide at a concentration above the CAC (0.2 mM and 0.4 mM, Fig. 4B) display a PPII CD spectrum, with a minimum at 203 nm analogous to the SA2 peptide. The 200 nm CD signal of this SA7 peptide is more intense, which is attributed to the strong negative 200 nm signal of glutamic acids [178]. Throughout the concentration series the characteristic PPII spectrum was maintained (Fig. 4B). Some detailed but significant changes were observed when approaching the CAC. At the CAC the minimum in the CD spectrum showed a 5 nm blue-shift, and at concentrations below the CAC the 220 nm signal increased; at 10 μM a neutral 220 nm value and at 5.0 μM a positive value of 1.6 10^3 deg cm^2 $dmol^{-1}$ were reached (Fig. 4B). The spectra below the CAC may represent a typical charged, solvated PPII conformation [179]. Clearly, the PPII conformation is already present in the monomeric peptide and as such favors self-assembly into vesicles.

Conclusion

In conclusion, we have shown that the amphiphilic oligopeptides when self-assembled in vesicles predominantly exhibit a PPII conformation, giving these nanoscale structures a strikingly stable conformation that can withstand exposure to high temperatures and high concentration of chaotropic agent. Destabilization of the secondary conformation of the self-assembled peptides is accompanied by disruption of the self-organized state of the peptide, whereas in the presence of the PPII conformation preserving chaotropic agent GND, the peptide vesicles are stable. These findings point to a crucial role of the PPII structure in the molecular self-assembly of amphiphilic oligopeptides that has until now remained unexplored.

Materials and Methods

Peptide synthesis and self-assembly

Peptides were recombinantly produced in *E. coli* as described before (Chapter 2). Briefly, BL21(DE3) cells were transformed with the DNA construct encoding the peptide - Small Ubiquitin Modifiying (SUMO) fusion protein. Expression of the protein took place upon addition of IPTG (1.0 mM final concentration) in 5 liter fed-batch fermentation and the fusion protein was purified from the bacterial lysate by nickel affinity chromatography. The purified fusion protein was enzymatic cleaved by SUMO protease (LifeSensors, Malvern, USA) for 1 hour at 30°C and overnight at 5°C. The released peptides were purified using a second nickel affinity purification step and analyzed as reported previously (purity > 98%). The N-terminus of the peptides was acetylated in a 25% acetic anhydride (Fluka, St. Gallen, Switzerland), 50% methanol solution (v/v). Solvents were removed by reduced pressure evaporation and the peptides were taken up in water, precipitated by acidification with HCl and pelleted by centrifugation for 45 minutes at 17 000 g. Peptide self-assembly was performed after removing the supernatant by restoring the peptide pellet in a 10 mM sodium phosphate, pH 8.0 and subsequent incubation at RT for 4 hours. The concentration of the peptides were determined with UV spectroscopy, using the absorbance of tryptophan $\lambda_{max}(H_2O)$/nm 280 (ε/dm^3 mol^{-1} cm^{-1} 5690).

Spectroscopic analysis

For spectroscopic analysis peptides were diluted from aqueous stock to 0.5 mM in 10 mM sodium phosphate, pH 7.0, unless indicated otherwise. Acid-aggregation was done by addition of 1.0 M HCl until pH < 2.0. For acetonitrile-induced aggregation, the peptide stock and the acetonitrile were preheated to 68°C and 25 µl of 30 nmol peptide was injected into 300 µl acetonitrile and directly measured with DLS, taking into account the refractive index of acetonitrile (1.344). For subsequent FTIR analysis, the solvents were evaporated and the white aggregates were resuspended in 10 µl D_2O.

Circular dichroism was measured in a double beam DSM 1000 CD spectrometer (Online Instrument Systems, Bogart, GA, USA) using quartz cuvettes of different path lengths (0.5 – 10 mm) (Hellma, Müllheim, Germany). Ten measurements of

1.0 nm increment were averaged and background spectra of the buffer were subtracted. The results are expressed in terms of molar residue CD.
FTIR measurements were performed on a BioRad FTS 6000 spectrometer (Varian, Inc., Palo Alto, CA, USA) using a liquid sample cell at a 10 µm path length with CaF_2 windows and. Peptides were taken up in D_2O at a peptide concentration of 2.5 mM or higher. 1 024 scans were accumulated for a single spectrum, and an H_2O vapor spectrum was measured for background subtraction.

Dynamic light scattering

The samples, described above, were assessed for dynamic light scattering at 90° angle in a Malvern ALV CGS-3 goniometer (Malvern Instruments, Malvern, UK) containing a He-Ne laser source (λ 632.8 nm, 22 mW output power). The DLS time correlation was analyzed by ALV Correlator 3.0 software (ALV, Langen, Germany).

Chapter 5

Hydrophobic interactions and intermolecular hydrogen bonding in interdigitated oligopeptide-vesicle membranes

Albert J van Hell[1]

Andrey Klymchenko[2]

Pepijn Burgers[3]

Ed E Moret[3]

Wim Jiskoot[4]

Daan JA Crommelin[1]

Wim E Hennink[1]

Enrico Mastrobattista[1]

[1] Department of Pharmaceutics, Utrecht Institute for Pharmaceutical Sciences, Utrecht University, The Netherlands

[2] Laboratoire de Pharmacologie et Physicochimie, Universite Louis Pasteur, Illkirch, France

[3] Medicinal Chemistry and Chemical Biology, Department of Pharmaceutics, Utrecht University, The Netherlands

[4] Division of Drug Delivery Technology, Leiden / Amsterdam Center for Drug Research, Leiden University, The Netherlands

To be submitted

Abstract

Several lipid-like peptides have shown to self-assemble spontaneously into peptide nanotubes or, for example the SA2 peptides (Ac-Ala-Ala-Val-Val-Leu-Leu-Leu-Trp-Glu-Glu-COOH), into well-defined nanovesicles in an aqueous environment. We have previously shown that the polyproline type II conformation is the dominant conformation of these non-proline containing oligopeptides when assembled into vesicles. Here, the intermolecular interactions that contribute to the formation and stabilization of the SA2 oligopeptide assemblies were determined. Firstly, upon assembly the formation of a hydrophobic domain was demonstrated using hydrophobic fluorescent probes and intrinsic tryptophan fluorescence in the peptide assemblies. The polarity of this hydrophobic microenvironment was comparable to that in negatively charged lipid bilayers. However, in contrast to lipid bilayers the SA2 oligopeptide vesicles could not be disrupted by addition of sodium dodecyl sulphate (SDS), suggesting an additional intermolecular interaction besides hydrophobic clustering. The effects of different solvents on the stability of the peptide assemblies suggested that intermolecular hydrogen bonds additionally stabilize the peptide assembly. All-atom molecular dynamics simulations confirmed the formation of intermolecular hydrogen bonds. In the interdigitated oligopeptide membrane, the peptide backbones in the hydrophobic domain either connected together directly by hydrogen bonding, or two peptide backbones were stably bridged by single water molecules. In conclusion, based on the data presented here we propose a model of an interdigitated peptide membrane which is stabilized by intermolecular hydrogen bonds, in addition to the hydrophobic interactions in the oligopeptide vesicles.

Introduction

The self-assembly of peptides is an attractive route to obtain new, functional materials, which may find application in a variety of different fields, including tissue engineering and drug delivery. Dependent on the amino acid sequence amphiphilic oligopeptides were shown in aqueous media to assemble into either vesicles or nanotubes with a hydrophilic interior [47, 50]. These oligopeptides consist of a hydrophobic tail of 6 - 10 hydrophobic amino acids, and a hydrophilic domain

of charged amino acids, which vary in length from 1 - 7 residues [50]. In view of their hydrophobic block lengths, such amphiphilic peptides have also been referred to as lipid-like or detergent-like peptides. Moreover, the SA2 peptides that assemble into vesicles have a conical geometry, in which the hydrophobic amino acids side chains increased in size towards the hydrophilic domain (Ac-Ala-Ala-Val-Val - Leu-Leu-Leu-Trp-Glu-Glu-COO^-) (Chapter 2).

Such peptides exhibit a lipid-like design and display similarity in their supramolecular architecture to phospholipids, e.g. vesicular assemblies [56, 157, 186]. In contrast, the supramolecular characteristics of these peptides assemblies are significantly different. The SA2 peptides self-assemble into nano-sized vesicles spontaneously, without the need for any particle sizing [50]. The polar nature of the peptide backbone may partially explain the distinguished self-assembling characteristics of oligopeptides as compared to e.g. lipids. The amide hydrogen and carbonyl oxygen atoms are hydrogen bond donor and acceptors and the free energetic penalty of burying a non-hydrogen bonded amide and carbonyl in a dehydrated environment has been estimated at 2.5 kcal/mol [69]. In contrast, the gain in free energy of apolar amino acid side chain desolvation is at maximum 2.2 kcal/mol, and for the amino acid side chains of alanine or valine these values are smaller [70]. Therefore, hydrogen bonding of the peptide's backbone is favorable in a desolvated environment, and indeed, in proteins burial of non-hydrogen bonded amides and carbonyls in the hydrophobic interior of proteins is rarely found [71].

Previously, we have shown that the SA peptides assembled into vesicles adopt the polyproline type II (PPII) conformation as the dominant intramolecular organization (Chapter 4). The PPII conformation is a stretched conformation [87, 187] and, in contrast to e.g. the α-helix, leaves the backbone amide hydrogen and oxygen atoms available for intermolecular hydrogen bonds. The aim of this study is to reveal the stabilizing forces that dominate the SA2 oligopeptide assemblies. Hydrophobic domain formation was assessed using the fluorescent probe pyrene and the fluorescence of tryptophan (Trp) in the peptide assemblies. A 3-Hydroxyflavone based probe was used to reveal the degree of hydration and polarity within the hydrophobic cavity. In addition, by both experimental

techniques and *in silico* molecular simulations, intermolecular hydrogen bonding within the hydrophobic domain was examined.

Materials and Methods

Materials

All the chemicals were from Sigma-Aldrich (St. Louis, USA), unless indicated otherwise. Probe F was synthesized as reported elsewhere [209].

Peptide production

Peptides were recombinantly produced in *E. coli* as described before [50]. Briefly, BL21(DE3) cells were transformed with the DNA construct encoding the peptide - Small Ubiquitin Modifiying (SUMO) fusion protein. Expression of the protein took place upon addition of IPTG (1.0 mM final concentration) in 5 liter fed-batch fermentation and the fusion protein was purified from the bacterial lysate by nickel affinity chromatography. The purified fusion protein was enzymatic cleaved by SUMO protease (LifeSensors, Malvern, USA) for 1 hour at 30°C and overnight at 5°C. The released peptides were purified using a second nickel affinity purification step and analyzed as reported previously (purity > 98%). The N-terminus of the peptides was acetylated in 25% acetic anhydride (Fluka, St. Gallen, Switzerland), 50% methanol solution, 25% water (v/v). Solvents were removed by reduced pressure evaporation and the peptides were taken up in water, precipitated by acidification with HCl and pelleted by centrifugation for 45 minutes at 17 000 g. Peptide self-assembly was performed after removing the supernatant by restoring the peptide pellet in a 20 mM sodium phosphate, pH 8.0 and subsequent incubation at ambient temperature for 4 hours. The concentration of the peptides was determined with UV spectroscopy (Nanodrop, ThermoScientific, Wilmington, USA) using the absorbance of tryptophan $\lambda_{max}(H_2O)$/nm 280 (ε/dm^3 mol^{-1} cm^{-1} 5690).

Fluorescence spectroscopy

Dilution series of the peptide (1000 - 0.1 µg/ml) were prepared in 5 mM Hepes, pH 8.0. Pyrene (Fluka, Buchs, Switzerland) in acetone was added to a final concentration of 5.4 x 10^{-6} M. Acetone did not exceed 1% of the total volume. After minimally 14 hours of incubation in the dark, fluorescence excitation spectra

were measured using a Horiba Fluorolog fluorometer (Horiba Jobin Yvon, Longjumeau Cedex, France). Excitation spectra were recorded between 300 nm and 360 nm, with an emission wavelength of 390 nm. Excitation and emission band slits were 4 and 2 nm, respectively. The intensity ratio of I_{338}/I_{333} was plotted against the peptide concentration [32].

For probe F experiments, the samples were prepared in a 20 mM sodium phosphate, pH 8.0 at a 0.5 mM peptide concentration. Acidification was done by addition of 1.0 M HCl until pH < 2.0. For acetonitrile induced aggregation the peptide stock and the acetonitrile were preheated to 68°C and 25 µl of 30 nmol peptide was injected into 300 µl acetonitrile solution. The solvents were removed by reduced pressure evaporation and the peptides were hydrated 20 mM sodium phosphate, pH 8.0. Probe F was added to a 4.0 µM concentration from a DMSO stock solution. The final DMSO concentration was <1% (v/v). Deconvolution of probe F fluorescence into three bands (N*, H-N* and T*) was performed as previously described[20] using the Siano software kindly provided by Dr. A.O. Doroshenko (Kharkov, Ukraine). The program is based on an iterative nonlinear least-squares method that is itself based on the Fletcher-Powell algorithm. The individual emission bands were approximated by a log-normal function [210].

Tryptophan fluorescence was measured SA2 peptide or NATA concentration of at a 75 µM, diluted in 20 mM sodium phosphate, pH 8.0 from aqueous stock solution. Quantum yields were based on measurements with NATA as a reference (quantum yield NATA 0.14). For iodide quenching, to the peptide diluted to 350 µM iodide was added from 4.0 M potassium iodide stock solution. For the forced co-assembly with SDS, 0.15 µmol SA2 peptide and 2.4 µmol SDS were diluted from an aqueous stock solution in 25 ml methanol. Solvents were removed by reduced pressure evaporation after which the resulting film was hydrated in a 20 mM sodium sodium phosphate, pH 8.0. All emission spectra were recorded with excitation wavelengths at 280 nm.

Circular dichroism

Circular dichroism was measured in a double beam DSM 1000 CD spectrometer (Online Instrument Systems, Bogart, GA, USA) using quartz cuvettes of 0.5 mm path length (Hellma, Müllheim, Germany) and peptide dispersions (0.5 mM) in 10

mM sodium phosphate, pH 8.0. Five measurements of 1.0 nm increment were averaged and background spectra of the buffer were subtracted. The results are expressed in terms of molar residue CD.

Dynamic light scattering

Dynamic light scattering (DLS) measurements were performed at 90° angle in a Malvern ALV CGS-3 goniometer (Malvern Instruments, Malvern, UK) containing a HeNe laser source (λ = 632.8 nm, 22 mW output power). The DLS time-correlation was analyzed with ALV Correlator 3.0 software (ALV, Langen, Germany) taking into account the refractive indices of the different solvents.

Molecular dynamics simulations

Molecular dynamics was performed with the program YASARA version 8.3.3 [211] in an Amber-99 force field. Explicit water molecules were placed at random positions within the box until the water density was 1.00 g/ml. Periodic boundary conditions were used and every run was started with a steepest descent energy minimisation until the maximum atom speed dropped below 2200 m/s, followed by 500 annealing steps. The particle mesh Ewald method was applied for long-range electrostatic interactions, with a 7.86 Ångstrom Van der Waals forces cut-off. pH was 7.0, temperature was set at 300K and the density was maintained at 1.00 g/ml. From a 750 picosecond simulation random conformations of the SA2 peptides were selected and 18 peptides were placed in boxes of 37x39x79 (opposing layers) and 36x45x60 Ångstrom (interdigitated layers) in the presence of water and 54 sodium ions. Simulations were run for 15 ns and coordinates were saved every 7.5 ps. The results were analysed using analysis programs written in Python in our laboratory.

Results and Discussion

Pyrene partitioning in oligopeptide vesicles

The SA2 amphiphilic oligopeptides were designed to self-assemble based on the hydrophobic interactions of its apolar amino acids (Chapter 2). In light of the observation by electron microscopy that closely related oligopeptides assemble into a peptide membrane [37], it might be expected that these small peptides indeed form a distinguished hydrophobic microdomain. To confirm the formation of a hydrophobic domain, the apolar fluorescent probe pyrene was used. Partitioning in a hydrophobic environment results in a red-shift of the peak at 338 nm in the excitation spectra [188]. In Figure 1A the I_{333}/I_{338} ratio is plotted against the SA2 peptide concentration. Above the critical association concentration (CAC; 0.5 µg/ml)[50] an increase in I_{333}/I_{338} ratio was observed at increasing peptide concentrations. The fluorescence analysis shows that pyrene partitioned into a marked hydrophobic domain in the self-assembled peptides, which is in good agreement with previous investigations on similar self-assembling amphiphilic oligopeptides [157].

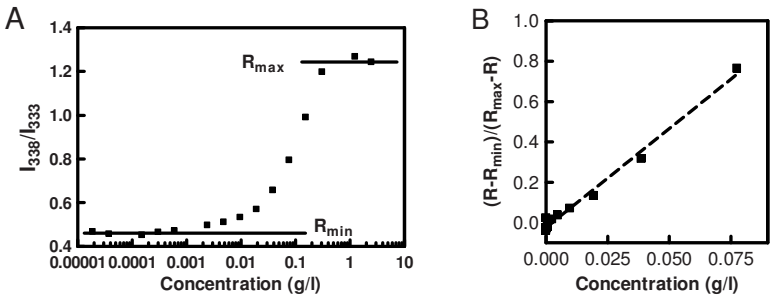

Figure 1. A. Pyrene excitation red shift (I_{333}/I_{338}) plotted against the SA2 peptide concentration. B. Pyrene partitioning equilibrium analysis. At a constant pyrene concentration, the relative increase of excitation I_{333}/I_{338} ratio (R) is plotted against the peptide concentration (c in g/l). The calculated binding constant was 1.6×10^4, assuming a mean density of the hydrophobic block of 1.27 g/cm^3.

In order to obtain more insight into the apolarity of the hydrophobic cavity, the partitioning equilibrium of pyrene in the peptide assemblies, relative to pyrene in the bulk water, was examined [188]. A linear correlation (r^2 0.99) between 7.7 x 10^{-2} and 9.0 x 10^{-6} g/l SA2 peptide was observed (Fig. 1B). The CAC as derived from pyrene partitioning is defined at the intersection with the x-axis [188]. For the SA2 peptides the CAC value measured with pyrene was higher (2.1 μM) compared to the CAC determined with Trp fluorescence anisotropy (0.5 μM) [50], something found more frequently when using pyrene for CAC determination of amphiphiles [147, 189].

The pyrene partitioning equilibrium constant (K_v) defined by

$$(R-R_{min})/(R_{max}-R) = K_v*\chi_h c/1000\rho_h \quad (1)$$

, where χ_h is the mass fraction of the hydrophobic block and ρ_h is the density of the hydrophobic domain and R is the ratio I_{333}/I_{338}. The R_{min} and R_{max} are determined as the lower and upper limit of the I_{333}/I_{338} ratio (Fig. 1A). Assuming a mean density of the solid amino acids of the hydrophobic domain (1.27 g/cm^3), pyrene partitions into the peptide assemblies with K_v of 1.6 x 10^4. The K_v of the peptide vesicles is an order of magnitude lower than reported for e.g. polystyrene-*b*-polyethylene glycol micelles of various polystyrene molecular weights and more closely resembles that of methoxy poly(ethylene glycol)-*b*-oligo(caprolactone) micelles containing 2 caprolactone units [188, 190]. The pyrene partitioning into the peptide vesicles indeed demonstrated the formation of a hydrophobic domain, while this domain may be relatively polar or hydrated.

Analysis of 3-hydroxyflavone probe in the peptide vesicles

3-Hydroxyflavone based membrane probes[191, 192] are suitable for independently assessing the polarity and the hydration of hydrophobic domains in lipid bilayers [193, 194]. Due to intramolecular proton transfer in their excited states, these probes exhibit emission of both the normal (N*) form and a strongly red-shifted tautomeric (T*) form, and thereby provide additional information on the environment of the probe. 4'-N,N-dimethylamino-3-hydroxyflavone (probe F) was used for the investigation of SA2 peptide assemblies. Whereas below the CAC of the SA2 peptides only minor probe F fluorescence was observed, probe F in the presence of the SA2 assemblies showed dual emission (Fig. 2), similarly to that observed for this dye in lipid bilayers [193].

To extract the hydration and polarity parameters from these data, we used a method previously developed for probe F in lipid vesicles, which consists of deconvolution of the fluorescence spectrum into three bands: normal (N*), H-bonded normal (H-N*) and tautomer (T*) [193]. The polarity of the assembles was estimated as the intensity ratio I_N^*/I_T^*, while the hydration parameter was calculated as a relative contribution of the H-N* band, namely $I_{H\text{-}N^*}/(I_{N^*}+0.5\times I_{T^*})$.The results of the analysis presented in Table 1 were compared with previous data on large unilamellar vesicles (LUVs). It is clear that the obtained values of polarity and hydration are significantly different from those for LUVs composed of the neutral lipid, egg yolk phosphatidylcholine (PC), while they are remarkably close to those observed for the vesicles composed of the anionic lipid, bovine brain phosphatidylserine (PS). This especially concerns the polarity parameter, which, in SA2 vesicles, is *ca* 2.4-fold larger than in the PC vesicles, while it is nearly the same as in the PS vesicles.

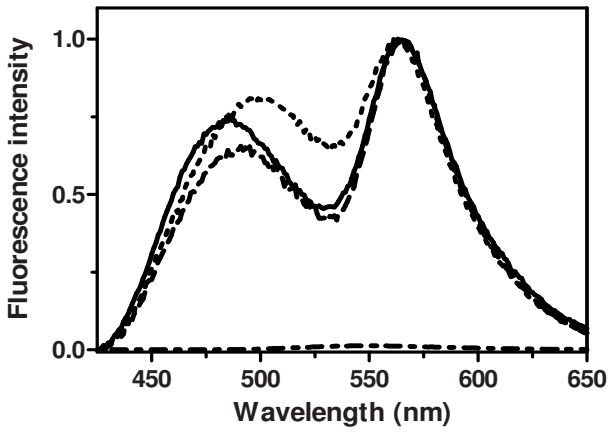

Figure 2. Fluorescence spectra of the 3-hydroxyflavone based probe in peptide vesicles (dotted line), aggregated peptides by decrease of the pH values (solid line) and peptides aggregated by injection into hot acetonitrile (dashed line). The spectra were normalized at the T* band maximum. The spectrum of probe F in the presence of SA2 below CAC, presented for comparison (dashed-dotted line), was normalized to its relative intensity (1.3 %) with respect to that of probe F in SA2 vesicles. Excitation wavelength was 400 nm.

The similarity of the SA2 vesicles with PS vesicles in terms of polarity of the probe binding site can be attributed to the presence of anionic glutamic acid residues in SA2 molecule. Indeed, like in the case of PS lipid, the anionic head group of SA2 should contribute to a large negative surface charge at the membrane-water interface. Moreover, similarities between SA2 and PS vesicles indicate common structural features between the organization of lipid membranes and SA2 membranes, namely the presence of low polar region formed by hydrophobic interactions of the amphiphiles (evident from the observed relatively low polarity) and presence of hydrated membrane-water interface (observed as the hydrated form of the dye, H-N*).

Table 1. Values of polarity and hydration estimated from spectra of probe F in assemblies of SA2 and in large unilamellar vesicles (LUV) of lipids

Sample	Polarity[a]	Hydration[a]
SA2 Vesicles	0.915	0.429
SA2 pH-aggr	0.858	0.141
SA2 AcN-aggr	0.710	0.168
LUV, PC[b]	0.382	0.874
LUV, PS[b]	1.012	0.636

[a]Polarity = I_{N^*}/I_{T^*}; hydration = $I_{H\text{-}N^*}/(I_{N^*}+0.5\times I_{T^*})$, where $I_{H\text{-}N^*}$,I_{N^*} and I_{T^*} are peak intensities of the three bands obtained by band-separation analysis of the fluorescence spectra of probe F.

[b]PC - egg yolk phosphatidylcholine; PS – bovine brain phosphatidylserine. The data were from ref. 193.

It was previously shown that disruption of the SA2 peptide self-organization could be obtained by either decreasing the pH below the pK_a of the glutamic acids, or by a combination of heat (weakening hydrogen bonds) with solvent change (injection into hot acetonitrile). These conditions resulted in the formation of large, visible peptide aggregates. The pH induced aggregation was found to be fully reversible, in contrast to the acetonitrile induced aggregation (Chapter 2).

However, in both cases, peptide aggregation was accompanied by a conformation switch of the peptides towards β-sheets as measured by circular dichroism and Fourier transform infrared spectroscopy (Chapter 4). As can be seen from Figure 2B, the dual emission of probe F maintained in the aggregated peptides, while the emission spectral profiles were considerably different. In the aggregated assemblies of SA2, the position of the short-wavelength band was considerably shifted to the blue as compared to the SA2 vesicles. Deconvolution analysis confirmed that the aggregation resulted in strong dehydration of the assemblies (Table 1), while the polarity parameter was modified only to a minor extent. The observed dehydration can be explained by formation of the β-sheet molecular packing, which is much tighter compared to the packing in vesicular membranes, and thus much more dehydrated [195].

Tryptophan fluorescence

The Trp in the SA2 peptides (Ac-Ala-Ala-Val-Val-Leu-Leu-Leu-Trp-Glu-Glu-COOH) is located subsequent to the glutamic acids that constitute the hydrophilic domain of the peptides. In order to address the polarity of the hydrophobic domain in the SA2 assemblies at this hydrophobic-hydrophilic interface, Trp fluorescence was investigated (Fig. 3). The Trp in vesicular assembly showed a fluorescence emission maximum at 355 nm (quantum yield 0.05). This is a 10 nm blue-shift as compared to the fully hydrated N-acetyl-tryptophan-amide (NATA; Fig. 3). The shift in polarity of the Trp in the vesicles can be compared to changing the environment of a charged Trp from water to ethanol [150, 196]. The Trp of the peptide below the CAC showed an emission maximum at 368 nm, indicating full hydration of the Trp of monomeric SA2 peptides. When the peptides were aggregated by acidification (Fig. 3, grey line) a more extensive Trp emission shift to the blue was observed (quantum yield 0.02) as compared to the vesicular assemblies. When the polarity of the Trp species was now compared to Trp emission in well-known solvents, the λ_{max} of the aggregated peptides resembles closely the fluorescence of Trp in n-butanol (λ_{max} at 331 nm) [196]. Overall, the Trp fluorescence data suggest that the peptide vesicles at the hydrophilic-hydrophobic interface are considerably hydrated. Such degree of hydration in peptide vesicles around the Trp as well as dehydration upon aggregation of the peptides both are in agreement with the data obtained with probe F (Table 1).

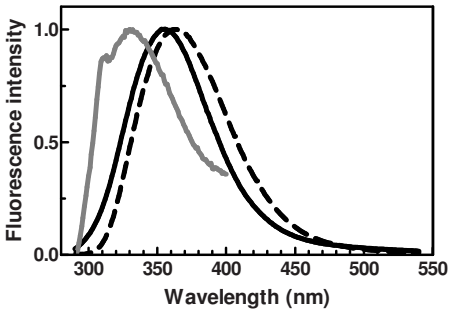

Figure 3. Tryptophan fluorescence emission spectra of the peptides in vesicular (solid black line) and in aggregated form (solid grey line) as compared to the fully hydrated NATA (dashed line). Excitation wavelength was 280 nm.

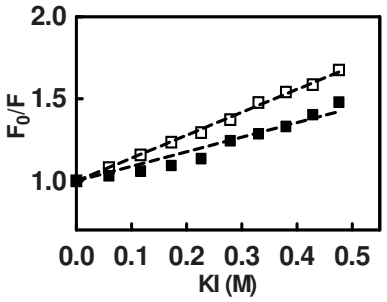

Figure 4. Iodide quenching of the Trp in the SA2 peptides in assembly (0.2 mM, closed blocks) and at a concentration (10 μM, open blocks) approaching the CAC.

Iodide quenching

The Trp quenching by iodide above and approaching the CAC of the SA2 peptides are displayed in Figure 4. At significant iodide concentrations quenching was observed and the extent of collisional quenching was analyzed using:

$$F_0/F=1+K_{SV}[Q] \quad (2)$$

F_0 and F are the fluorescence intensities in the absence and presence of the quencher, K_{SV} is the Stern-Volmer quenching constant and Q is the molar concentration of the quencher [150]. The Stern-Volmer analysis for the vesicle assemblies showed a relatively low quenching efficiency (K_{SV} 0.89 (+/- 0.02) M^{-1}), indicating that the Trp in peptide assemblies is poorly accessible to iodide. When the peptides were diluted close to the critical association concentration (10 μM), a slight increase of the slope towards K_{SV} = 1.4 was observed (Fig. 4, open blocks), suggesting that the relative increase of the molar fraction of the monomeric peptides indeed contributed to an enhanced accessibility of Trp moieties to iodide.

The Trp in the SA2 assembly was shown to be located in a relative hydrated environment (Fig. 3), while almost inaccessible for iodide ions. Previous reports have shown that peptide amphiphile nanofibers, even those which had the Trp

located more deeply buried in the self-assembled structure, display a more extensive iodide quenching (10-20 x higher K_{SV} values) [197]. Therefore, burial of the Trp into apolar domains of the SA2 vesicles only may not be a sufficient explanation for the poor iodide quenching. Likely, efficient shielding of the assembled structures by the repulsive charges of the glutamic acids may significantly contribute to a minimal accessibility of the Trp in the vesicles [150].

Stability of the SA2 vesicles in the presence of SDS

Sodium dodecyl sulphate (SDS) rapidly inserts into phospholipid bilayers and disrupts liposomal structures. Typically such liposomal disruption starts already at low concentrations of SDS, below its CMC (8.2 mM) [198, 199]. To assess whether SDS inserts and disrupts the oligopeptide vesicles, DLS analysis on mixtures of SA2 peptide vesicles and SDS was performed. The 100 nm peak in Figure 5C, corresponding to peptide vesicles (Fig. 5B), remained even at high concentrations of SDS and in significant molar excess (35 mM, above the CMC) compared to the peptides (0.1 mM). The smaller light scattering peak (Fig. 5C) displayed a hydrodynamic radius of around the radius of SDS micelles (2.5 nm) [198]. Molecular mixing of SDS with peptides and proteins may also induce extensive aggregation [200, 201]. The DLS analysis additionally showed that no aggregation of the peptides occurred by addition of SDS (Fig. 5C). Clearly, SDS did not disrupt the peptide vesicles. Since SDS is known to disturb secondary conformations of peptides at low concentrations [46, 202], circular dichroism (CD) measurements were performed. No significant changes in the SA2 secondary conformation were observed in the presence of SDS (Fig. 5D). The CD spectra did not change over time (>2 months, RT) and were independent of the SDS concentration. The CD spectra in the presence or absence of SDS both showed the characteristics of the conformation of the vesicular SA2 assembly, dominated by the PPII conformation.

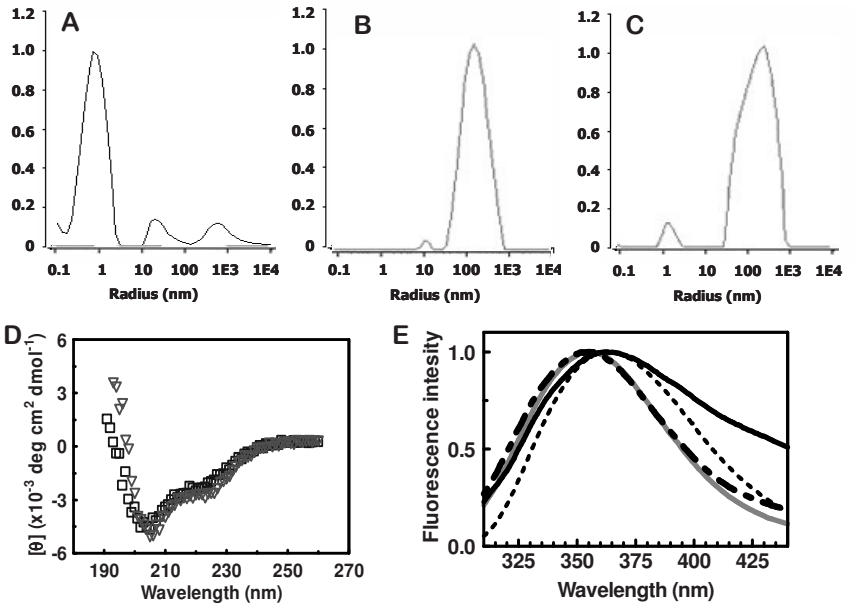

Figure 5. Stability of the SA2 assembly in presence of SDS. DLS analysis of SDS in aqueous solution (A), the SA2 peptide (0.1 mM) assemblies in absence (B) or in co-existence with SDS (35 mM) micelles (C). D. Circular dichroism analysis of the SA2 peptides (0.5 mM) in presence (triangles) or absence (blocks) of SDS (8.2 mM). E. Normalized tryptophan fluorescence of SA2 (0.1 mM) peptide vesicles (dashed line), and in co-existence with SDS (35 mM) micelles (grey line). As a control, tryptophan fluorescence of the SA2 peptides, forced to molecularly intermix with SDS is shown (solid line), in addition to NATA as a reference (dotted line).

To now confirm that the addition of SDS to already assembled peptide vesicles did not result in spontaneous molecular intermixing of both self-assembling molecules, the Trp fluorescence of peptide vesicles and SDS co-added was investigated. As can be seen in Figure 5E, the Trp fluorescence of the peptide vesicles after addition of SDS (dashed line) was comparable to the Trp fluorescence of the assemblies without SDS (solid grey line). The Trp fluorescence contrasts the Trp fluorescence of the SDS and SA2 peptides forced to intermix (solid line, see text below), suggesting a lack of spontaneous insertion of significant amounts of SDS into the peptide vesicles in agreement with the DLS data (Fig. 5C). The data are in anology to the independent assembly of surfactants and low molecular weight hydrogelators, the latter shown to form

intermolecular hydrogen bonds in their assembly by X-ray diffraction [203, 204]. Independent molecular assembly of the SA2 peptides and SDS micelles indicates that an additional intermolecular interaction stabilizes the peptide assemblies, different from those involved in SDS assembly.

For forced intermixing of SDS with the peptides, both the peptides and SDS were diluted in methanol. DLS measurements showed full disintegration of the SA2 peptide assemblies in methanol (results not shown). By gentle evaporation a film was created. After hydration of the SA2 peptides and SDS film, successful molecular intermixing was suggested by changes of the supramolecular assemblies formed as well as the fluorescence profile of the Trp. Using optical particle size analysis, large structures of sizes up to 10 μm were detected in the dispersions and the molecular intermixing resulted in a red-shift of the SA2 Trp fluorescence (Fig. 5E). The λ_{max} of the peptide SDS mixture (365 nm) corresponded to the λ_{max} of NATA (365 nm, Table 1). The increase in polarity of the environment of Trp can have various causes, like an increased fraction of the dissolved peptides, proximity of the negatively charged SDS molecules to the Trp in the intermixed system, or an increased hydration of the Trp microenvironment by the SDS intermixing.

Solvent effects on the peptide assembly

To examine the presence of intermolecular hydrogen bonds within the peptide assemblies, the colloidal stability of the peptide assemblies in different solvents was monitored by DLS. The results of the DLS analyses are shown in Table 2. As a reference, the mean count rate of the SA2 vesicles in water was 850 kcps, displaying a mean particle radius of 65 nm and a relatively low particle polydispersity. When the particles were injected in THF significant particle light scattering was observed, and DLS analysis showed a comparable mean particle size combined with an even lower particle polydispersity as compared to the peptide vesicles water. Peptide vesicles also remained after addition of acetonitrile or ethanol with a moderate increase (ethanol) or decrease (acetonitrile) in average particle radius as compared to the peptide vesicles in water, which may be related to considerable differences in electrostatic interactions induced by the change of solvent. As the scattering intensity relates to the difference between the refractive index of the particle and the solvent, the

absolute scattering intensities can not be directly compared. However, the observed maintenance (THF) or increase (acetontrile, ethanol) of significant light scattering signal, as well as the absence of any large (aggregated) structures both indicated pronounced stability of the assemblies in the tested solvents. Clearly, the solvents acetonitrile, ethanol and THF were not able to disrupt the peptide assembly, whereas the tested solvents all caused complete disintegration of negatively charged EPG liposomes (data not shown).

Table 2. Stability of the peptide assemblies in different solvents examined by dynamic light scattering

	Water	THF	Acetonitrile	Ethanol	DMF	DMSO
Mean count rate (kcps)	850	650	1450	1540	70	65
radius (nm)	65	74	38	98	No correlation	No correlation
Particle polydispersity	0.28	0.23	0.24	0.12	-	-

Kcps - kilocounts per second; THF - Tetrhydrofuran; DMF - N,N-dimethylformamide; DMSO – Dimethylsulfoxide

DMF and DMSO are good hydrogen bond breaking solvents [205] and therefore these solvents were used subsequently to investigate the presence of any stabilizing intermolecular hydrogen bonds in the peptide vesicles. Upon injecting the peptide vesicles in DMF or DMSO, scattering intensity was immediately lost, and background scattering was observed only (Table 2). Clearly, these hydrogen bond breaking solvents instantaneously disintegrated the peptide assemblies. These findings are an additional indication that the peptide assemblies are stabilized by intermolecular hydrogen bonds in addition to hydrophobic interactions.

Molecular dynamics

SA2 peptide assemblies were also investigated by molecular dynamics. Using periodic boundary conditions 18 peptides were simulated for 15 ns in the all-atom Amber 99 force field. Firstly, in analogy to the classical lipid bilayer model, a peptide bilayer in which two sets of 9 parallel peptides face each other at the

hydrophobic tail ends was used. This particular peptide bilayer conformation was unstable (Fig. 6A, B). Both monolayers dissociated over time and individual peptides became more disordered. In contrast, when peptides were arranged in an interdigitated manner with respect to the hydrophobic blocks (Fig. 6C), the peptide arrangement remained stable throughout 15 ns simulations (Fig. 6D). The degree of insertion of the hydrophobic blocks was optimal when the hydrophilic head protruded 4.5 Ångstrom out from the peptide membrane. In the hydrophobic domain of the interdigitated layer, the peptides remained flexible and the hydrophobic tails of the peptides retained a small but significant degree of conformational freedom (Fig. 6D), characteristic of an amorphous assembly. Lateral movement along the peptide interdigitated layer surface was minimal and was restricted by the bulkiness of amino acid side chains, and the conical shape of the SA2 peptides may further contribute to efficient peptide packing.

Although it is known that current force fields are suboptimal for the simulation of the PPII conformation in non-proline containing peptides [87, 206, 207], the PPII conformation in assembled form was present for approximately 1/3 of the amino acids throughout the simulations. In contrast, when a monomeric SA2 peptide was simulated in water, the PPII conformation was fully lost within 1.0 ns (data not shown), underscoring the significance of the assembled state for the PPII peptide conformation.

In agreement with experimental data (Chapter 3 of this thesis), the peptides lacked extended α-helical or β-sheeted conformations. These two conformations would saturate the hydrogen bond abilities of the peptides backbone by the well defined intra- (α-helix) or intermolecular (β-sheet) hydrogen bond patterning. However, the PPII conformation leaves the amide and carbonyl in the peptide backbone open for intermolecular interaction. Indeed, the molecular simulations showed significant hydrogen bonding between the peptides. Within the hydrophobic domain (Ac-Ala-Ala-Val-Val-Leu-Leu-Leu-Trp) of the 18 peptides in the simulation the total number of hydrogen bonds fluctuated around 8 (Fig. 7A), so that on average 16 out of 18 peptides were hydrogen bonded to another peptide within the hydrophobic domain.

After 7.5 ns simulation the number of water molecules located in the peptide hydrophobic domain was stable (Fig. 8). The water molecules in between the hydrophobic tails were found to bind the peptide backbones and frequently these bound water molecules directly bridged two peptides together (Fig. 7C). Such peptide – water – peptide bridges were markedly stable, lasting up to 3 nanoseconds. The binding of these water molecules is in contrast with the stability of hydrogen bonds among water molecules that typically switch positions within < 0.5 ps [208]. On average 19 of such water bridges were present (2.1 for each peptide) in the hydrophobic domain (Fig. 7B). Thus, each of these SA2 peptides were on average involved in at least 3.0 hydrogen bonds in the hydrophobic domain by either direct intermolecular hydrogen bonds or single water molecules mediated intermolecular hydrogen bonds and bridges involving 2 or more water molecules were found as well. Moreover, hydrogen bonds and stable water bridges occurred as well intramolecularly, which can be expected to further reduce the energetic penalty of peptide backbone desolvation.

Other computational simulations have demonstrated that similar amphiphilic oligopeptides (Ac-V_6D) indeed can form a stable spherical mesoscale assembly [48]. A tail-to-tail peptide layer was used in these simulations and the simulations did not involve water molecules [48]. Our findings underscore that the presence of water is indeed crucial for the correct modeling of the interactions that stabilize the peptide assemblies. Overall, the presence of hydrogen bonds in the hydrophobic domain significantly contributes to the stability of the SA2 peptide vesicles.

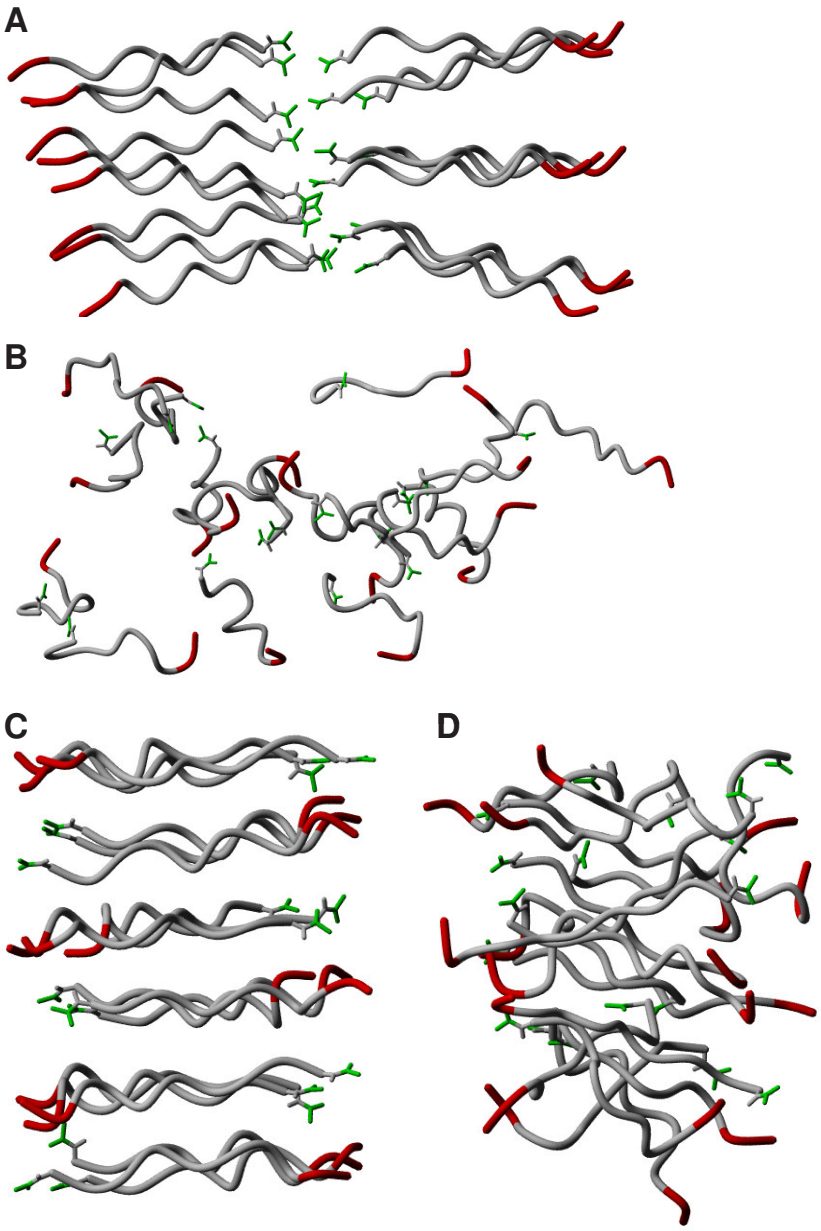

Figure 6. Snapshots of 18 peptides (tube display) before and after simulation. The tail-to-tail bilayer (A, B) and the interdigitated peptide layer (C, D) at start after energy minimization and simulated annealing (A, C) and after 15 ns simulation (B, D). Glutamic acids are displayed in red, peptide ends (acetyl) in green. For clarity, water molecules and counter ions were removed before constructing the snapshots.

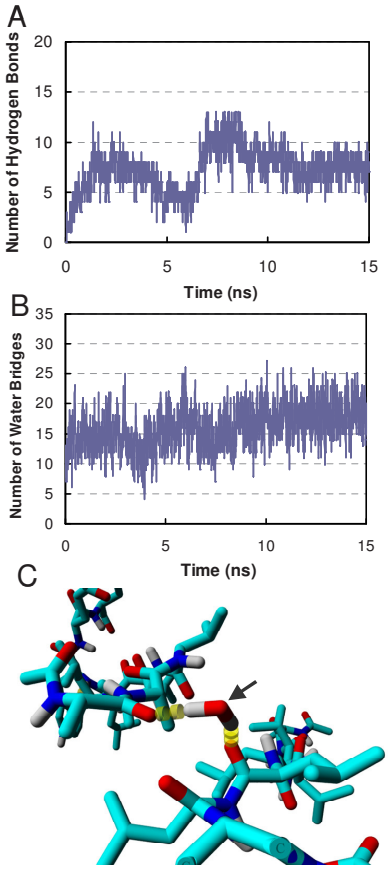

←Figure 7. Intermolecular hydrogen bonding within the hydrophobic domain of 18 SA2 peptides. A. Time profile of number of peptide backbone-backbone hydrogen bonds in between the peptides. B. Time profile of the number of single water molecules bridging two peptide backbones by hydrogen bonding. C. Close-up view in the hydrophobic domain of the peptide assembly. The depicted water molecule (arrow) bridged two peptides by hydrogen bonding. For clarity other water molecules are not depicted. Colouring: red is oxygen, blue is nitrogen, white is hydrogen and hydrogen bonds are indicated as yellow dashed lines.

↓Figure 8. Average number of water molecules (blocks, left y-axis) in a sliding window crossing the interdigitated peptide membrane. A. At 7.5 ns simulation stage. B. At 15 ns simulation (end) stage. The glutamate side chains (triangles, rigth y-axis) are indicated as a reference.

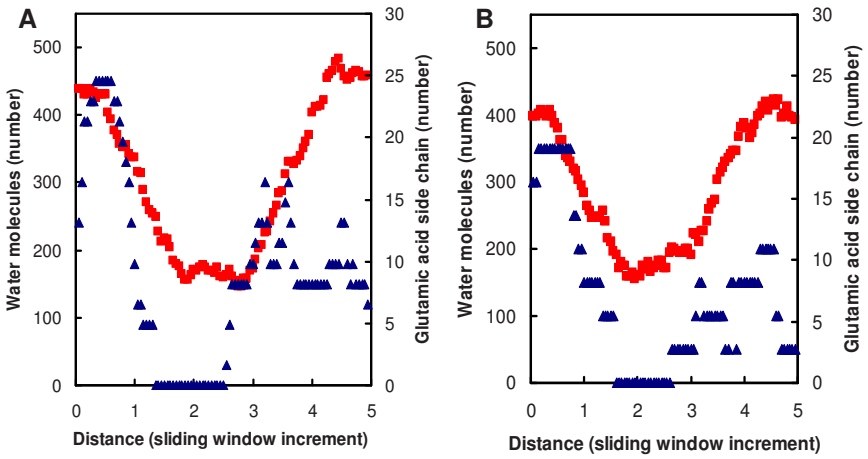

Conclusion

The described results provide insight into the intermolecular interactions that govern the SA2 peptide assembly and shed light onto the dynamic character of such oligopeptide membrane. As may be expected from their design, hydrophobic forces play a significant role in the oligopeptide assembly. The hydrophobic domain was shown to closely resemble the polarity of negatively charged lipid bilayers. In the oligopeptide vesicles Trp residues located at the hydrophobic-hydrophilic interface of the peptides significantly sense the presence of water molecules surrounding the charged glutamic acid residues. The anionic glutamic acids efficiently shield the Trp for the iodide quencher, indicating a molecular organization in which the glutamic acids expose outward to the bulk water. In addition, both the experimental findings and the molecular dynamics simulations demonstrated that peptide backbone hydrogen bonds additionally stabilize the oligopeptide vesicles. Within the interdigitated peptide membrane water molecules are significantly present in the hydrophobic domain and these water molecules are involved in stably bridging peptides by hydrogen bonding. In summary, additional to hydrophobic interactions, intermolecular hydrogen bonding stabilizes the oligopeptide-vesicle assembly, either directly between peptide backbones or mediated by bridging water molecules.

Acknowledgements

We thank dr. Aurelie Brizard and prof. dr. Jan van Esch from the Technical University Delft for valuable discussion.

Chapter 6

Peptide vesicles for the intracellular delivery of drugs

Albert J van Hell

Marjan M Fretz

Daan JA Crommelin

Wim E Hennink

Enrico Mastrobattista

Department of Pharmaceutics, Utrecht Institute for Pharmaceutical Sciences, Utrecht University, The Netherlands

To be submitted

Abstract

Previously we have shown that recombinantly produced amphiphilic oligopeptides with amino acid sequence Ac-Ala-Ala-Val-Val-Leu-Leu-Leu-Trp-Glu-Glu-COOH spontaneously assemble into nano-sized vesicles. Moreover, such peptide vesicles could be stabilized by introducing multiple cysteine residues within the hydrophobic domain of these amphiphilic oligopeptides, allowing the formation of intermolecular disulfide bridges. In this study, the cellular association and internalization of such vesicle-forming peptides was assessed. Furthermore, the potential of these vesicle-forming peptides as delivery system for photosensitizers was explored. It was demonstrated that the water-insoluble phthalocyanine (Zn-Pt-NH_2) could be quantitatively entrapped within the hydrophobic domains of these peptide vesicles. Flow cytometry and confocal laser-scanning microscopy showed, that vesicle-forming peptides were internalized by cells predominantly via adsorptive pinocytosis. To exclude the possibility that peptide vesicles disintegrate into monomeric peptides before cellular internalization, the intracellular localization of fluorescently-labeled peptides and the entrapped phthalocyanine was monitored by multiphoton microscopy. It was demonstrated that the peptides co-localized with the phthalocyanine, suggesting intact cellular internalization. Upon illumination, the phthalocyanine-containing oligopeptide vesicles showed an active photodynamic response towards the cells resulting in effective cell killing. In contrast, the free phthalocyanine or empty peptide vesicles did not show any cytotoxicity. In conclusion, we have demonstrated that peptide vesicles can be used to deliver photosensitizers into cells in culture resulting in effective cell killing after irradiation with visible light.

Introduction

Recently, the self-assembling behavior of lipid-like peptides has been exploited for the controlled formation of nano-sized objects [37, 50, 157]. Dependent on their amino acid sequence, these peptides spontaneously form either tubes (e.g. G_8D_2) or vesicles (Ac-Ala-Ala-Val-Val-Leu-Leu-Leu-Trp-Glu-Glu-COOH; SA2), exhibiting diameters of 40-60 nm [47, 50]. Moreover, by introducing multiple cysteine residues into the hydrophobic domain of the SA2 peptides, the formed peptide vesicles can be conveniently stabilized via disulfide bond formation in between the peptides (Chapter 3 of this thesis).

Oligopeptide vesicles can potentially be used in a variety of applications, including drug delivery [7-9, 12, 212]. The potential advantages of such vesicles as drug delivery systems are numerous. Firstly, peptides made of natural amino acids are mostly likely enzymatically degradable and consequently do yield natural amino acids as non-toxic degradation products. Secondly, peptides can adopt a secondary conformation or can change their structure in response to the environment (pH or temperature), which may be used as a trigger for destabilization of the vesicles [50, 213]. Thirdly, peptide ligands can be conveniently incorporated into the hydrophilic domain of the self-assembling peptides allowing cell-specific targeting without the need for chemical modifications of the carrier or ligand [53, 55, 59]. So far, oligopeptide vesicles have not been studied as a drug delivery vehicle. Two recent reports have demonstrated that (poly-)peptide vesicles can efficiently translocate into the cytosol using (poly)arginines in the hydrophilic block [51, 142]. However, whether such peptide vesicles can be used to deliver drugs or other pharmacologically active compounds into the cell's interior has not been investigated. The aim of this study was to determine the interaction with cells *in vitro* of non-functionalized oligopeptide vesicles. In addition, it was studied whether these peptide vesicles can be used to deliver hydrophobic drugs into cells and establish an active therapeutic response. For this, we used phthalocyanines, which are clinically used as photosensitizers for treatment of various diseases and hold promise for cancer treatment [214-216]. However, the poor water solubility of the highly aromatic molecules hinders their intravenous application and therefore such drugs profit in particular from entrapment in nanoparticles [217].

Results and Discussion

In order to assess cytotoxicity of the vesicle-forming peptides, *in vitro* cultured COS-7 cells were incubated for 6 hours with the crosslinked (SA2C3; Ac-Ala-Cys-Val-Cys-Leu-Cys-Leu-Trp-Glu-Glu-COOH) and non-crosslinked peptide (SA2; Ac-Ala-Ala-Val-Val-Leu-Leu-Leu-Trp-Glu-Glu-COOH) vesicles after which cell viability was determined. Both types of vesicle-forming peptides showed no inhibitory effects on cell growth up to 100 μM peptide concentrations. Compared to the PBS control, cells incubated with SA2 or SA2C3 showed a significant higher viability ($P<0.05$), particularly for the non-crosslinked peptide vesicles 6 hours after adding the peptides (Fig. 1). At the highest tested concentration (100 μM) of the crosslinked vesicles the cell viability slightly declined, but still remained indifferent from the PBS control ($P<0.05$), showing that the peptide vesicles are non-cytotoxic within the tested concentration range.

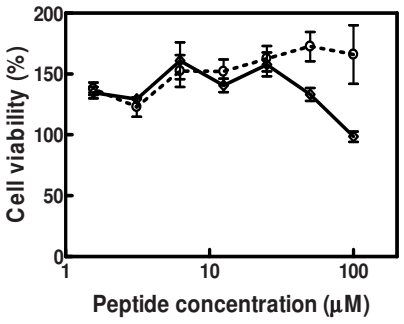

Figure 1. Relative cell viability 6 hours after addition of different concentrations of the crosslinked (diamonds, filled lined) and the non-crosslinked (circles, dotted line) peptide vesicles to COS-7 cells as compared to addition of buffer (PBS). Experiments were performed in triplicate.

AF633-labeled SA2C3 peptide vesicles were used for cellular uptake studies. Two tumor cell lines (C26, COS-7) as well as a primary human vascular endothelial cell line (HUVEC) were incubated with the SA2C3 vesicle-forming peptides at different concentrations for 2 hours at 37°C prior to analysis by flow cytometry to determine cell-associated peptide fluorescence. As can be seen in Figure 2, all three cell lines showed a shift in fluorescence of the mean cell population upon incubation with the fluorescently labeled peptides. Moreover, the association of the peptides with the cells (either in free form or assembled in vesicles) was not influenced by the presence of serum components (Fig. 2E). The cellular fluorescence was not due to traces of free label present in the vesicle dispersions, as incubations with high concentrations (50 μM) of free label resulted

in minor cellular fluorescence intensity as compared to the fluorescence shift by the peptide vesicles (Fig. 2F). The cellular association was observed for the general cell population, although a small subset of cells could be detected that showed a more extensive (almost two orders of magnitude) or off-scale fluorescence (Fig. 2A, B). Further studies are needed to identify this subset of cells and the observation may be related to the divisional state of the cells.

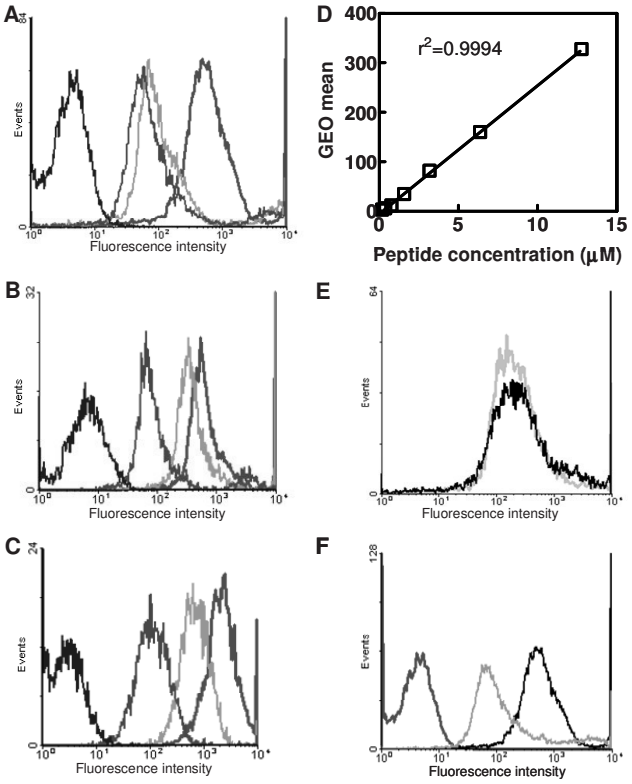

Figure 2. Cellular association of the vesicle-forming peptides, analyzed by flow cytometry. Increasing amounts of fluorescently labelled peptide vesicles were incubated at 37°C with COS-7 (A), C26 (B) and HUVEC (C) cells, and compared to the cells without peptide vesicles. The histograms (from left to right) display cell-associated fluorescence after incubation without, with 1.3, 2.9 and 6.0 µM SA2C3 peptide vesicles, respectively. D. The increase in geometric (GEO) mean cell-associated fluorescence intensity showed a linear correlation with the concentration of peptide vesicles added to the cells (r^2 =0.9994). E. COS-7 cells with vesicle-forming SA2C3 peptides in presence (grey) or absence of (black) 10% serum. F. From left to right: untreated cells, free label (50 µM), and vesicle forming SA2C3 (2.9 µM), incubated for 1 hour at 37°C with COS-7 cells.

Using a concentration series of the vesicle-forming peptides, the correlation of the mean cell-associated fluorescence intensity to peptide concentration is plotted in Figure 2D. Over the range of tested concentrations a linear correlation with the cell fluorescence intensity was observed. Typically, cellular association by means of active receptor-mediated binding displays a sigmoidal curve, and therefore the linearity observed in Figure 2 suggests a receptor-independent process, although it cannot be excluded that at higher peptide concentrations, saturation of cellular uptake may occur.

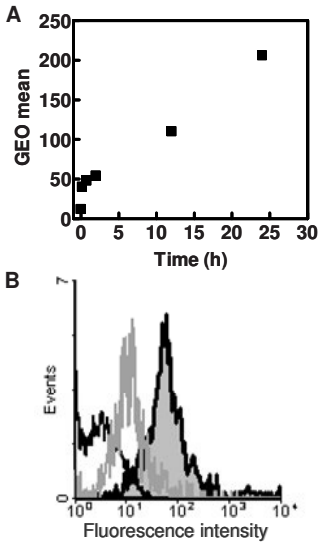

Figure 3. A. Time dependency of cellular association of SA2 peptides with COS-7 cells, analyzed by flow cytometry. Cells were incubated with peptide vesicles over different time periods at 8.0 µM peptide concentration. The geometrical mean of cell-associated fluorescence is plotted against incubation time. B. Washing of the cells directly after addition of the peptide vesicles already revealed a marked shift of the fluorescent cell population, as is shown in the grey line. As a reference, cells incubated without peptide vesicles (black line, empty) and cells incubated with the same concentration of peptide vesicles for 2 hours (black line, filled).

Figure 3 shows that the cellular fluorescence increased upon increased incubation time. Addition of the vesicle-forming peptides to cells directly followed by extensive washing of the cells to remove unbound vesicle-forming peptides, resulted already in an increase in cellular fluorescence. The shift of the cell population (Fig. 3B; grey curve) indicated that cellular association of the vesicle-forming peptides is very rapid, suggesting non-specific adsorption of the vesicle-forming peptides onto the cell membrane.

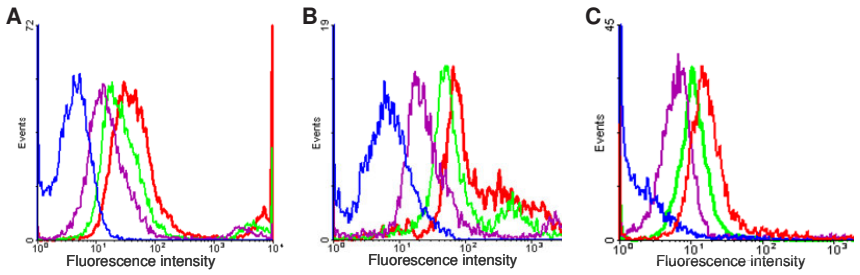

Figure 4. Cell association of the vesicle-forming SA2C3 peptides after 1 hour incubation at 0°C with COS-7 (A), C26 (B) and HUVEC (C) cells. The purple, green and red histograms display cell-associated fluorescence observed after incubation with 1.3, 2.9 and 6.0 μM peptide concentration, respectively. Cells in suspension were washed with ice-cold PBS and analyzed by flow cytometry. The blue histogram represents control cells, not incubated with fluorescently labeled SA2-peptides. The purple, green and red histograms represent cells incubated with increasing concentrations of SA2C3 peptides.

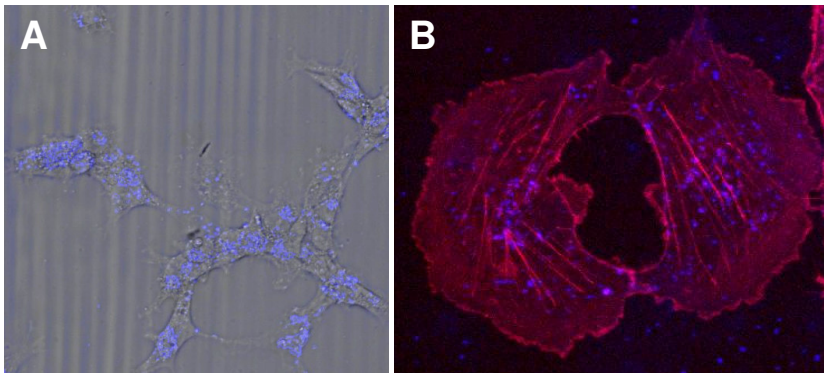

Figure 5. Cellular uptake of the SA2C3 peptides (4.0 μM) after 2 hours incubation of peptides with COS-7 at 37°C in serum-free medium. A. Differential interference contrast image and confocal fluorescence image with the peptide fluorescence in blue. B. Z-stacked fluorescence confocal micrograph of two cells stained for the actin cytoskeleton (purple) with the peptides labeled in blue.

To confirm cellular binding of the vesicle-forming SA2C3 peptides, incubations were performed on ice. All three cell lines showed a significant fluorescent shift of the cell population after 1 hour incubation (Fig. 4), as compared to the cells without peptide vesicles (blue lines). The fluorescence shift was peptide concentration dependent, as increasing concentrations of peptide resulted in an increase in cell-associated fluorescence (purple, green and red lines). These results show that cell binding of vesicle-forming SA2C3 peptides occurs.

To study the cellular internalization of SA2C3 peptide vesicles, cells were analyzed by confocal laser-scanning microscopy (CLSM). Many spots of peptide fluorescence (blue) were observed associated with the cells, as is shown in Figure 5A. Actin-cytoskeleton stained cells (Fig. 5B) were used to scan the confocal plane over the z-axis of the cells, which confirmed the intracellular localization of the peptide assemblies. As is also visible from Figure 5B, the fluorescence was spread throughout the cell (with the exception of the nucleus). The peptide fluorescence was present in a dotted pattern, characteristic for an endosomal compartmentalization. The observed fluorescence was not due to the presence of traces of free label, as incubations with high concentrations of free fluorophore (50 μM) resulted in vague background fluorescence intensity as well as the fluorescence uniformly spread throughout the cells.

To investigate whether the internalization of the vesicle-forming SA2C3 peptides was receptor-independent as suggested by the cytometry experiments (Fig. 2D), transferrin co-localization with the peptides was examined by CLSM. Transferrin is rapidly taken up via clathrin-coated pits by receptor-mediated endocytosis [172, 218, 219]. After co-incubation both the fluorescently labeled peptides (blue, Fig. 6) and the transferrin (green) were visualized by confocal microscopy. While both the peptide vesicles and transferrin could be traced intracellularly, co-localization of fluorescence was not observed (Fig. 6B), indicating that clathrin dependent internalization was not a major route of uptake. In contrast, when a marker for receptor independent endocytosis was used, i.e. fluorescently labeled dextran 10 000, extensive co-localization with the peptides was found (Fig. 6B). Characteristically, pinocytosis (fluid-phase uptake) including macropinocytosis is directly proportional to the concentration of the solute the cells are exposed to [172],

as was reported before for the peptide vesicles in Figure 2D. Adsorptive pinocytosis, due to aspecific association with cells, which was observed for the peptides (Fig. 3, Fig. 4) explains the relatively efficient cellular uptake of the peptide vesicles, for example when compared to uptake of negatively charged liposomes [172, 220]. Taken together, the data demonstrate that the SA2C3 peptides are internalized via aspecific pinocytotic uptake routes. In contrast, negatively charged liposomes were found to enter cells via clathrin coated pits [220].

In figures 2-6 it was demonstrated that vesicle-forming SA2C3 peptides bind to and are taken up by different cell types. As the vesicles are stabilized by covalent crosslinking it is expected that these peptides are presented to the cells as vesicles rather than monomeric peptides and are taken up as such. To prove the vesicular nature of the peptides when taken up by cells in culture, an essentially water-insoluble zinc-phthalocyanine was entrapped in the peptide vesicles. This molecule requires a micellar or vesicular carrier for cellular delivery as the free phthalocyanine precipitates in aqueous media. Hydration of a film of only the phthalocyanine resulted in a blue precipitate and clear supernatant due to its limited aqueous solubility (Fig. 7A). In contrast, when a film composed of the phthalocyanine and the self-assembling peptides were hydrated, a clear blue dispersion was obtained with the peptide vesicles (Fig. 7A). The size (distribution) of the peptide vesicles did not increase by the presence of the phthalocyanine as was shown by dynamic light scattering.

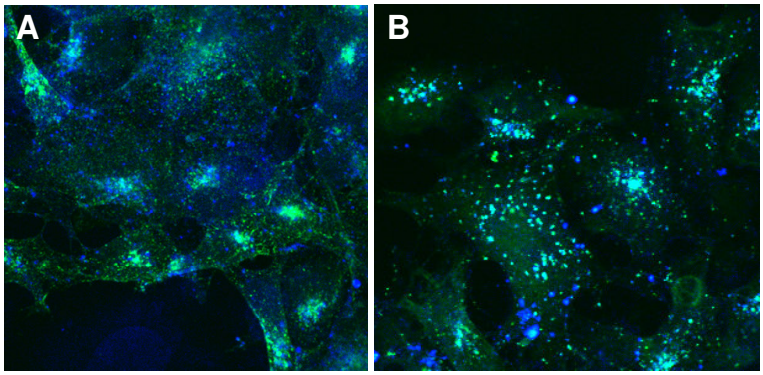

Figure 6. Route of uptake of the vesicle-forming SA2C3 peptides. A. Co-localization of the peptides (blue) with transferrin, a marker for receptor-mediated endocytosis (green) was absent in COS-7 cells. B. Co-incubation with dextran 10 000, a marker for fluid-phase endocytosis (green) resulted in multiple spots of dotted patterned co-localization (cyan).

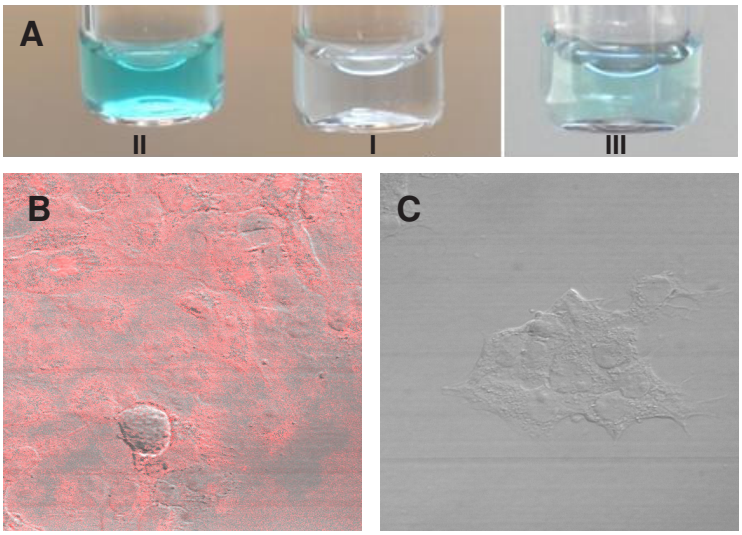

Figure 7. Entrapment of phthalocyanine in the peptide vesicles and delivery to cells. A. Zn-Pt -NH_2 was entrapped by hydration of a film of phthalocyanine and peptides in PBS. Non-crosslinked as well as disulfide crosslinked peptide vesicles were used to entrap the blue colored phthalocyanine, whereas peptides were left out as a control (PBS). The pictures show supernatants obtained after hydration of a film of Zn-Pt -NH_2 in the absence (I) or presence of SA2 (II) or SA2C3 (III) peptides and subsequent removal of precipitates by centrifugation B. Cell-associated phthalocyanine fluorescence (red) 2 hours after incubation with the phthalocyanine peptide vesicles. Results with the crosslinked vesicles are shown. As a control the cells were imaged that were incubated with free phthalocyanine (C). Micrographs were taken at identical exposure time and light intensity.

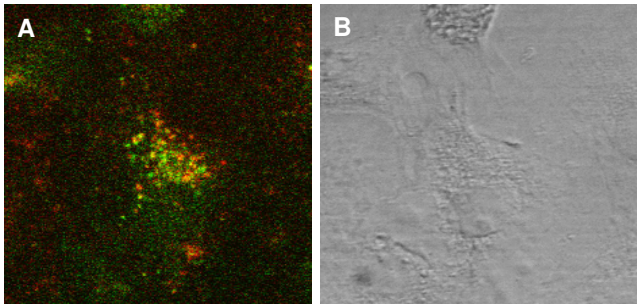

Figure 8. Co-localization of phthalocyanine with the peptides inside cells. A. Multiphoton excitation microscopy was performed on COS-7 cells internalizing the peptide assemblies (green) and the phthalocyanine (red). The multiple sites of co-localization of the phthalocyanine and the peptides are indicated in yellow. B. Corresponding differential interference contrast image.

Quantification of the entrapped phthalocyanine by UV-Vis absorbance measurements showed the quantative entrapment of the phthalocyanine. Further, UV-Vis spectroscopy analysis revealed absorbance band broadening (data not shown), indicative for location of phthalocyanines in hydrophobic domains [221]. As can be seen in Figure 7A, the phthalocyanine encapsulation in the crosslinked peptide vesicles was somewhat lower; approximately 50% of the phthalocyanine quantity was encapsulated (1.2 µg per 25 nmol peptide) as compared the non-crosslinked vesicles (2.2 µg phthalocyanine) at identical peptide quantities. Likely, the disulfide bridges in the hydrophobic domain may reduce the space available for entrapment of the relatively large phthalocyanine molecules.

It was investigated whether the loading of phthalocyanine in the SA2C3 peptide vesicles could result in effective cellular delivery of this poorly water-soluble compound. Since the zinc-phthalocyanine is not phototoxic towards cells, cytotoxic effects during analysis could be avoided. Utilizing the intrinsic fluorescent properties of the phthalocyanine, confocal microscopy revealed significant phthalocyanine fluorescence inside the cells when entrapped in the both the SA2 and SA2C3 (crosslinked) peptide vesicles, (Fig. 7B). In contrast, when the phthalocyanine was incubated with cells without the peptide vesicles as a carrier, at identical imaging and light exposure settings no cellular fluorescence was observed (Fig. 7C).

Subsequently, cellular co-localization of the entrapped phthalocyanine with the peptide assemblies was investigated. Multiphoton excitation fluorescence microscopy excites the fluorophores in the confocal plane of the excitation light beam, thereby enhancing signal-to-background ratio while reducing photo-damaging effects. As can be seen from Figure 8, both the peptides (green) and the phthalocyanine (red) were observed inside the cells and, as is evident from the yellow spots in Figure 8, the phthalocyanine clearly co-localized with the peptide assemblies. This co-localization demonstrates that peptide vesicles do not dissociate prior to cellular internalization as this would lead to loss of phthalocyanine fluorescence due to precipitation (see Fig. 7C). The dotted pattern of these spots of co-localization confirmed the endocytotic compartmentalization, as was observed earlier by the confocal microscopy investigations (Fig. 6).

Photodynamic therapy activates photosensitizers (PS) by illumination with visible light (670 nm), generating cytotoxic effects [215, 216]. In order to investigate these therapeutic relevant effects, a phototoxic, axially solketal-substituted silicon phthalocyanine [217, 221] was entrapped in the peptide vesicles and the PS-SA2 peptide dispersions were subsequently incubated with COS-7 cells. As is shown in Figure 9, incubation of COS-7 cells with the phthalocyanine-loaded peptide vesicles in the dark did not result in any cytotoxicity. Furthermore, incubation with different dilutions of free phthalocyanine showed no concentration dependent cytotoxic effect (Fig. 9). Importantly, by entrapping the PS inside SA2 peptide vesicles, a clear concentration dependent photodynamic effect was observed (open blocks). The phototoxic effect was evident already at low phthalocyanine concentrations (from 0.7 nM phthalocyanine onwards), resulting in IC_{50} values of about 2.8 nM phthalocyanine. The observed photodynamic effect of this PS using peptide vesicles as carriers is comparable to previously reported delivery vehicles of this photosensitizer (IC_{50} 3.2 nM, in 10% serum) [217, 221]. These polymeric micelles were not significantly taken up by cells, and merely exerted their therapeutic effect via indirect delivery routes [221]. Our data demonstrate that the peptide vesicles actively contribute to the delivery of the poorly water-soluble photosensitizer inside the cells, establishing efficient photodynamic effects *in vitro*.

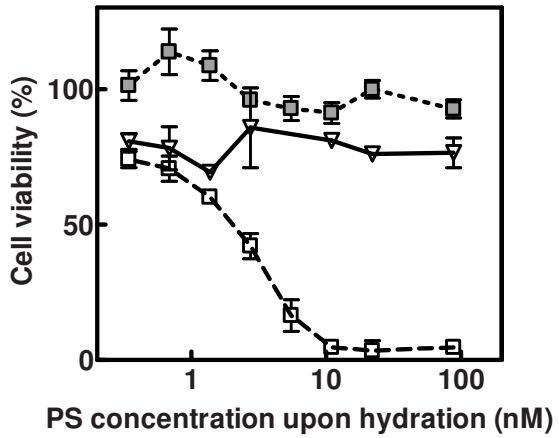

Figure 9. COS-7 cell viability after 6 hours incubation the SA2 peptide vesicles loaded with phthalocyanine and subsequent infrared (670 nm) illumination (open squares). Cell viability after incubation with the phthalocyanine loaded oligopeptide vesicles without illumination (filled squares) and, as an additional control, dilution series of the phthalocyanine without peptide vesicles were incubated with the cells and subsequently illuminated (triangles).

Conclusions

In this study it was demonstrated that oligopeptide vesicles bind to different cell lines *in vitro* resulting in effective cellular internalization. Cellular adsorptive pinocytosis routes provide explanation for the efficient process of vesicle internalization. The vesicle-forming peptides did not show any cytotoxicity at the concentration range tested. Co-entrapment of an otherwise water-insoluble phthalocyanine resulted in effective intracellular delivery of this photosensitizer with clear co-localization of the PS and peptides inside endocytic compartments, which strongly suggests that peptide vesicles do not dissociate prior to internalization. Overall, the data demonstrate that the oligopeptide vesicles successfully function as a carrier for the cellular delivery of hydrophobic drugs.

Materials and Methods

Materials

All chemicals were purchased from Sigma (Zwijndrecht, The Netherlands), unless indicated otherwise.

Peptide production

Peptides were produced using recombinant DNA technology in *E. coli* as previously described (Chapter 2). Briefly, the dsDNA encoding the peptides was cloned in frame with a SUMO gene, facilitating expression and purification [65]. After expression in cells of *E. coli* BL21(DE3), the peptide attached to the SUMO protein was purified using Ni-NTA affinity purification and subsequently cleaved off the SUMO protein by incubation with SUMO protease. Purification of the peptides from the SUMO and SUMO protease was performed either by a second Ni-NTA affinity purification (non-crosslinked) or size exclusion chromatography (crosslinked), and peptides were N-terminally acetylated.

Peptide labeling

The peptides were labeled by covalent coupling of an AlexaFluor 633 C5-Maleimide fluorophore (Invitrogen, Carlsbad, USA) to the thiols within the hydrophobic domain of the SA2C3 peptides. Typically, 150 nmol of peptide was reduced (20 mM DTT, 20 mM sodium phosphate, pH 8.0, 1 hour, 45°C). The peptides were acid-precipitated by addition of 1.0 M HCl until pH <1.5, centrifuged for 10 minutes at 13 000 xg, and the peptide pellet was rehydrated in 20 mM degassed phosphate buffer, pH 7.0, and argon was applied on top. From a freshly prepared stock solution in water, the label was added to a peptide sample in a 1:50 (label:peptide) molar ratio. After overnight reaction (4°C, argon) the AlexaFluor C5-Maleimide was quenched by addition of DTT to a 20 mM concentration and 1 hour incubation at room temperature. Subsequently, the peptides were acid-precipitated to remove the DTT and the residual label, and the peptide pellet was washed in 10 mM HCl, until no fluorescence could be detected in the supernatant (typically after two washing steps). Peptides were rehydrated in sterile PBS (164 mM NaCl, 140 mM Na_2HPO_4, 11 mM NaH_2PO_4, pH 7.4) and exposed to air for 1 hour for intermolecular crosslinking. Efficient labeling was verified by fluorescence measurements on the peptide vesicles and GPC analysis confirmed minimal amounts of free label (<10%). Dynamic light scattering in DMF

was performed to confirm intermolecular crosslinking of the vesicles, which was shown to fully disrupt peptide vesicles without intermolecular disulfide crosslinks (Chapter 3 of this thesis).

Cell culture

COS-7 and C26 cells were cultured in Dulbecco's modified Eagle's medium (Gibco, Breda, The Netherlands), supplemented with 10% (v/v) fetal calf serum, 100 units/ml penicillin, 100 µg/ml streptomycin, 5 mM glucose and 4 mM L-glutamine. Human umbilical vein endothelial cells (HUVECs) were cultured in endothelial cell growth medium-2 (Cambrex, East Rutherford, USA) consisting of EBM-2 medium supplemented with an EGM-2 bullet kit (containing growth factors, 2% FBS, and antibiotics). Cells were maintained in a water-saturated atmosphere containing 5% CO_2 at 37°C.

Cell viability

Cells were incubated for 6 hours with the peptide in serum-free medium at 37°C, after which the cells were washed twice in PBS. Serum-containing medium was added and next day the cell viability was determined by a colorimetric XTT assay (Sigma-Aldrich, St. Louis, USA), according to the manufacturers instructions.

Flow cytometry

For cellular association studies, cells were detached from the culture flask by trypsin/EDTA solution (0.05% (w/v) trypsin and 0.02% (w/v) EDTA in PBS). 1×10^5 cells were incubated either for 2 hours at 37°C or for 1 hour on ice (COS-7 and C26) or at 4°C (HUVEC) with different concentrations of peptide vesicles. HUVEC cells incubated at 37°C were detached after peptide incubation. Cells were washed twice by centrifugation (300 ×g, 5 min, 4°C) and addition of 1 ml cold PBS. After centrifugation, the cells were resuspended in 400 µl PBS and analyzed by flow cytometry using a FACSCalibur (Becton&Dickinson, Mountain View, USA).

Confocal laser scanning microscopy

COS-7 cells were cultured on 16 wells glass slides to 70-80% confluency. Cells were washed in PBS, changed to serum-free medium and incubated for 2 hours with 4.0 µM of the peptide vesicle. Transferrin Alexafluor 488 (Invitrogen) or dextran 10 000 Alexafluor 488 (fixable, Invitrogen) were added 2 hours after

addition of the peptide vesicles, and co-incubated with the peptide vesicle for an additional 4 hours. Cells were fixed (10 min in 4% (w/v) paraformaldehyde in PBS), and mounted in Fluorsave Reagent (Invitrogen). Actin was stained for 20 minutes with Phalloidin 568 (Invitrogen) after fixing of the cells. Samples were examined with a Leica TCS-SP confocal laser scanning microscope equipped with a 488 nm Argon, 568 nm Krypton and 647 nm HeNe laser.

Cellular delivery of phthalocyanines and photodynamic effects

For imaging studies a non-phototoxic zinc phthalocyanine ($ZnPcNH_2$, MW 759) kindly provided by prof. dr. Torres (Universidad Autónoma de Madrid, Spain) was used. Typically, 25 nmol of the SA2 and reduced SA2C3 peptides was diluted in methanol (90% methanol, 10 % water) to which 2.0 µg phthalocyanine was added (from a 10 mg/ml THF stock solution, final volume THF < 1%). Solvents were gently evaporated and the resulting film was hydrated in 100 µl PBS. For the SA2C3 during hydration anearobic conditions were maintained, after which crosslinked was achieved by air-exposure for 16 hours. The samples were centrifuged (13 000 xg, 10 minutes) twice to remove unencapsulated phthalocyanine. 4.0 µM of the peptide vesicles were incubated with COS-7 cells for 2 hours in serum-free culture medium.

For photodynamic effects on cells a photoactive axially solketal-substituted silicon phthalocyanine was used, synthesized as described before [217]. A film of 50 nmol of SA2 peptides and 2.0 µg of the phthalocyanine (from a methanol stock solution) were hydrated in 100 µl sterile PBS, after which the samples were centrifuged twice (13 000 xg, 10 minutes). Dilution series of the peptide vesicles entrapping the silicon phthalocyanine were made in PBS and subsequently incubated with COS-7 cells in serum free medium for 6 hours. After incubation, the cells were washed extensively and illuminated for 10 minutes using a 37°C water-thermostated 96 LED lamp device at a 3.5 mW/cm^2 light intensity (670 ± 10 nm), as described previously by Hofman et al [217]. The cells in serum containing medium were incubated overnight at 37°C under a 5% CO_2 atmosphere. The cell viability was determined by a XTT assay, as described above. For determination of the IC_{50} value viability of the non-illuminated cells incubated with the vesicles entrapping the phthalocyanine were set as 100% and quantification of the silicon phthalocyanine entrapped in the non-crosslinked

peptide vesicles was performed by UV606 absorbance measurements in methanol, using dilution series of silicon phthalocyanine in methanol.

Multiphoton microscopy

A Radiance 2100MP multiphoton excitation microscope (Bio-Rad, Hemel Hempstead, United Kingdom) equipped with a Nikon TE300 inverted microscope (Nikon, Tokyo, Japan) was used for imaging. Two hours after incubation of the COS-7 cells with the zinc-phtalocyanine entrapped in SA2C3 peptide vesicles labelled with AlexaFluor 488, cells were fixed and mounted as described above. Excitation of the phtalocyanine and the AlexaFluor 488 was achieved by multiphoton excitation at 780 nm using a mode-locked Titanium:Sapphire laser (Tsunami; Spectra Physics, San Jose, CA) pumped by a 10-W solid state laser (Millennia Xs; Spectra Physics). Samples were viewed using a 40x/1.3 oil objective (Nikon, Tokyo, Japan). Images were recorded and analyzed using LaserSharp 2000 software (Bio-Rad).

Acknowledgements

We wish to thank Anko de Graaf (Department of Biochemistry and Cell Biology, Veterinary Medicine, Utrecht University) for his help on the multiphoton microscopy and prof. dr. Torres (Department of Organic Chemistry, Universidad Autónoma de Madrid, Spain) for kindly providing the zinc-phthalocyanine.

Chapter 7

Summary and Perspectives

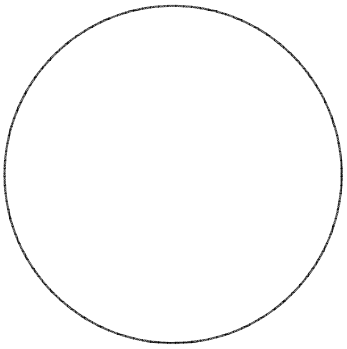

Albert J van Hell

Department of Pharmaceutics, Utrecht Institute for Pharmaceutical Sciences, Utrecht University, The Netherlands

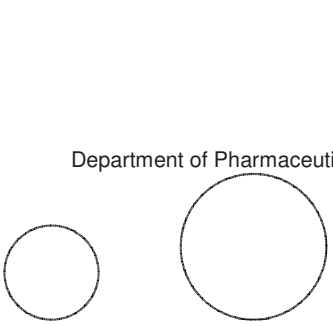

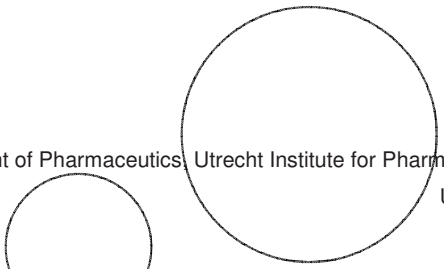

1. Summary

The aim of this thesis was to design amphiphilic peptides that self-assemble into supramolecular structures, like nano-sized vesicles that can be of use for drug delivery purposes. Detailed analysis of the obtained self-assembled, vesicular structures has provided insight into their characteristics. This will guide the design of further studies on oligopeptide vesicles.

In order to obtain self-assembling peptides that form nano-sized vesicles, amphiphilic oligopeptides were designed and produced by recombinant techniques (Chapter 2). The 8 amino acid hydrophobic block exhibits a conical shape, in which the amino acid side chains increased in size towards the hydrophilic domain. The length of the hydrophilic block was varied, from 25% (SA2) to 50% (SA7) mass fraction of the hydrophilic block. As an alternative to solid-phase synthesis, these peptides were produced by recombinant techniques. By using a small hydrophilic fusion protein the recombinant route of production of such amphiphilic peptides is feasible without causing premature degradation inside *E. coli*, as is often the case with recombinant production of small peptides lacking tertiary structures. The yield of SA peptides after purification was typically 6 mg out of 1 liter high density fermentation culture (25 g of bacteria, dry cell weight). Electron microscopy, static light scattering and calcein entrapment assays showed that both SA2 and SA7 peptides spontaneously assemble into nano-sized vesicles (Chapter 2). Thus, within the chosen range self-assembly of the oligopeptides into vesicles is insensitive to the hydrophobic:hydrophilic block length ratio. The peptide self-assembly into relatively monodisperse vesicles takes place spontaneously in aqueous solutions at physiological pH and is insensitive to salt concentrations up to physiological values. Moreover, exposure to low pH causes aggregation and precipitation of peptides, which was fully reversible upon increasing the pH to neutral values.

In order to stabilize these amphiphilic oligopeptide vesicles by crosslinking, either two or three cysteines were introduced in the hydrophobic domain of the oligopeptides. Dynamic light scattering showed that the introduction of 2 or 3 cysteines did not affect the self-assembling behavior of the oligopeptides

(Chapter 3). The intermolecular crosslinking by disulfide bond formation rendered the oligopeptide vesicle stable under disruptive conditions, such as injection into dimethylformamide. Due to the enhanced stability of the crosslinked vesicles, their size distribution could be more closely examined. Whereas dynamic light scattering showed average sizes of the assemblies between 60 and 120 nm in radius, atomic force microscopy, negative stain and cryogenic electron microscopy all demonstrated a lower average size of 10 to 30 nm. The overestimation of average size by dynamic light scattering is explained by the much greater contribution of larger particles to the overall light scattering compared to smaller particles. The vesicular architecture was further demonstrated by both static light scattering, showing an Rg /Rh ratio which is typical for vesicles, and encapsulation of the hydrophilic molecule calcein, which was released from the peptide vesicles slowly over time.

Insight into the secondary structure of peptides is critical for understanding their self-assembling behavior. Circular dichroism and Fourier transform infrared spectroscopy showed that, when assembled into vesicles, the oligopeptides exhibit the polyproline type II (PPII) conformation as their predominant intramolecular organization (Chapter 4). The addition of chaotropic salts like guanidinium which is known to stabilize existing PPII conformations did not disrupt the peptide self-assembled structure, which further underscores the significance of the PPII conformation for oligopeptide assembly. If these SA peptides adopt beta-sheets the self-organization of the peptides was disrupted, and the peptides aggregated into large structures, and precipitated from the solution.

Unlike the alpha-helix and the beta-sheet, the PPII is a flexible conformation that leaves the peptide's backbone hydrogen bond donors and acceptors open for intermolecular interaction. The aim of chapter 5 was to investigate the intermolecular interactions that stabilize the peptide vesicles. Fluorescence analysis using hydrophobic fluorescent probes and the tryptophan in the peptides assemblies demonstrated the formation of a hydrophobic domain in the peptide vesicles. The polarity of the hydrophobic domain is comparable to that in negatively charged phospholipid bilayers. Both experimental data and molecular

dynamics simulation demonstrated that intermolecular hydrogen bonds and water bridges in the hydrophobic domain additionally stabilize the peptide assemblies. The presence of residual water in the hydrophobic compartment is critical for the peptide self-organization and dehydration of the assemblies resulted in irreversible peptide aggregation.

In Chapter 6 the feasibility to use these peptide vesicles as a drug carrier were tested on cells in culture. Cell viability assays showed that both the crosslinked and the non-crosslinked oligopeptide vesicles were well-tolerated by cultured cells. The negatively charged oligopeptides are internalized by the cells via receptor-independent routes, most likely via non-specific adsorptive pinocytosis. Besides hydrophilic molecules (Chapter 2 and 3), the oligopeptide vesicles could entrap hydrophobic phthalocyanines. As shown by co-localization using multiphoton microscopy, the vesicles could co-deliver the phthalocyanines inside the cells. Due to the poor aqueous solubility of these compounds, photosensitizers require a delivery into cells, and it was demonstrated for the first time that peptide vesicles could be used as a delivery system for photosensitizers resulting in an active photodynamic effect towards cells in culture

In summary, this thesis demonstrates that amphiphilic oligopeptides can be designed to spontaneously self-organize into nano-sized vesicles. The predominant (> 90% in number) size of such vesicles is between 20 and 60 nm in diameter. The intramolecular organization of these peptides is dominated by the flexible PPII conformation, which leaves the hydrogen bond capabilities of the peptide backbone open for intermolecular hydrogen bonding. The peptide assembly is indeed stabilized by intermolecular hydrogen bonding in the hydrophobic domain, in addition to hydrophobic interactions, which is in contrast to many other nanovesicles like liposomes and polymersomes whose self-assembly is solely driven by amphiphilicity. The oligopeptide vesicles can be conveniently crosslinked in the hydrophobic domain using cysteines. The peptide vesicles hold promise, for example, as a drug carrier to actively deliver drug molecules like phthalocyanines into cells.

2. Perspectives

In this thesis we report on the assembly of amphiphilic oligopeptides into vesicles. Selection of the proper peptide sequence or additive stabilizing molecules can adjust vesicle characteristics. In chapter 3 it is shown that by introducing multiple cysteine residues within the hydrophobic domain of the SA peptides, stabilization of the peptide vesicles could be obtained by covalently crosslinking of the peptides within the vesicle assembly. The insights into the intermolecular interactions (Chapter 5) and peptide secondary conformation (Chapter 4) may facilitate further optimization of SA peptide design in order to obtain favorable characteristics of the peptide assemblies required for a specific application. The peptide vesicles like the ones described in this thesis (crosslinked, non-crosslinked) hold promise for delivery of hydrophobic drug molecules (Chapter 6) - other applications, such as delivery of small hydrophilic drugs, might require further optimization of the vesicle characteristics.

Optimization of vesicle characteristics

The successful use of oligopeptide vesicles for the delivery of hydrophilic small molecular weight drugs might first require a decrease in the vesicle membrane permeability. Different strategies may be opted for to achieve the optimization of this particular vesicle characteristic. First, the barrier function of the peptide membrane may be enhanced by increasing the hydrophobicity of the peptide itself. For example, one or multiple phenylalanines can be introduced in the peptide sequence. Different self-assembling peptides containing two phenylalanines in the peptide sequence have been shown to pack remarkably tight and rigid, most likely due to the π-π stacking of the benzenes [10, 38, 41]. Incorporation of phenylalanine(s) in the currently described oligopeptides may therefore significantly enhance the stability and reduce the permeability of oligopeptide vesicles. Given the fact that in the interdigitated membrane the least hydrophilic part is in the middle of the peptide (Chapter 5), this location may be optimal, and the introduction of a phenylalanine there leaves the conical geometry of the peptides unaffected.

Alternatively, for further stabilization SA2 and SA2C2 peptides could be derivatized at their N-termini or, in case of SA2C2, by a thiol linkage with benzyl

or naphtyl groups. Preliminary data on the behavior of the N-terminal benzylated SA2 peptide indeed showed that addition of the benzyl moiety increases the apolarity of the hydrophobic peptide domain and lowered the critical aggregation concentration. Also, various modifications of the peptides may be feasible using natural enzymes. Significant increase of hydrophobicity via palmitoylation or myristoylation by amide or thiol linkage is frequently found in nature and could be readily applied on the recombinantly produced SA peptides as well [222].

Longer hydrophobic peptide segments could be selected to optimize vesicle characteristics, as they may enhance favorable secondary peptide conformations. Indeed, it was shown that a 20 leucine hydrophobic block adopts an alpha-helical conformation in the peptide vesicle membrane and decreases the permeability of small hydrophilic molecules. Longer domains may yield vesicles that are even completely impermeable to salt molecules [28, 39].

Importantly, increase in peptide length coincides with increase in vesicle size. Amphiphilic polypeptides of 200 amino acids display 1000-fold larger vesicles than the oligopeptide vesicles reported in this thesis: about 40 µm in diameter [28]. As our findings show that small peptides of 10 amino acids form vesicles of 20-60 nm, variation of the peptide length, may steer the peptide vesicle size. This may be subject of future studies.

In the oligopeptide membrane water molecules play an important role by stably bridging peptide backbones (Chapter 5), which explains the high degree of permeability observed for small hydrophilic molecules like calcein (Chapter 3). In order to energetically stabilize the peptide membrane and reduce its permeability, an alternative substitute for water may be added to bridge two peptide backbones by hydrogen bonding in the hydrophobic domain. In lipid membranes, cholesterol enhances the barrier function as it decreases the permeability of the membrane. Addition of cholesterol to the amphiphilic oligopeptides may already reduce the permeability of the oligopeptide vesicles. In addition, the hydrophobic molecule added to the peptide membranes may function as a hydrogen bond donor and acceptor, capable of bridging two peptide backbones together. Examples include

sterols that, besides their hydroxyl hydrogen bond donor additionally contain an amide hydrogen bond acceptor [223].

Secondary conformation and vesicle characteristics

The secondary peptide conformation plays a major role in establishing the desired supramolecular characteristics of peptide assemblies [39]. PPII conformations (Chapter 4) as well as alpha-helical peptides [39] occur in peptide vesicles. The alpha-helix is rod-like and therefore a more rigid conformation as compared to the flexible PPII conformation of non-proline containing oligopeptides [96]. Hydrophobic peptide segments of an alpha-helical conformation expose their apolar residues outward with a defined periodicity of 3.6 amino acid residues per turn of 360°. By their well defined patterning of intramolecular hydrogen bonding, the ability for water molecules to penetrate and interact with the peptides backbone may be expected to be reduced significantly. Therefore, membrane permeability of self-assembling oligopeptides vesicles may be attuned by adopting different degrees of alpha-helical conformations by selecting amino acids with a high helical propensity (e.g. alanines) in their hydrophobic block.

Although mainly unexplored so far, also beta-sheeted peptides may be of interest for peptide vesicle assembly. As a general consideration, the balance of the hydrophobic interactions and the directional hydrogen bonds in the oligopeptides are expected to be essential for the vesicular architecture. If no beta-sheet breaking amino acids are present (like proline) and the peptide exhibits too much hydrophobicity, the strong hydrophobic collapse may force the hydrogen bonds in between the peptide backbones to induce beta-sheet formation. Notably, the beta-sheet is a cooperative conformation and typically results in strong peptide aggregation or fibrilization. [224]

Similar to the PPII conformation but unlike the alpha-helix conformation, beta-sheets allow the formation of intermolecular hydrogen bonding. In contrast to the PPII conformation, the beta-sheets form hydrogen bonds in a well-defined pattern, thereby stabilizing the assembly more rigidly. A combination of short beta-sheet sequences interchanged with proline sequences may be studied as a well-defined partial beta-sheet forming peptides that allow vesicle self-assembly and prevent fibril formation.

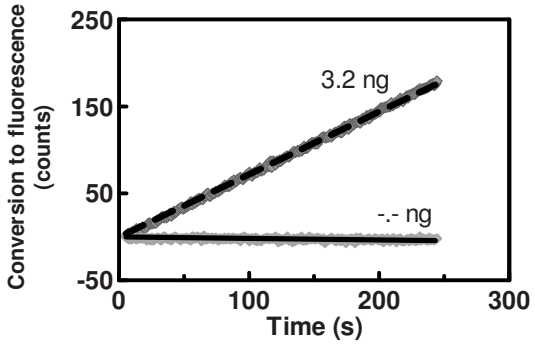

Figure 1. Protection of ß-galactosidase inside SA2 peptide vesicles against trypsin digestion. Acid precipitated SA2 peptides (50 µM) were allowed to assemble into vesicles by hydrating with a solution of 200 µg/ml of ß-galactosidase. As a control, ß-galactosidase was added to already assembled vesicles (solid line). After 24 hours of trypsin cleavage (7.5 mg/ml) conversion of fluorescein-di-3-D-Galactopyranoside into fluorescein by ß-galactosidase was monitored. The amount of entrapped ß-galactosidase was quantified using the Fluorescein-di-3-D-Galactopyranoside conversion rate and compared with a calibration curve of know amounts of β-galactosidase.

Applications of oligopeptide vesicles

The oligopeptides vesicles studied in this thesis could entrap hydrophobic phthalocyanines (Chapter 6) and larger hydrophilic molecules, like enzymes. For example, beta-galactoside can be stably entrapped and shielded from the environment over extended periods of time (Figure 1). As the peptide vesicle membranes are very permeable for small hydrophilic molecules (see Chapter 3), the entrapped enzymes could still convert substrates into product. Therefore, a possible application of these oligopeptide vesicles may be to serve as protective cages in which enzymes are protected from being degraded or opsonized by antibodies after local or systemic administration.

The small size of the oligopeptide vesicles (Chapter 3) renders them promising drug carriers for penetration into diseased tissues, like cancer or inflamed tissue. Penetration into such tissues is critically affected by particle size, as particles larger than 50 nm poorly diffuse into tumors [126, 170]. The amphiphilic oligopeptides studied in this thesis spontaneously assemble into vesicles of sizes below 40 nm, without the need for downsizing by extrusion or sonication (Chapter 2 and 3).

However, the small size of vesicles negatively affects the loading capacity for drugs into the hydrophilic interior. In order to overcome drug loading problems, efficient coupling of drug molecules using small linker systems can be investigated, like the recently developed platinum linker system [225]. The methione residue required for this type of linker system is readily introduced in the peptide sequence, for example as a part of its hydrophilic domain.

The vesicle-forming nature of these oligopeptides may also present a platform for vaccine development. Multivalent presentation of multiple antigens, or highly repetitive patterns of single antigens both are known to significantly enhance immune responses [226-228]. Oligopeptide vesicles can be used to present antigens, either before vesicle assembly by direct extension of the peptide sequence with antigenic peptide sequences or after vesicle formation by coupling antigens for example with amines or thiols that constitute the hydrophilic block. Immunostimulating molecules can be added as well, e.g. muramyl di- or tripeptide derivatives and modified lipopolysaccharides.

In Chapter 2 it is shown that the vesicular architecture is relatively insensitive to variations in the length of the hydrophillic domain, which is in contrast to many other polymeric vesicles [128]. Our findings demonstrate that in peptide vesicles the hydrophilic : hydrophobic block length ratio can be varied from 1:4 up to 1:1 [138]. Other reports on polypeptide showed that this hydrophilic : hydrophobic ratio can even be further extended up to 3:1 [39, 229]. As a consequence, the hydrophilic domain may be conveniently used to incorporate functional peptide sequences, for example cellular targeting sequences. Recently, two independent reports demonstrated that peptide vesicles can be functionalized as they showed that vesicle forming peptides, containing membrane translocation (polyarginine) sequences in the hydrophilic domain, retain their biofunctionality in assembly and indeed rapidly translocated over cellular membranes [51, 142]. Moreover, hydrophilic peptide sequences may function as stealth coatings of the nano-carriers to enhance *in vivo* circulation kinetics [230-232] and the hydrophobic domain of the peptides may be used to incorporate pH-triggered endosomal escape sequences [126, 233].

In conclusion, this thesis describes the first steps for peptide based, nano-sized drug delivery systems with a wide variety of physico-chemical characteristics and which may readily incorporate biofunctionalities. Modification of the vesicle characteristics is guided by the insights in the intermolecular peptide interactions offering rational optimization strategies for further peptide and vesicle membrane design.

References

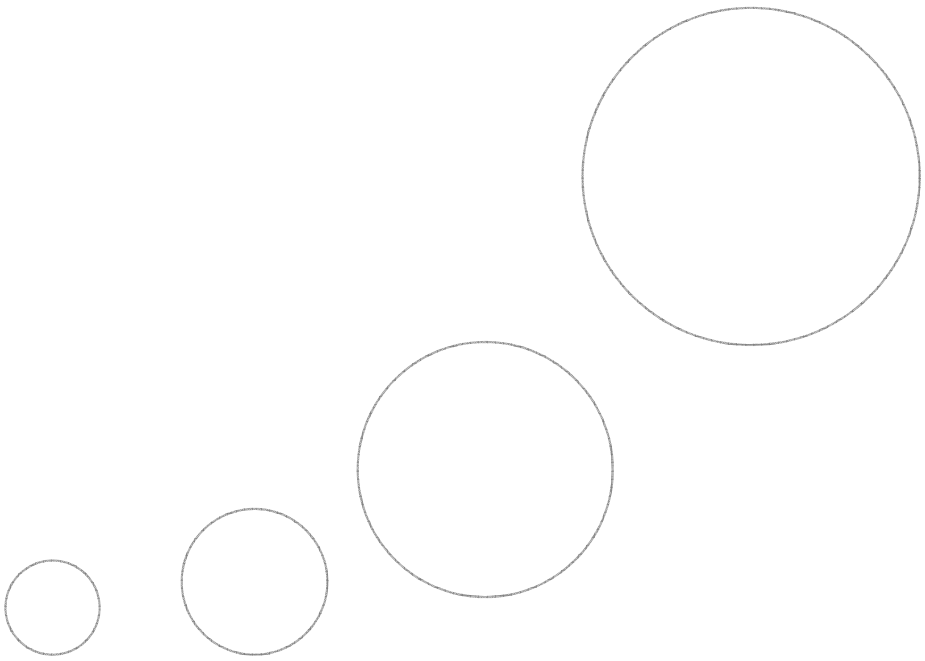

1. Whitesides GM, Mathias JP and Seto CT (1991) **Molecular Self-Assembly and Nanochemistry - a Chemical Strategy for the Synthesis of Nanostructures**. *Science* 254(5036): p1312-1319.

2. Whitesides GM and Grzybowski B (2002) **Self-assembly at all scales**. *Science* 295(5564): p2418-21.

3. Davis AV, Yeh RM and Raymond KN (2002) **Supramolecular assembly dynamics**. *Proceedings of the National Academy of Sciences of the United States of America* 99(8): p4793-6.

4. Menger FM (2002) **Supramolecular chemistry and self-assembly**. *Proceedings of the National Academy of Sciences of the United States of America* 99(8): p4818-4822.

5. Lendlein A and Kelch S (2002) **Shape-memory polymers**. *Angewandte Chemie-International Edition* 41(12): p2034-2057.

6. Cordier P, Tournilhac F, Soulie-Ziakovic C and Leibler L (2008) **Self-healing and thermoreversible rubber from supramolecular assembly**. *Nature* 451(7181): p977-980.

7. Stadler B, Bally M, Grieshaber D, Voros J, Brisson A and Grandin HM (2006) **Creation of a functional heterogeneous vesicle array via DNA controlled surface sorting onto a spotted microarray**. *Biointerphases* 1(4): p142-145.

8. Dirksen A, Langereis S, de Waal BFM, van Genderen MHP, Hackeng TM and Meijer EW (2005) **A supramolecular approach to multivalent target-specific MRI contrast agents for angiogenesis**. *Chemical Communications* (22): p2811-2813.

9. Nahrendorf M, Zhang H, Hembrador S, Panizzi P, Sosnovik DE, Aikawa E, Libby P, Swirski FK and Weissleder R (2008) **Nanoparticle PET-CT Imaging of Macrophages in Inflammatory Atherosclerosis**. *Circulation* 117(3): p379-387.

10. Reches M and Gazit E (2003) **Casting metal nanowires within discrete self-assembled peptide nanotubes**. *Science* 300(5619): p625-7.

11. Santoso SS, Vauthey S and Zhang S (2002) **Structures, function and applications of amphiphilic peptides**. *Current Opinion in Colloid & Interface Science* 7(5-6 SU -): p262-266.

12. Ryadnov MG (2007) **A self-assembling peptide polynanoreactor**. *Angewandte Chemie-International Edition* 46(6): p969-972.

13. Meyer DE, Kong GA, Dewhirst MW, Zalutsky MR and Chilkoti A (2001) **Targeting a genetically engineered elastin-like polypeptide to solid tumors by local hyperthermia**. *Cancer Research* 61(4): p1548-54.

14. Heath JR and Davis ME (2008) **Nanotechnology and Cancer**. *Annual Review of Medicine* 59(1): p251-265.

15. Lee KB, Park SJ, Mirkin CA, Smith JC and Mrksich M (2002) **Protein nanoarrays generated by dip-pen nanolithography**. *Science* 295(5560): p1702-1705.

16. Piner RD, Zhu J, Xu F, Hong SH and Mirkin CA (1999) **"Dip-pen" nanolithography**. *Science* 283(5402): p661-663.

17. Bansiddhi A, Sargeant TD, Stupp SI and Dunand DC (2008) **Porous NiTi for bone implants: A review**. *Acta Biomaterialia* 4(4): p773-782.

18. Coviello T, Matricardi P, Marianecci C and Alhaique F (2007) **Polysaccharide hydrogels for modified release formulations**. *Journal of Controlled Release* 119(1): p5-24.

19. Lasic DD and Needham D (1995) **The "Stealth" liposome: A prototypical biomaterial**. *Chemical Reviews* 95(8): p2601-2628.

20. Langer R and Tirrell DA (2004) **Designing materials for biology and medicine**. *Nature* 428(6982): p487-92.

21. Goldberg M, Langer R and Jia XQ (2007) **Nanostructured materials for applications in drug delivery and tissue engineering**. *Journal of Biomaterials Science-Polymer Edition* 18(3): p241-268.

22. Megeed Z, Haider M, Li D, O'Malley BW, Jr., Cappello J and Ghandehari H (2004) **In vitro and in vivo evaluation of recombinant silk-elastinlike hydrogels for cancer gene therapy**. *Journal of Controlled Release* 94(2-3): p433-45.

23. Haider M, Megeed Z and Ghandehari H (2004) **Genetically engineered polymers: status and prospects for controlled release**. *Journal of Controlled Release* 95(1): p1-26.

24. Zhang S, Marini DM, Hwang W and Santoso S (2002) **Design of nanostructured biological materials through self-assembly of peptides and proteins**. *Current Opinion in Chemical Biology* 6(6): p865-71.

25. Lowik DW and van Hest JC (2004) **Peptide based amphiphiles**. *Chemical Society Reviews* 33(4): p234-45.

26. Gazit E (2007) **Self-assembled peptide nanostructures: the design of molecular building blocks and their technological utilization**. *Chemical Society Reviews* 36(8): p1263-9.

27. Ulijn RV and Smith AM (2008) **Designing peptide based nanomaterials**. *Chemical Society Reviews* 37(4): p664-75.

28. Deming TJ (2007) **Synthetic polypeptides for biomedical applications**. *Progress in Polymer Science* 32(8-9): p858-875.

29. Ian WH (2007) **Peptide Fibrillization**. *Angewandte Chemie International Edition* 46(43): p8128-8147.

30. Colombo G, Soto P and Gazit E (2007) **Peptide self-assembly at the nanoscale: a challenging target for computational and experimental biotechnology**. *Trends Biotechnology*.

31. Zhang S (2002) **Emerging biological materials through molecular self-assembly**. *Biotechnology Advances* 20(5-6): p321-39.

32. Haines LA, Rajagopal K, Ozbas B, Salick DA, Pochan DJ and Schneider JP (2005) **Light-activated hydrogel formation via the triggered folding and self-assembly of a designed peptide**. *Journal of the American Chemical Society* 127(48): p17025-9.

33. Nagai Y, Unsworth LD, Koutsopoulos S and Zhang S (2006) **Slow release of molecules in self-assembling peptide nanofiber scaffold**. *Journal of Controlled Release* 115(1): p18-25.

34. Aggeli A, Bell M, Carrick LM, Fishwick CWG, Harding R, Mawer PJ, Radford SE, Strong AE and Boden N (2003) **pH as a trigger of peptide beta-sheet self-assembly and reversible switching between nematic and isotropic phases**. *Journal of the American Chemical Society* 125(32): p9619-9628.

35. Ryadnov MG and Woolfson DN (2003) **Introducing branches into a self-assembling peptide fiber**. *Angewandte Chemie-International Edition* 42(26): p3021-3.

36. Ryadnov MG and Woolfson DN (2005) **MaP peptides: programming the self-assembly of peptide-based mesoscopic matrices**. *Journal of the American Chemical Society* 127(35): p12407-15.

37. Vauthey S, Santoso S, Gong H, Watson N and Zhang S (2002) **Molecular self-assembly of surfactant-like peptides to form nanotubes and nanovesicles**. *Proceedings of the National Academy of Sciences of the United States of America* 99(8): p5355-60.

38. Kol N, Adler-Abramovich L, Barlam D, Shneck RZ, Gazit E and Rousso I (2005) **Self-assembled peptide nanotubes are uniquely rigid bioinspired supramolecular structures**. *Nano Letters* 5(7): p1343-1346.

39. Holowka EP, Pochan DJ and Deming TJ (2005) **Charged polypeptide vesicles with controllable diameter**. *Journal of the American Chemical Society* 127(35): p12423-8.

40. Ringler P and Schulz GE (2003) **Self-assembly of proteins into designed networks**. *Science* 302(5642): p106-9.

41. Reches M and Gazit E (2004) **Formation of Closed-Cage Nanostructures by Self-Assembly of Aromatic Dipeptides**. *Nano Letters* 4(4): p581-585.

42. Mahler A, Reches M, Rechter M, Cohen S and Gazit E (2006) **Rigid, Self-Assembled Hydrogel Composed of a Modified Aromatic Dipeptide**. *Advanced Materials* 18(11): p1365-1370.

43. Niu L, Chen X, Allen S and Tendler SJB (2007) **Using the Bending Beam Model to Estimate the Elasticity of Diphenylalanine Nanotubes**. *Langmuir* 23(14): p7443-7446.

44. Deming TJ (1997) **Facile synthesis of block copolypeptides of defined architecture**. *Nature* 390(6658): p386-9.

45. Nowak AP, Breedveld V, Pakstis L, Ozbas B, Pine DJ, Pochan D and Deming TJ (2002) **Rapidly recovering hydrogel scaffolds from self-assembling diblock copolypeptide amphiphiles**. *Nature* 417(6887): p424-8.

46. Zhang S, Holmes T, Lockshin C and Rich A (1993) **Spontaneous assembly of a self-complementary oligopeptide to form a stable macroscopic membrane**. *Proceedings of the National Academy of Sciences of the United States of America A* 90(8): p3334-8.

47. Santoso S, Hwang W, Hartman H and Zhang S (2002) **Self-assembly of surfactant-like peptides with variable glycine tails to form nanotubes and nanovesicles**. *Nano Letters* 2(7): p687-691.

48. Tsai CJ, Zheng J and Nussinov R (2006) **Designing a nanotube using naturally occurring protein building blocks**. *PLoS Computational Biology* 2(4): pe42.

49. Israelachvili J. (1991) **Intermolecular & surface forces**. Second ed.; Academic Press: London, p 366-394.

50. van Hell AJ, Costa CI, Flesch FM, Sutter M, Jiskoot W, Crommelin DJ, Hennink WE and Mastrobattista E (2007) **Self-assembly of recombinant amphiphilic oligopeptides into vesicles**. *Biomacromolecules* 8(9): p2753-61.

51. Yoon YR, Lim YB, Lee E and Lee M (2008) **Self-assembly of a peptide rod-coil: a polyproline rod and a cell-penetrating peptide Tat coil**. *Chemical Communications (Camb)* (16): p1892-4.

52. Holmes TC, de Lacalle S, Su X, Liu G, Rich A and Zhang S (2000) **Extensive neurite outgrowth and active synapse formation on self-assembling peptide scaffolds**. *Proceedings of the National Academy of Sciences of the United States of America* 97(12): p6728-33.

53. Narmoneva DA, Oni O, Sieminski AL, Zhang S, Gertler JP, Kamm RD and Lee RT (2005) **Self-assembling short oligopeptides and the promotion of angiogenesis**. *Biomaterials* 26(23): p4837-46.

54. Genove E, Shen C, Zhang S and Semino CE (2005) **The effect of functionalized self-assembling peptide scaffolds on human aortic endothelial cell function**. *Biomaterials* 26(16): p3341-51.

55. Semino CE (2008) **Self-assembling peptides: from bio-inspired materials to bone regeneration**. *Journal of Dental Research* 87(7): p606-16.

56. Schneider A, Garlick JA and Egles C (2008) **Self-assembling Peptide nanofiber scaffolds accelerate wound healing**. *PLoS ONE* 3(1): pe1410.

57. Zhang S, Holmes TC, DiPersio CM, Hynes RO, Su X and Rich A (1995) **Self-complementary oligopeptide matrices support mammalian cell attachment**. *Biomaterials* 16(18): p1385-93.

58. Salick DA, Kretsinger JK, Pochan DJ and Schneider JP (2007) **Inherent antibacterial activity of a peptide-based beta-hairpin hydrogel**. *Journal of the American Chemical Society* 129(47): p14793-14799.

59. Ellis-Behnke RG, Liang YX, You SW, Tay DK, Zhang S, So KF and Schneider GE (2006) **Nano neuro knitting: Peptide nanofiber scaffold for brain repair and axon regeneration with functional return of vision**. *Proceedings of the National Academy of Sciences of the United States of America* 103(13): p5054-9.

60. Adams DJ, Holtzmann K, Schneider C and Butler MF (2007) **Self-assembly of surfactant-like peptides**. *Langmuir* 23(25): p12729-36.

61. Baneyx F (1999) **Recombinant protein expression in Escherichia coli**. *Current Opinion in Biotechnology* 10(5): p411-21.

62. Makrides SC (1996) **Strategies for achieving high-level expression of genes in Escherichia coli**. *Microbiology Reviews* 60(3): p512-38.

63. LaBean TH and Kauffman SA (1993) **Design of synthetic gene libraries encoding random sequence proteins with desired ensemble characteristics**. *Protein Science* 2(8): p1249-54.

64. Kwon I, Kirshenbaum K and Tirrell DA (2003) **Breaking the degeneracy of the genetic code**. *Journal of the American Chemical Society* 125(25): p7512-3.

65. Marblestone JG, Edavettal SC, Lim Y, Lim P, Zuo X and Butt TR (2006) **Comparison of SUMO fusion technology with traditional gene fusion systems: enhanced expression and solubility with SUMO**. *Protein Science* 15(1): p182-9.

66. Young L and Dong Q (2004) **Two-step total gene synthesis method**. *Nucleic Acids Research* 32(7): pe59.

67. Fass R, Vandewalle M, Shiloach A, Joslyn A, Kaufman J and Shiloach J (1991) **Use of High-Density Cultures of Escherichia-Coli for High-Level Production of Recombinant Pseudomonas-Aeruginosa Exotoxin-A**. *Applied Microbiology and Biotechnology* 36(1): p65-69.

68. Malakhov MP, Mattern MR, Malakhova OA, Drinker M, Weeks SD and Butt TR (2004) **SUMO fusions and SUMO-specific protease for efficient expression and purification of proteins**. *Journal of Structural and Functional Genomics* 5(1-2): p75-86.

69. Baldwin RL (2003) **In search of the energetic role of peptide hydrogen bonds**. *Journal of Biological Chemistry* 278(20): p17581-8.

70. Guy HR (1985) **Amino acid side-chain partition energies and distribution of residues in soluble proteins**. *Biophysical Journal* 47(1): p61-70.

71. Sticke DF, Presta LG, Dill KA and Rose GD (1992) **Hydrogen bonding in globular proteins**. *Journal of Molecular Biology* 226(4): p1143-1159.

72. Papapostolou D, Smith AM, Atkins ED, Oliver SJ, Ryadnov MG, Serpell LC and Woolfson DN (2007) **Engineering nanoscale order into a designed protein fiber**. *Proceedings of the National Academy of Sciences of the United States of America* 104(26): p10853-8.

73. Ryadnov MG and Woolfson DN (2004) **Fiber recruiting peptides: noncovalent decoration of an engineered protein scaffold**. *Journal of the American Chemical Society* 126(24): p7454-5.

74. Ryadnov MG and Woolfson DN (2003) **Engineering the morphology of a self-assembling protein fibre**. *Nature Matererials* 2(5): p329-32.

75. Wagner DE, Phillips CL, Ali WM, Nybakken GE, Crawford ED, Schwab AD, Smith WF and Fairman R (2005) **Toward the development of peptide nanofilaments and nanoropes as smart materials**. *Proceedings of the National Academy of Sciences of the United States of America* 102(36): p12656-61.

76. Lamm MS, Rajagopal K, Schneider JP and Pochan DJ (2005) **Laminated morphology of nontwisting beta-sheet fibrils constructed via peptide self-assembly**. *Journal of the American Chemical Society* 127(47): p16692-700.

77. Haines-Butterick LA, Rajagopal K, Lamm M, Pochan DJ and Schneider JP (2007) **Controlling hydrogelation kinetics via peptide design for three-dimensional encapsulation and injectable delivery of cells**. *Biopolymers* 88(4): p518-518.

78. Aggeli A, Nyrkova IA, Bell M, Harding R, Carrick L, McLeish TC, Semenov AN and Boden N (2001) **Hierarchical self-assembly of chiral rod-like molecules as a model for peptide beta -sheet tapes, ribbons, fibrils, and fibers**. *Proceedings of the National Academy of Sciences of the United States of America* 98(21): p11857-62.

79. Aggeli A, Bell M, Boden N, Keen JN, Knowles PF, McLeish TC, Pitkeathly M and Radford SE (1997) **Responsive gels formed by the spontaneous self-assembly of peptides into polymeric beta-sheet tapes**. *Nature* 386(6622): p259-62.

80. Nagarkar RP, Hule RA, Pochan DJ and Schneider JP (2008) **De Novo Design of Strand-Swapped Beta-Hairpin Hydrogels**. *Journal of the American Chemical Society* 130(13): p4466-4474.

81. Aggeli A, Bell M, Boden N, Carrick LM and Strong AE (2003) **Self-assembling peptide polyelectrolyte beta-sheet complexes form nematic hydrogels**. *Angewandte Chemie-International Edition* 42(45): p5603-5606.

82. Woolfson DN and Ryadnov MG (2006) **Peptide-based fibrous biomaterials: some things old, new and borrowed**. *Current Opinion in Chemical Biology* 10(6): p559-567.

83. Hamley IW, Ansari IA, Castelletto V, Nuhn H, Rosler A and Klok HA (2005) **Solution self-assembly of hybrid block copolymers containing poly(ethylene glycol) and amphiphilic beta-strand peptide sequences**. *Biomacromolecules* 6(3): p1310-5.

84. Babin J, Rodriguez-Hernandez J, Lecommandoux S, Klok HA and Achard MF (2005) **Self-assembled nanostructures from peptide-synthetic hybrid block copolymers: Complex, stimuli-responsive rod-coil architectures**. *Faraday Discussions* 128: p179-192.

85. Vandermeulen GWM, Tziatzios C and Klok HA (2003) **Reversible self-organization of poly(ethylene glycol)-based hybrid block copolymers mediated by a De Novo four-stranded alpha-helical coiled coil motif**. *Macromolecules* 36(11): p4107-4114.

86. Schweitzer-Stenner R, Eker F, Griebenow K, Cao XL and Nafie LA (2004) **The conformation of tetraalanine in water determined by polarized raman, FT-IR, and VCD spectroscopy (vol 126, pg 2768, 2004)**. *Journal of the American Chemical Society* 126(34): p10794-10794.

87. Shi ZS, Chen K, Liu ZG and Kallenbach NR (2006) **Conformation of the backbone in unfolded proteins**. *Chemical Reviews* 106(5): p1877-1897.

88. Stapley BJ and Creamer TP (1999) **A survey of left-handed polyproline II helices**. *Protein Science* 8(3): p587-595.

89. Schweitzer-Stenner R, Measey T, Kakalis L, Jordan F, Pizzanelli S, Forte C and Griebenow K (2007) **Conformations of alanine-based peptides in water probed by FTIR, Raman, vibrational circular dichroism, electronic circular dichroism, and NMR spectroscopy**. *Biochemistry* 46(6): p1587-1596.

90. Shi Z, Olson CA, Rose GD, Baldwin RL and Kallenbach NR (2002) **Polyproline II structure in a sequence of seven alanine residues**. *Proceedings of the National Academy of Sciences of the United States of America* 99(14): p9190-5.

91. Ding L, Chen K, Santini PA, Shi ZS and Kallenbach NR (2003) **The pentapeptide GGAGG has PII conformation**. *Journal of the American Chemical Society* 125(27): p8092-8093.

92. Avbelj F, Grdadolnik SG, Grdadolnik J and Baldwin RL (2006) **Intrinsic backbone preferences are fully present in blocked amino acids**. *Proceedings of the National Academy of Sciences of the United States of America* 103(5): p1272-1277.

93. Kelly MA, Chellgren BW, Rucker AL, Troutman JM, Fried MG, Miller AF and Creamer TP (2001) **Host-guest study of left-handed polyproline II helix formation**. *Biochemistry* 40(48): p14376-14383.

94. Chen K, Liu ZG, Zhou CH, Shi ZS and Kallenbach NR (2005) **Neighbor effect on PPII conformation in alanine peptides**. *Journal of the American Chemical Society* 127(29): p10146-10147.

95. Chen K, Liu Z and Kallenbach NR (2004) **The polyproline II conformation in short alanine peptides is noncooperative**. *Proceedings of the National Academy of Sciences of the United States of America* 101(43): p15352-7.

96. Zagrovic B, Lipfert J, Sorin EJ, Millett IS, van Gunsteren WF, Doniach S and Pande VS (2005) **Unusual compactness of a polyproline type II structure**. *Proceedings of the National Academy of Sciences of the United States of America* 102(33): p11698-703.

97. Law B, Weissleder R and Tung CH (2006) **Peptide-based biomaterials for protease-enhanced drug delivery**. *Biomacromolecules* 7(4): p1261-5.

98. Kickhoefer VA, Garcia Y, Mikyas Y, Johansson E, Zhou JC, Raval-Fernandes S, Minoofar P, Zink JI, Dunn B, Stewart PL and Rome LH (2005) **Engineering of vault nanocapsules with enzymatic and fluorescent properties**. *Proceedings of the National Academy of Sciences of the United States of America* 102(12): p4348-52.

99. Geng Y, Dalhaimer P, Cai SS, Tsai R, Tewari M, Minko T and Discher DE (2007) **Shape effects of filaments versus spherical particles in flow and drug delivery**. *Nature Nanotechnology* 2(4): p249-255.

100. Verma A, Uzun O, Hu Y, Hu Y, Han H-S, Watson N, Chen S, Irvine DJ and Stellacci F (2008) **Surface-structure-regulated cell-membrane penetration by monolayer-protected nanoparticles**. *Nature Materials* 7(7): p588-595.

101. Ferrari M (2005) **Cancer nanotechnology: Opportunities and challenges**. *Nature Reviews Cancer* 5(3): p161-171.

102. Ferrari M (2008) **Nanogeometry: Beyond drug delivery**. *Nature Nanotechnology* 3(3): p131-132.

103. Kim KY (2007) **Nanotechnology platforms and physiological challenges for cancer therapeutics**. *Nanomedicine* 3(2): p103-10.

104. McKee TD, Grandi P, Mok W, Alexandrakis G, Insin N, Zimmer JP, Bawendi MG, Boucher Y, Breakefield XO and Jain RK (2006) **Degradation of fibrillar collagen in a human melanoma xenograft improves the efficacy of an oncolytic herpes simplex virus vector**. *Cancer Research* 66(5): p2509-2513.

105. Yuan F, Leunig M, Huang SK, Berk DA, Papahadjopoulos D and Jain RK (1994) **Microvascular permeability and interstitial penetration of sterically stabilized (stealth) liposomes in a human tumor xenograft**. *Cancer Research* 54(13): p3352-6.

106. van Etten B, ten Hagen TLM, de Vries MR, Ambagtsheer G, Huet T and Eggermont AMM (2002) **Prerequisites for effective adenovirus mediated gene therapy of colorectal liver metastases in the rat using an intracellular neutralizing antibody fragment to p21-Ras**. *British Journal of Cancer* 86(3): p436-442.

107. Saleh N, Koner AL and Nau WM (2008) **Activation and stabilization of drugs by supramolecular pK(a) shifts: Drug-delivery applications tailored for cucurbiturils**. *Angewandte Chemie-International Edition* 47(29): p5398-5401.

108. Duncan R and Sat YN (1998) **Tumour targeting by enhanced permeability and retention (EPR) effect**. *Annals of Oncology* 9: p39-39.

109. Schiffelers RM, Molema G, Ten Hagen TLM, Janssen APCA, Schraa AJ, Kok RJ, Koning GA and Storm G (2002) **Targeting of liposomes to angiogenic endothelial cells**. *Cellular & Molecular Biology Letters* 7(2): p255-255.

110. Leckband D and Israelachvili J (2001) **Intermolecular forces in biology**. *Quarterly Reviews of Biophysics* 34(2): p105-267.

111. Crommelin DJ and Storm G (2003) **Liposomes: from the bench to the bed**. *Journal of Liposome Research* 13(1): p33-6.

112. Israelachvili J, Mitchell D and Ninham B (1976) **Theory of self-assembly of hydrocarbon amphiphiles into micelles and bilayers**. *Journal of chemical society, Faraday Transactions 2* 72(12): p1525-1568.

113. Lasic DD (1998) **Novel applications of liposomes**. *Trends in Biotechnology* 16(7): p307-321.

114. Drummond CJ and Fong C (1999) **Surfactant self-assembly objects as novel drug delivery vehicles**. *Current Opinion in Colloid & Interface Science* 4(6): p449-456.

115. Schreier H and Bouwstra J (1994) **Liposomes and Niosomes as Topical Drug Carriers - Dermal and Transdermal Drug-Delivery**. *Journal of Controlled Release* 30(1): p1-15.

116. Torchilin VP (2006) **Multifunctional nanocarriers**. *Advanced Drug Delivery Reviews* 58(14): p1532-55.

117. Veldman RJ, Koning GA, van Hell A, Zerp S, Vink SR, Storm G, Verheij M and van Blitterswijk WJ (2005) **Coformulated N-octanoyl-glucosylceramide improves cellular delivery and cytotoxicity of liposomal doxorubicin**. *Journal of Pharmacology and Experimental Therapeutics* 315(2): p704-10.

118. Bennett CL and Calhoun EA (2004) **Pharmacoeconomics of liposomal anthracycline therapy**. *Seminars in Oncology* 31(6 Suppl 13): p191-5.

119. Ewer MS, Martin FJ, Henderson C, Shapiro CL, Benjamin RS and Gabizon AA (2004) **Cardiac safety of liposomal anthracyclines**. *Seminars* in *Oncology* 31(6 Suppl 13): p161-81.

120. Muggia FM (2001) **Liposomal encapsulated anthracyclines: new therapeutic horizons**. *Current Oncology Reports* 3(2): p156-62.

121. Fretz MM, Mastrobattista E, Koning GA, Jiskoot W and Storm G (2005) **Strategies for cytosolic delivery of liposomal macromolecules**. *International Journal of Pharmaceutics* 298(2): p305-9.

122. Boeckler C, Frisch B, Muller S and Schuber F (1996) **Immunogenicity of new heterobifunctional cross-linking reagents used in the conjugation of synthetic peptides to liposomes**. *Journal of Immunological Methods* 191(1): p1-10.

123. Gaucher G, Dufresne MH, Sant VP, Kang N, Maysinger D and Leroux JC (2005) **Block copolymer micelles: preparation, characterization and application in drug delivery**. *Journal of Controlled Release* 109(1-3): p169-88.

124. LaVan DA, McGuire T and Langer R (2003) **Small-scale systems for in vivo drug delivery**. *Nature Biotechnology* 21(10): p1184-1191.

125. Kataoka K, Harada A and Nagasaki Y (2001) **Block copolymer micelles for drug delivery: design, characterization and biological significance**. *Advanced Drug Delivery Reviews* 47(1): p113-131.

126. Zamboni WC (2008) **Concept and clinical evaluation of carrier-mediated anticancer agents**. *Oncologist* 13(3): p248-60.

127. Discher BM, Won YY, Ege DS, Lee JC, Bates FS, Discher DE and Hammer DA (1999) **Polymersomes: tough vesicles made from diblock copolymers**. *Science* 284(5417): p1143-6.

128. Discher DE and Eisenberg A (2002) **Polymer vesicles**. *Science* 297(5583): p967-73.

129. Yu K and Eisenberg A (1998) **Bilayer morphologies of self-assembled crew-cut aggregates of amphiphilic PS-b-PEO diblock copolymers in solution**. *Macromolecules* 31(11): p3509-3518.

130. van Hest JC, Delnoye DA, Baars MW, van Genderen MH and Meijer EW (1995) **Polystyrene-Dendrimer Amphiphilic Block Copolymers with a Generation-Dependent Aggregation**. *Science* 268(5217): p1592-1595.

131. Biloti DN, Santana MHA and Pessine FBT (2003) **Lipid membrane with low proton permeability**. *Biochimica et Biophysica Acta (BBA) - Biomembranes* 1611(1-2): p1-4.

132. Sommerdijk NAJM, Holder SJ, Hiorns RC, Jones RG and Nolte RJM (2000) **Self-Assembled Structures from an Amphiphilic Multiblock Copolymer Containing Rigid Semiconductor Segments**. *Macromolecules* 33(22): p8289-8294.

133. Meier W and Winterhalter CNM (2000) **Reconstitution of Channel Proteins in (Polymerized) ABA Triblock Copolymer Membranes**. *Angewandte Chemie International Edition* 39(24): p4599-4602.

134. Lee JCM, Bermudez H, Discher BM, Sheehan MA, Won YY, Bates FS and Discher DE (2001) **Preparation, stability, and in vitro performance of vesicles made with diblock copolymers**. *Biotechnology and Bioengineering* 73(2): p135-145.

135. Luo L and Eisenberg A (2001) **Thermodynamic stabilization mechanism of block copolymer vesicles**. *Journal of the American Chemical Society* 123(5): p1012-3.

136. Rothemund PW (2006) **Folding DNA to create nanoscale shapes and patterns**. *Nature* 440(7082): p297-302.

137. Hartgerink JD, Beniash E and Stupp SI (2002) **Peptide-amphiphile nanofibers: a versatile scaffold for the preparation of self-assembling materials**. *Proceedings of the National Academy of Sciences of the United States of America* 99(8): p5133-8.

138. Rodriguez-Hernandez J and Lecommandoux S (2005) **Reversible inside-out micellization of pH-responsive and water-soluble vesicles based on polypeptide diblock copolymers**. *Journal of the American Chemical Society* 127(7): p2026-7.

139. Hartgerink JD, Beniash E and Stupp SI (2001) **Self-assembly and mineralization of peptide-amphiphile nanofibers**. *Science* 294(5547): p1684-8.

140. Garreta E, Genove E, Borros S and Semino CE (2006) **Osteogenic differentiation of mouse embryonic stem cells and mouse embryonic fibroblasts in a three-dimensional self-assembling peptide scaffold**. *Tissue Engineering* 12(8): p2215-27.

141. von Maltzahn G, Vauthey S, Santoso S and Zhang SU (2003) **Positively charged surfactant-like peptides self-assemble into nanostructures**. *Langmuir* 19(10): p4332-4337.

142. Holowka EP, Sun VZ, Kamei DT and Deming TJ (2007) **Polyarginine segments in block copolypeptides drive both vesicular assembly and intracellular delivery**. *Nature Materials* 6(1): p52-7.

143. Rovira-Bru M, Thompson DH and Szleifer I (2002) **Size and structure of spontaneously forming liposomes in lipid/PEG-lipid mixtures**. *Biophysical Journal* 83(5): p2419-2439.

144. Riley T, Stolnik S, Heald CR, Xiong CD, Garnett MC, Illum L, Davis SS, Purkiss SC, Barlow RJ and Gellert PR (2001) **Physicochemical evaluation of nanoparticles assembled from poly(lactic acid)-poly(ethylene glycol) (PLA-PEG) block copolymers as drug delivery vehicles**. *Langmuir* 17(11): p3168-3174.

145. Reed DC, Barnard GC, Anderson EB, Klein LT and Gerngross TU (2005) **Production and purification of self-assembling peptides in Ralstonia eutropha**. *Protein Expression* and *Purification*

146. Killian JA and von Heijne G (2000) **How proteins adapt to a membrane-water interface**. *Trends in Biochemical Sciences* 25(9): p429-34.

147. Carstens MG, Bevernage JJL, van Nostrum CF, van Steenbergen MJ, Flesch FM, Verrijk R, de Leede LGJ, Crommelin DJA and Hennink WE (2007) **Small oligomeric micelles based on end group modified mPEG-oligocaprolactone with monodisperse hydrophobic blocks**. *Macromolecules* 40(1): p116-122.

148. Yoo Y, Rote K and Rechsteiner M (1989) **Synthesis of peptides as cloned ubiquitin extensions**. *Journal of Biological Chemistry* 264(29): p17078-83.

149. Butt TR, Edavettal SC, Hall JP and Mattern MR (2005) **SUMO fusion technology for difficult-to-express proteins**. *Protein Expression and Purification* 43(1): p1-9.

150. Lakowicz J. (2006) **Principles of fluorescence Spectroscopy**. 3 ed.

151. Kastantin M, Ananthanarayanan B, Lin B, Ressl J, Black M and Tirrell M (2007) **Increase of fluorescence anisotropy upon self-assembly in headgroup-labeled surfactants**. *Macromolecular Bioscience* 7(2): p189-94.

152. Benoit H and Froehlich D. (1972) In **Light Scattering From Polymer Solutions.** Huglin, M. B., Ed. Academic Press: London, pp 520-535.

153. Burger C, Hao J, Ying Q, Isobe H, Sawamura M, Nakamura E and Chu B (2004) **Multilayer vesicles and vesicle clusters formed by the fullerene-based surfactant C60(CH3)5K**. *Journal of Colloid and Interface Science* 275: p632–641.

154. Nie T, Zhao Y, Xie ZW and Wu C (2003) **Micellar formation of poly(caprolactone-block-ethylene oxide-block-caprolactone) and its enzymatic biodegradation in aqueous dispersion**. *Macromolecules* 36(23): p8825-8829.

155. Carstens MG, van Nostrum CF, Ramzi A, Meeldijk JD, Verrijk R, de Leede LL, Crommelin DJ and Hennink WE (2005) **Poly(ethylene glycol)--oligolactates with monodisperse hydrophobic blocks: preparation, characterization, and behavior in water**. *Langmuir* 21(24): p11446-54.

156. Fry DW, White JC and Goldman ID (1978) **Rapid separation of low molecular weight solutes from liposomes without dilution**. *Analytical Biochemistry* 90(2): p809-15.

157. Yang SJ and Zhang SG (2006) **Self-assembling behavior of designer lipid-like peptides**. *Supramolecular Chemistry* 18(5): p389-396.

158. Gao WP, Bai Y, Chen EQ, Li ZC, Han BY, Yang WT and Zhou QF (2006) **Controlling vesicle formation via interpolymer hydrogen-bonding complexation between poly(ethylene oxide)-block-polybutadiene and poly(acrylic acid) in solution**. *Macromolecules* 39(14): p4894-4898.

159. Antonietti M and Forster S (2003) **Vesicles and liposomes: A self-assembly principle beyond lipids**. *Advanced Materials* 15(16): p1323-1333.

160. Kayes JB (1977) **Pharmaceutical suspensions: relation between zeta potential, sedimentation volume and suspension stability**. *Journal of Pharmacy and Pharmacology* 29(4): p199-204.

161. Vandermeulen GW and Klok HA (2004) **Peptide/protein hybrid materials: enhanced control of structure and improved performance through conjugation of biological and synthetic polymers**. *Macromolecular Bioscience* 4(4): p383-98.

162. Lemmel C, Weik S, Eberle U, Dengjel J, Kratt T, Becker HD, Rammensee HG and Stevanovic S (2004) **Differential quantitative analysis of MHC ligands by mass spectrometry using stable isotope labeling**. *Nature Biotechnology* 22(4): p450-4.

163. Pencer J and Hallett FR (2003) **Effects of vesicle size and shape on static and dynamic light scattering measurements**. *Langmuir* 19(18): p7488-7497.

164. Olson F, Hunt CA, Szoka FC, Vail WJ and Papahadjopoulos D (1979) **Preparation of liposomes of defined size distribution by extrusion through polycarbonate membranes**. *Biochimica Et Biophysica Acta* 557(1): p9-23.

165. Zhang S, Lockshin C, Cook R and Rich A (1994) **Unusually stable beta-sheet formation in an ionic self-complementary oligopeptide**. *Biopolymers* 34(5): p663-72.

166. Hartgerink JD (2004) **Covalent capture: a natural complement to self-assembly**. *Current Opinion in Chemical Biology* 8(6): p604-9.

167. Horcas I, Fernandez R, Gomez-Rodriguez JM, Colchero J, Gomez-Herrero J and Baro AM (2007) **WSXM: a software for scanning probe microscopy and a tool for nanotechnology**. *Review of Scientific Instruments* 78(1): p013705.

168. Cui H, Hodgdon TK, Kaler EW, Abezgauz L, Danino D, Lubovsky M, Talmon Y and Pochan DJ (2007) **Elucidating the assembled structure of amphiphiles in solution via cryogenic transmission electron microscopy**. *Soft Matter* 3(8): p945-955.

169. Heinz L (1995) **Comparative Test of Methods to Determine Particle Size and Particle Size Distribution in the Submicron Range**. *Particle and Particle Systems Characterization* 12(3): p148-157.

170. Sutton D, Nasongkla N, Blanco E and Gao J (2007) **Functionalized micellar systems for cancer targeted drug delivery**. *Pharmaceutical Research* 24(6): p1029-46.

171. Sheldon K, Liu D, Ferguson J and Gariepy J (1995) **Loligomers: design of de novo peptide-based intracellular vehicles**. *Proceedings of the National Academy of Sciences of the United States of America* 92(6): p2056-60.

172. Conner SD and Schmid SL (2003) **Regulated portals of entry into the cell**. *Nature* 422(6927): p37-44.

173. Ueno M, Yoshida S and Horikoshi I (1991) **Characteristics of the Membrane-Permeability of Temperature-Sensitive Liposome**. *Bulletin of the Chemical Society of Japan* 64(5): p1588-1593.

174. Crestfield AM, Moore S and Stein WH (1963) **The preparation and enzymatic hydrolysis of reduced and S-carboxymethylated proteins**. *Journal of Biological Chemistry* 238: p622-7.

175. Jiskoot W and Crommelin DJ. (2005) **Methods for Structural Analysis of Protein Pharmaceuticals**. American Association of Pharmaceutical scientists: p 1-26.

176. Riddles PW, Blakeley RL and Zerner B (1983) **Reassessment of Ellman's reagent**. *Methods Enzymology* 91: p49-60.

177. Shi Z, Woody RW and Kallenbach NR (2002) **Is polyproline II a major backbone conformation in unfolded proteins?** *Advances in Protein Chemistry* 62: p163-240.

178. Shi Z, Chen K, Liu Z, Ng A, Bracken WC and Kallenbach NR (2005) **Polyproline II propensities from GGXGG peptides reveal an anticorrelation with beta-sheet scales**. *Proceedings of the National Academy of Sciences of the United States of America* 102(50): p17964-8.

179. Schweitzer-Stenner R, Eker F, Perez A, Griebenow K, Cao XL and Nafie LA (2003) **The structure of tri-proline in water probed by polarized Raman, Fourier**

transform infrared, vibrational circular dichroism, and electric ultraviolet circular dichroism spectroscopy. *Biopolymers* 71(5): p558-568.

180. Jackson M and Mantsch HH (1995) **The use and misuse of FTIR spectroscopy in the determination of protein structure**. *Critical Reviews in Biochemistry and Molecular Biology* 30(2): p95-120.

181. Jackson M, Haris PI and Chapman D (1989) **Fourier-Transform Infrared Spectroscopic Studies of Lipids, Polypeptides and Proteins**. *Journal of Molecular Structure* 214: p329-355.

182. Sreerama N and Woody RW (2003) **Structural composition of beta(I)- and beta(II)-proteins**. *Protein Science* 12(2): p384-388.

183. Whittington SJ, Chellgren BW, Hermann VM and Creamer TP (2005) **Urea promotes polyproline II helix formation: Implications for protein denatured states**. *Biochemistry* 44(16): p6269-6275.

184. Liu ZG, Chen K, Ng A, Shi ZS, Woody RW and Kallenbach NR (2004) **Solvent dependence of PII conformation in model alanine peptides**. *Journal of the American Chemical Society* 126(46): p15141-15150.

185. Pappu RV and Rose GD (2002) **A simple model for polyproline II structure in unfolded states of alanine-based peptides**. *Protein Science* 11(10): p2437-55.

186. Yaghmur A, Laggner P, Zhang S and Rappolt M (2007) **Tuning curvature and stability of monoolein bilayers by designer lipid-like peptide surfactants**. *PLoS ONE* 2(5): pe479.

187. Chen K, Liu Z, Zhou C, Bracken WC and Kallenbach NR (2007) **Spin relaxation enhancement confirms dominance of extended conformations in short alanine peptides**. *Angewandte Chemie-International Edition* 46(47): p9036-9.

188. Wilhelm M, Zhao CL, Wang YC, Xu RL, Winnik MA, Mura JL, Riess G and Croucher MD (1991) **Polymer Micelle Formation .3. Poly(Styrene-Ethylene Oxide) Block Copolymer Micelle Formation in Water - a Fluorescence Probe Study**. *Macromolecules* 24(5): p1033-1040.

189. Jones G and Vullev VI (2001) **Contribution of a Pyrene Fluorescence Probe to the Aggregation Propensity of Polypeptides**. *Organic Letters* 3(16): p2457-2460.

190. Almgren M, Grieser F and Thomas JK (1980) **Photochemical and photophysical studies of organized assemblies. Interaction of oils, long-chain alcohols, and surfactants forming microemulsions**. *Journal of the American Chemical Society* 102(9): p3188-3193.

191. Shynkar VV, Klymchenko AS, Kunzelmann C, Duportail G, Muller CD, Demchenko AP, Freyssinet JM and Mely Y (2007) **Fluorescent biomembrane probe for**

ratiometric detection of apoptosis. *Journal of the American Chemical Society* 129(7): p2187-2193.

192. Klymchenko AS, Duportail G, Ozturk T, Pivovarenko VG, Mely Y and Demchenko AP (2002) **Novel two-band ratiometric fluorescence probes with different location and orientation in phospholipid membranes**. *Chemistry & Biology* 9(11): p1199-1208.

193. Klymchenko AS, Duportail G, Demchenko AP and Mely Y (2004) **Bimodal distribution and fluorescence response of environment-sensitive probes in lipid bilayers**. *Biophysical Journal* 86(5): p2929-2941.

194. Klymchenko AS, Mely Y, Demchenko AP and Duportail G (2004) **Simultaneous probing of hydration and polarity of lipid bilayers with 3-hydroxyflavone fluorescent dyes**. *Biochimica Et Biophysica Acta-Biomembranes* 1665(1-2): p6-19.

195. Velichko YS, Stupp SI and de la Cruz MO (2008) **Molecular simulation study of peptide amphiphile self-assembly**. *Journal of Physical Chemistry B* 112(8): p2326-2334.

196. Mozo-Villarias A (2002) **Second derivative fluorescence spectroscopy of tryptophan in proteins**. *Journal of Biochemical and Biophysical Methods* 50(2-3): p163-78.

197. Tovar JD, Claussen RC and Stupp SI (2005) **Probing the interior of peptide amphiphile supramolecular aggregates**. *Journal of the American Chemical Society* 127(20): p7337-45.

198. Bales BL, Messina L, Vidal A, Peric M and Nascimento OR (1998) **Precision Relative Aggregation Number Determinations of SDS Micelles Using a Spin Probe. A Model of Micelle Surface Hydration**. *Journal of Physical Chemistry B* 102(50): p10347-10358.

199. Lopez O, Cocera M, Wehrli E, Parra JL and de la Maza A (1999) **Solubilization of liposomes by sodium dodecyl sulfate: New mechanism based on the direct formation of mixed micelles**. *Archives of Biochemistry and Biophysics* 367(2): p153-160.

200. Xu Q and Keiderling TA (2004) **Effect of sodium dodecyl sulfate on folding and thermal stability of acid-denatured cytochrome c: a spectroscopic approach**. *Protein Science* 13(11): p2949-59.

201. Gonzalez-Perez A, Ruso JM, Prieto G and Sarmiento F (2004) **Physicochemical study of ovalbumin in the presence of sodium dodecyl sulphate in aqueous media**. *Colloid and Polymer Science* 282(4): p351-356.

202. Wu CS, Ikeda K and Yang JT (1981) **Ordered conformation of polypeptides and proteins in acidic dodecyl sulfate solution**. *Biochemistry* 20(3): p566-70.

203. Heeres A, van der Pol C, Stuart M, Friggeri A, Feringa BL and van Esch J (2003) **Orthogonal self-assembly of low molecular weight hydrogelators and surfactants**. *Journal of the American Chemical Society* 125(47): p14252-14253.

204. van Esch J, Schoonbeek F, de Loos M, Kooijman H, Spek AL, Kellogg RM and Feringa BL (1999) **Cyclic bis-urea compounds as gelators for organic solvents**. *Chemistry-a European Journal* 5(3): p937-950.

205. Michel Berthelot CLMLCRRWT (1996) **Partition coefficients and intramolecular hydrogen bonding. 2. The influence of partition solvents on the intramolecular hydrogen-bond stability of salicyclic acid derivatives**. *Journal of Physical Organic Chemistry* 9(9): p626-630.

206. Garcia AE (2004) **Characterization of non-alpha helical conformations in Ala peptides**. *Polymer* 45(2): p669-676.

207. Sreerama N and Woody RW (1999) **Molecular dynamics simulations of polypeptide conformations in water: A comparison of alpha, beta, and poly(Pro)II conformations**. *Proteins-Structure Function and Genetics* 36(4): p400-406.

208. Xenides D, Randolf BR and Rode BM (2006) **Hydrogen bonding in liquid water: An ab initio QM/MM MD simulation study**. *Journal of Molecular Liquids* 123(2-3): p61-67.

209. Ormson SM, Brown RG, Vollmer F and Rettig W (1994) **Switching between Charge-Transfer and Proton-Transfer Emission in the Excited-State of a Substituted 3-Hydroxyflavone**. *Journal of Photochemistry and Photobiology a-Chemistry* 81(2): p65-72.

210. Siano DB and Metzler DE (1969) **Band shapes of the electronic spectra of complex molecules.** . *Journal of Chemical Physics* 51: p1856-1861.

211. Krieger E, Koraimann G and Vriend G (2002) **Increasing the precision of comparative models with YASARA NOVA--a self-parameterizing force field**. *Proteins* 47(3): p393-402.

212. Yeh JI, Du S, Tortajada A, Paulo J and Zhang S (2005) **Peptergents: Peptide Detergents That Improve Stability and Functionality of a Membrane Protein, Glycerol-3-phosphate Dehydrogenase**. *Biochemistry* 44(51): p16912-16919.

213. Nagarsekar A, Crissman J, Crissman M, Ferrari F, Cappello J and Ghandehari H (2002) **Genetic synthesis and characterization of pH- and temperature-sensitive silk-elastinlike protein block copolymers**. *Journal of Biomedical Materials Research* 62(2): p195-203.

214. Brown SB, Brown EA and Walker I (2004) **The present and future role of photodynamic therapy in cancer treatment**. *Lancet Oncology* 5(8): p497-508.

215. Wilson BC and Patterson MS (2008) **The physics, biophysics and technology of photodynamic therapy**. *Physics in Medicine and Biology* 53(9): pR61-R109.

216. Castano AP, Mroz P and Hamblin MR (2006) **Photodynamic therapy and anti-tumour immunity**. *Nature Reviews Cancer* 6(7): p535-545.

217. Hofman JW, van Zeeland F, Turker S, Talsma H, Lambrechts SAG, Sakharov DV, Hennink WE and van Nostrum CF (2007) **Peripheral and axial substitution of phthalocyanines with solketal groups: Synthesis and in vitro evaluation for photodynamic therapy**. *Journal of Medicinal Chemistry* 50(7): p1485-1494.

218. Jones AT (2008) **Gateways and tools for drug delivery: Endocytic pathways and the cellular dynamics of cell penetrating peptides**. *International Journal of Pharmaceutics* 354(1-2): p34-38.

219. Jones AT (2007) **Macropinocytosis: searching for an endocytic identity and role in the uptake of cell penetrating peptides**. *Journal of Cellular and Molecular Medicine* 11(4): p670-684.

220. Straubinger RM, Hong K, Friend DS and Papahadjopoulos D (1983) **Endocytosis of liposomes and intracellular fate of encapsulated molecules: encounter with a low pH compartment after internalization in coated vesicles**. *Cell* 32(4): p1069-79.

221. Rijcken CJF, Hofinan JW, van Zeeland F, Hennink WE and Van Nostrum CF (2007) **Photo sensitiser-loaded biodegradable polymeric micelles: Preparation, characterisation and in vitro PDT efficacy**. *Journal of Controlled Release* 124(3): p144-153.

222. Kleuss C and Krause E (2003) **G alpha(s) is palmitoylated at the N-terminal glycine**. *Embo Journal* 22(4): p826-832.

223. Hanson JR (2000) **Steroids: reactions and partial synthesis**. *Natural Product Reports* 17(5): p423-434.

224. Hamley IW (2007) **Peptide fibrillization**. *Angewandte Chemie-International Edition* 46(43): p8128-8147.

225. Gonzalo T, Talman EG, de Ven AV, Temming K, Greupink R, Beljaars L, Reker-Smit C, Meijer DKF, Molema G, Poelstra K and Kok RJ (2006) **Selective targeting of pentoxifylline platinum-based to hepatic stellate cells using a novel linker technology**. *Journal of Controlled Release* 111(1-2): p193-203.

226. Hermeling S, Crommelin DJA, Schellekens H and Jiskoot W (2004) **Structure-immunogenicity relationships of therapeutic proteins**. *Pharmaceutical Research* 21(6): p897-903.

227. Slutter B, Hagenaars N and Jiskoot W (2008) **Rational design of nasal vaccines**. *Journal of Drug Targetting* 16(1): p1-17.

228. Levine MM and Sztein MB (2004) **Vaccine development strategies for improving immunization: the role of modern immunology**. *Nature Immunology* 5(5): p460-4.

229. Checot F, Lecommandoux S, Gnanou Y and Klok HA (2002) **Water-soluble stimuli-responsive vesicles from peptide-based diblock copolymers**. *Angewandte Chemie-International Edition* 41(8): p1339-1343.

230. Romberg B, Metselaar JM, Baranyi L, Snel CJ, Bunger R, Hennink WE, Szebeni J and Storm G (2007) **Poly(amino acid)s: Promising enzymatically degradable stealth coatings for liposomes**. *International Journal of Pharmaceutics* 331(2): p186-189.

231. Romberg B, Oussoren C, Snel CJ, Carstens MG, Hennink WE and Storm G (2007) **Pharmacokinetics of poly(hydroxyethyl-L-asparagine)-coated liposomes is superior over that of PEG-coated liposomes at low lipid dose and upon repeated administration**. *Biochimica Et Biophysica Acta-Biomembranes* 1768(3): p737-743.

232. Romberg B, Flesch FM, Hennink WE and Storm G (2008) **Enzyme-induced shedding of a poly(amino acid)-coating triggers contents release from dioleoyl phosphatidylethanolamine liposomes**. *International Journal of Pharmaceutics* 355(1-2): p108-113.

233. Peer D, Karp JM, Hong S, Farokhzad OC, Margalit R and Langer R (2007) **Nanocarriers as an emerging platform for cancer therapy**. *Nature Nanotechnology* 2(12): p751-60.

Nederlandse Samenvatting

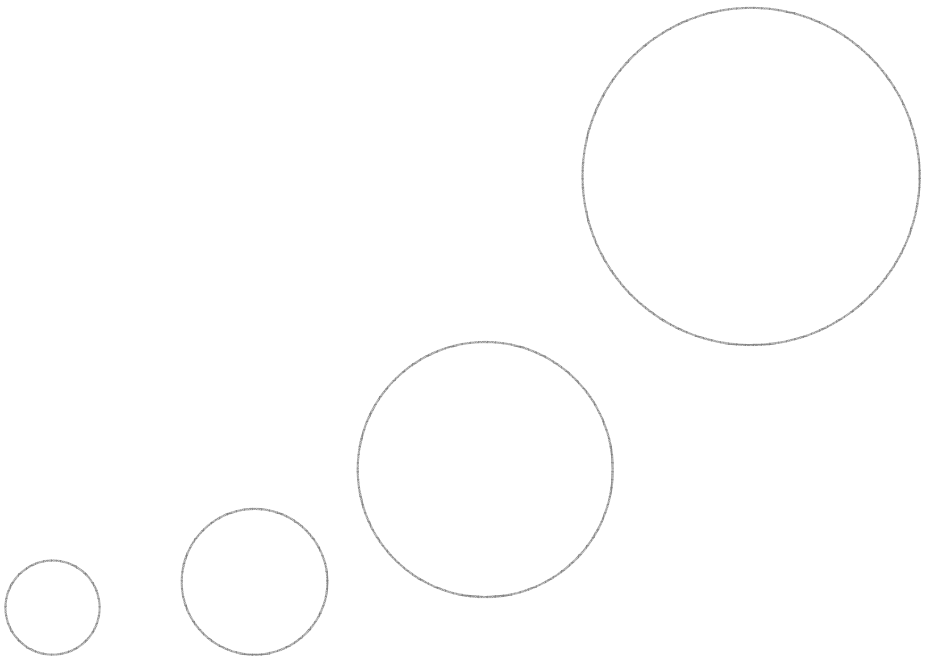

Nanodeeltjes

Nanodeeltjes worden gebruikt voor een breed scala aan toepassingen, van textielbescherming tot medische behandelingen. Door hun afmetingen (één nanometer is een 1 000 000 ste deel van een millimeter) hebben de deeltjes unieke eigenschappen. Zo kunnen ze op plaatsen doordringen die voor instrumenten of grotere deeltjes ontoegankelijk zijn. Bijvoorbeeld worden door het gebruik van nanodeeltjes medicijnen op de juiste plek van het zieke weefsel of kwaadaardige tumorcellen in het lichaam afgegeven (Engelse term: drug delivery). Medicijnen die ingesloten zijn in nanodeeltjes (kleiner dan 200 nanometer) blijven lange tijd in de bloedbaan circuleren, terwijl zij juist het tumorweefsel binnendringen. In de tumor komt daarmee naar rato meer medicijn terecht met behulp van zo'n nanodeeltje, wat de therapie effectiever maakt.

Het effect van een gecontroleerde afgifte van medicijnen wordt versterkt wanneer het nanodeeltje specifiek aan het zieke weefsel of de kwaadaardige tumorcellen bindt, terwijl het de gezonde gedeelten van het lichaam onaangetast laat. Via deze strategie zouden negatieve bijwerkingen van medicatie kunnen worden verminderd of zelfs voorkomen. Het is gemakkelijk voor te stellen dat dit voor behandelingen met zware medicatie zoals chemotherapie een enorme winst kan opleveren. Tot nog toe is het echter een uitdaging gebleken om nanodeeltjes te ontwikkelen die eenvoudig te modificeren zijn om bijvoorbeeld tumorcellen te binden of alleen in het zieke weefsel hun inhoud vrij te geven.

Moleculaire zelforganisatie

Door de kleine dimensies van de nanodeeltjes is het vaak al moeilijk de deeltjes zichtbaar te maken en zijn ook veel productiemethoden niet toepasbaar. Daarom is één van de meest krachtige strategieën om moleculen direct al zo te ontwerpen dat ze spontaan tot een geordende structuur zelforganiseren (Engelse term: self-assembly). In feite is dit een veelvoorkomend fenomeen dat bijvoorbeeld in het menselijk lichaam plaatsvindt. Zo ontstaan virussen door de spontane ordening van viruseiwitten en worden de membranen van cellen gevormd door zelforganisatie van lipide moleculen.

Door bepaalde eigenschappen van moleculen kunnen dus geordende structuren ontstaan. Via deze strategie is het ook mogelijk nieuwe, onnatuurlijke structuren

te vormen. Zo is bijvoorbeeld een afbeelding van de wereldkaart te maken op 10 bij 10 nanometer – door enkele duizenden unieke moleculen te ontwerpen (met behulp van wiskundige berekeningen) die vervolgens spontaan zelforganiseren tot zo'n gedetailleerde structuur. Omdat er nauwelijks instrumenten zijn die op de nanometer precies kunnen werken, is de zelforganisatie van moleculen dus een krachtig alternatief.

Een wereldkaart van 100 vierkante nanometer is medisch gezien niet van belang, en zal ook niet snel een dagelijkse toepassing vinden. Voor medische en farmaceutische doeleinden echter heeft de vorm van een bol al lang op belangstelling kunnen rekenen. Een holle bolvormige structuur zou kunnen worden gebruikt om medicijnen in te sluiten. Tussen de moleculen die de bol vormen passen vaak weer andere medicijnen. Op dit moment worden dit soort 'nanobolletjes' met succes in de kliniek gebruikt, onder meer in de behandeling van bepaalde vormen van kanker. Met behulp van deze lipide bolletjes (liposomen) worden de zware bijwerkingen van de toegepaste chemotherapie verminderd.

Echter, de bolletjes die op dit moment in de kliniek worden gebruikt, laten zich niet zo eenvoudig aan tumorcellen binden. Bovendien komt het medicijn niet altijd even gemakkelijk uit het bolletje vrij zodra het de tumor heeft bereikt. Daarom zou een nieuw type bolletje dat op moleculair niveau gemakkelijker aan te passen is, waardevol zijn voor medische doeleinden en andere toepassingen.

Inhoud onderzoekshoofdstukken (hoofdstukken 2-6)

Zoals gezegd zijn de bolletjes die op dit moment in patiënten worden gebruikt, gemaakt van lipiden. Dit zijn lichaamseigen moleculen. Andere nanobolletjes zijn gemaakt van polymeren, maar die zijn (nog) niet bij mensen toegepast. Verschillende polymeren zijn ook lichaamsvreemd, waardoor ze niet allemaal geschikt zijn voor medische toepassingen. Een andere belangrijke bouwsteen in het lichaam zijn eiwitten en peptiden. Een eiwit bestaat eigenlijk uit een netjes opgevouwen, lange keten van peptiden, en peptiden zijn weer opgebouwd uit aminozuren.

Dit proefschrift doet verslag van onderzoek of nanobolletjes kunnen worden gemaakt van peptiden. Hiervoor zijn korte peptiden ontworpen, van 10-15 aminozuren op een rij. De aminozuurvolgorde is zo gekozen dat het ene gedeelte van het peptide graag in contact staat met water (hydrofiel) en het andere gedeelte juist niet van water houdt (hydrofoob). Zodra de peptiden in contact met water komen, organiseren zij zich inderdaad spontaan tot een hol bolletje. Dit wordt aangetoond in **Hoofdstuk 2** van dit proefschrift.

De peptide bolletjes zouden in feite ook weer uit elkaar kunnen vallen, wat niet altijd wenselijk is. Daarom laat **Hoofdstuk 3** zien dat, door juist een paar aminozuren te vervangen door andere aminozuren (cysteines), de bolletjes kunnen worden gestabiliseerd door de zeer sterke covalente verbindingen tussen de peptiden onderling. Dit zorgt ervoor dat de peptide bolletjes als zodanig niet meer gemakkelijk uit elkaar vallen (Tabel 2, Hoofdstuk 3).

De ontworpen peptiden hebben ongeveer dezelfde lengte als lipiden en vormen ook bolletjes. Toch zijn de peptide bolletjes uniek als je ze vergelijkt met huidige lipide- en ook polymere bolletjes. Om nanobolletjes van lipiden of polymeren te maken zijn veelal geavanceerde technieken nodig. Hoofdstuk 2 en 3 laten al zien dat de nanodeeltjes spontaan worden gevormd enkel door de peptiden in water te brengen. Hoofdstuk 4 en 5 gaan dieper in op de exacte verschillen tussen deze peptide bolletjes en de lipide- (en ook de polymere) bolletjes.

Peptiden kunnen als individueel molecuul al een bepaalde mate van ordening aannemen. Sommige peptiden bijvoorbeeld vormen een helix (wenteltrap) structuur. Deze moleculaire ordening wordt de secondaire structuur van een peptide genoemd. **Hoofdstuk 4** laat zien dat deze peptiden de polyproline II structuur vormen. Deze structuur blijkt essentieel te zijn voor de peptiden om zich tot bolletje te organiseren.

Nadat de ordening binnen het molecuul opgehelderd is, wordt in **Hoofdstuk 5** de precieze ordening van de peptiden onderling bestudeerd. Hiervoor is gebruik gemaakt van zowel experimenten als computersimulaties. Op moleculair niveau steken twee lagen peptide in elkaar (Figuur 6 C & D, Hoofdstuk 5), zoals twee

haarborstels in elkaar worden gedrukt en zodoende blijven kleven. Hoofdstuk 5 laat verder zien dat de peptiden bij elkaar worden gehouden door hydrofobe interacties, terwijl de hydrofiele gedeelten van de peptiden in contact staan met het water. Echter, uit het hydrofobe gedeelte blijken niet alle watermoleculen verdwenen. De watermoleculen verbinden peptiden aan elkaar door waterstofbrugvorming. Ook staan de ruggengraten van peptiden in directe verbinding met elkaar door waterstofbrugvorming. Zo laat Hoofdstuk 5 zien dat verschillende unieke krachten die niet in lipide bolletjes worden gevonden wel een rol spelen in het stabiliseren van de peptiden tot nanobolletjes.

In het laatste onderzoekshoofdstuk, **Hoofdstuk 6**, is onderzocht of deze peptiden ook inderdaad kunnen worden gebruikt om medicijnen aan cellen af te leveren. Het laat zien, kort gezegd, dat bepaalde cellen de bolletjes “goed slikken”. Doordat de peptide bolletjes dus door de cellen worden opgenomen, kunnen tumorcellen worden bestreden met een lichtgevoelig medicijn dat is ingesloten in de peptide bolletjes. Deze bevindingen laten zien dat de peptide nanobolletjes inderdaad als moleculaire drager en afgiftesysteem van medicijnen kunnen functioneren.

Toekomstperspectieven

Om deze peptide bolletjes tot een medicijndrager te ontwikkelen die geschikt is voor gebruik in de kliniek, zijn verdere studies nodig. Zoals genoemd zou lichttherapie op tumorcellen een directe toepassing kunnen zijn van de peptide nanobolletjes. Dit zou in muizen verder kunnen worden onderzocht. De medicijnen die gebruikt zijn in de experimenten in Hoofdstuk 6 zitten tussen de peptiden die het bolletje vormen (hydrofobe gedeelte), omdat deze medicijnen ook hydrofoob zijn. Veel medicijnen zijn echter relatief kleine en hydrofiele moleculen. De bolletjes zullen nog verder moeten worden aangepast om hydrofiele medicijnen voor langere tijd in de bolletjes te houden. Dit kan bijvoorbeeld door de peptiden langer te maken, zodat de barrière voor hydrofiele moleculen groter wordt. Of door andere, meer hydrofobe aminozuren te kiezen in de peptiden. Wel moet worden opgelet of de secundaire structuur van de peptiden (Hoofdstuk 4) dan niet verandert ten nadele van de moleculaire organisatie tot nanobolletjes.

Het gebruik van peptiden als de bouwstenen van nanobolletjes levert bovendien het voordeel op dat de bouwstenen gemakkelijk uit te breiden zijn met grotere, functionele peptiden, of ook met eiwitten. Het is bekend dat bepaalde eiwitten tumorcellen kunnen herkennen en binden. Andere peptiden kunnen tegelijkertijd helpen om juist in de cellen het medicijn vrij te laten komen. De peptide bolletjes die gemaakt zijn in dit onderzoek blijken kleiner dan 60 nanometer in doorsnede te zijn (30 nanometer in radius; Figuur 6, Hoofdstuk 3). Dat is kleiner dan de huidige (lipide) bolletjes die voornamelijk 80-100 nanometer zijn en dit zou een groot voordeel op kunnen leveren. Wetenschappelijke studies laten namelijk zien dat juist deeltjes die kleiner zijn dan 80 nanometer gemakkelijk in tumorweefsels binnendringen.

In de chemische wetenschap is de laatste jaren gebleken dat controle over het zelforganiserend gedrag van moleculen kan leiden tot dat materiaal of nanodeeltje dat gewenst is. Met behulp van controle over zulke moleculen kunnen “intelligente” eigenschappen aan materialen worden meegegeven. Zoals een onlangs gesynthetiseerd rubber materiaal, dat, als het gebroken is, simpelweg door de twee einden een tijdje aan elkaar te houden zichzelf herstelt. Dit is mogelijk door een nauwgezette selectie in de kenmerken van de gebruikte moleculen. Juist aminozuren en de peptide ruggengraat bezitten een brede verscheidenheid aan moleculaire eigenschappen. Daarmee zijn peptiden uitermate geschikte moleculen om de kenmerken van nanodeeltjes ruimschoots te variëren en te optimaliseren. Het uitgangspunt om met peptiden nanobolletjes te vormen is in dit proefschrift aan het licht gebracht. Nu wacht de taak om deze bolletjes voor de afzonderlijk gewenste toepassingen verder te ontwikkelen.

Dankwoord

Curriculum Vitae

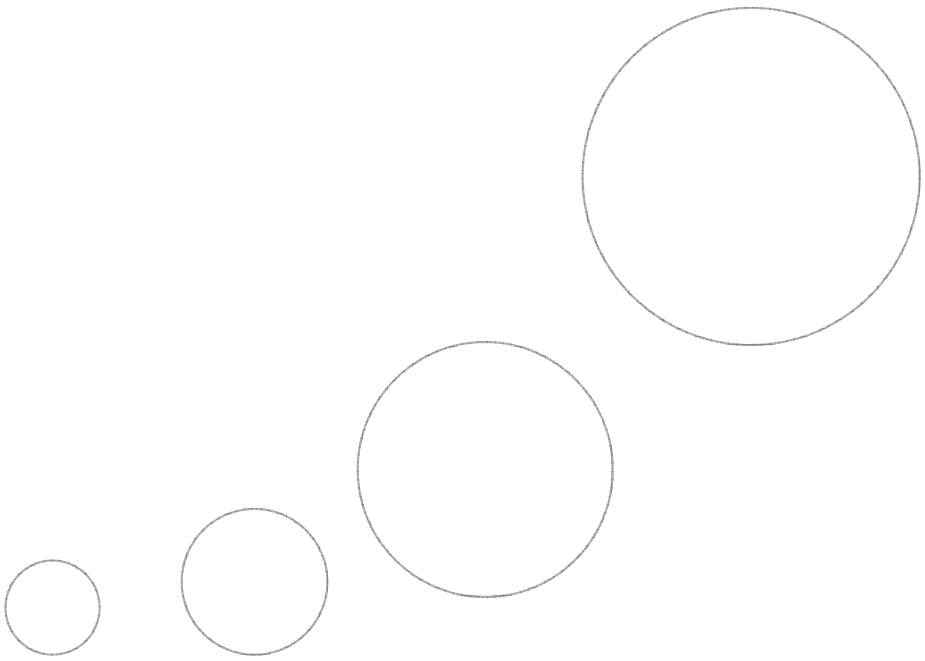

Dankwoord

Een woord van dank aan het einde van dit proefschrift – omdat je aan het begin niet weet hoeveel je geholpen wordt.

Allereerst wil ik jou, Enrico, bedanken voor je betrokkenheid bij het project en je vele ideeën die je telkens weer inbracht. Later in het traject, tijdens het schrijven van de artikelen, heb ik je positieve insteek waarmee je resultaten bekijkt, erg gewaardeerd. Wie weet kom je in de toekomst je eigen schrijfstijl nog tegen!

Wim en Daan, mijn beide promotoren, ik wil jullie hartelijk danken dat ik in jullie groep vier jaar onderzoek heb kunnen doen en van jullie ervaring heb kunnen leren. Twee van jullie eigenschappen heb ik in het bijzonder gewaardeerd. Ze gelden in feite voor jullie beiden maar ik wil het persoonlijk maken. Daan, jouw correctheid en werkethos zullen mij altijd bij blijven, mijn dank daarvoor. En Wim, je betrokkenheid bij de groep heeft me enorm geïnspireerd. Het doet goed om te merken hoezeer jullie, ondanks vele andere taken, je hebben ingezet voor de voortgang van mijn project en de onderlinge betrokkenheid binnen de groep.

Ook ben ik veel dank verschuldigd aan Wim “J”. Jammer dat jij (en Marc Sutter) richting het Wilde Westen vetrokken, waardoor ik alleen voor die (CD, FTIR & fluorescentie) lichtbundels stond. Uiteindelijk heeft jullie (overgedragen) kennis tot twee leuke hoofdstukken geleid.

Verder wil ik iedereen bedanken van wie ik heb geleerd hoe je zelfassociërende peptiden maakt, analyseert of toe weet te passen. Arjen, in het begin heb je geholpen om aan te tonen of mijn recombinant geproduceerde oligopeptiden er nu waren – of niet. Achter die joekel van een MALDI-TOF wist je uiteindelijk de correcte massa’s naar boven te toveren! Frits, zonder jouw hulp met de elektronen microscopie was dit boekje anders van inhoud geweest; dan had ik nog steeds niet geweten hoe m‘n peptiden er uit zien – stel je voor... Andrey Klymchenko thanks for the nice collaboration and showing us Strasbourg. Ed Moret, je hebt de peptiden laten droogzwemmen – hoewel computers er weken voor moesten draaien - werd het een erg leuk en nuttig experiment. Marjan, in het

bijzonder wil ik jou bedanken voor je hulp met de celstudies. Je leuke, doortastende manier van werken was erg stimulerend! Several students have been working on the project for half a year or more. Chantal, Cristina, Kees, Evi, Pepijn, thanks for your efforts to put the project a little step further. And Cris, in particular you and your parents thanks for the enjoyable time in Portugal and the beautiful city of Lisboa.

Iedereen die met het onderzoek heeft geholpen, zelfs als het een klein beetje was, mijn dank. Soms was er praktische hulp of kwamen er tips, soms ook niet – het maakt in feite niet zoveel uit – want iedereen die met het verloop van het onderzoek heeft meegeleefd, heeft eraan meegewerkt.

Daarom dank ik ook mijn wederzijdse familie, ouders, opa's en vrienden voor de betrokkenheid. Het was heerlijk om af en toe gewoon mijn verhaal te kunnen doen, zonder dat een wetenschappelijke inbreng was vereist. Ook de mede-biofarmacie-genoten. Het was erg leuk om bij Biofarmacie te zijn, niet alleen omdat er interessant onderzoek wordt gedaan (uiteraard dat ook), maar het was vooral erg sociaal en gezellig. In het bijzonder ook met mijn lab-genoten op Z611. Sophie, Natasa, Marion, later Frank en Niels: het was een leuke tijd en altijd was er gezelligheid. Daarbij alle anderen die het Went onveilig maakten – Amir, Martin, Roel, Rolf, en ook Holger, Ethlinn, Marcel, Joost, Joris, Sabrina, Ellen, Emmy: all - cordially - thanx.

Marion, je begon een maandje later, en eindigde een maandje eerder. Tsja, ik kan inderdaad niet ontkennen dat je soms een tikkeltje meer gestructureerd was. Maar goed, laat ik zeggen, des te gelukkiger ben ik dat jij, na vier jaar samen optrekken, tijdens het afsluitende zweet-uurtje mij bij staat! Aan de andere zijde – broer Bas. Na het werk samen drie kwartier tegen een balletje meppen – het doet de AIO goed. Nu kom je drie kwartier naast mij zitten, terwijl ik in m'n eentje inspanning sta te leveren – dat doet de ambtenaar vast goed.

Zo' n boekje komt soms met een zucht tot stand. Daarom nog een drievoudig dank. Aan hen die, misschien onbewust, mij wezenlijk hebben geholpen – zonder wie dit boekje er simpelweg niet was geweest. Mies, jij hielp op de momenten

waarop het echt nodig was. Ik weet niet hoe je aan die gave komt. Op het moment dat ik anders de deuren van het Went voorgoed achter me dicht had getrokken, kwam jij en ging jij de volgende 'uitdaging' aan. En je loste het probleem, zoals gebruikelijk, rustig op.

Mijn lieve Marlies: dank je voor alles wat je voor me hebt betekend. Jij hebt mij altijd geholpen, onafgebroken. Onder meer door er gewoon vertrouwen in te hebben dat het goed kwam. En ziehier – daar is 'tie dan. Voor jou misschien altijd vanzelfsprekend geweest – gelukkig heb je gelijk gekregen. Hier hoort ook Joëd bij, ons kleine zonnetje dat de vier jaar, van begin tot het einde, heeft geschenen. Je kunt het nu nog niet lezen, wist jij veel wat papa deed – je was gewoon altijd vrolijk!

Ten derde heb ik dit onderzoek vier jaar gedaan terwijl een ander zonnetje me continu heeft beschenen. Het deed me soms goed om naar het hoge gebouw van de Uni te kijken en daar het embleem, de zon van de UU te zien. Sol Iustitia Illustrae Nos. De zon van de gerechtigheid verlicht ons. Zonder die Zon – die Zoon was dit boek er niet geweest. Soli Deo Gloria – alleen God de eer.

Curriculum Vitae

Albert van Hell, geboren op 28 april 1981 te Pretoria (Zuid-Afrika), behaalde in 1999 zijn Gymnasium diploma aan het Driestar College te Gouda. Datzelfde jaar begon hij de studie Biomedische Wetenschappen aan de Vrije Universiteit (VU) in Amsterdam. Tijdens zijn Bachelor studie deed hij in het VU Medisch Centrum onderzoek naar het metaboliet Asymetrisch DiMethyl Arginine (dr. T. Teerlink), waarna hij in 2003 zijn Bachelor diploma behaalde. Tijdens de masterfase werd in 2004 onderzoek gedaan aan het Nederlands Kanker Instituut te Amsterdam (dr. W. van Blitterswijk) en bij Organon Pharmaceutics te Oss (dr. K.J. Dechering). Na het afronden van zijn scriptie over DNA methylering en kanker (dr. J. Kooter, VU), behaalde hij in 2005 zijn Master diploma en werd aansluitend als Assistent In Opleiding werkzaam bij de vakgroep Biofarmacie en Farmaceutische Technology aan de Universiteit Utrecht. Dit proefschrift beschrijft zijn onderzoek dat gedurende die periode werd verricht. Sinds november 2008 is de auteur werkzaam als post-doctoraal onderzoeker in de onderzoeksgroep van dr. W. van Blitterswijk en prof. M. Verheij aan het Nederlands Kanker Instituut te Amsterdam.